LATE HOLOCENE GLACIER FLUCTUATIONS IN SOUTHERNMOST PATAGONIA

by

Malyssa Kay Maurer

B.Sc., University of Northern British Columbia, 2009

THESIS SUBMITTED IN PARTIAL FULFILLMENT OF
THE REQUIREMENTS FOR THE DEGREE OF
MASTER OF SCIENCE
IN
NATURAL RESOURCES AND ENVIRONMENTAL STUDIES

UNIVERSITY OF NORTHERN BRITISH COLUMBIA

January 2015

Abstract

Documenting past climate dynamics aids in our understanding of the climate system. In order to assess future climate change it is valuable to examine the connectivity of climatic phenomena between the hemispheres. Although studies that estimate past climate fluctuations are common in the Northern Hemisphere, fewer well-constrained glacier chronologies exist in the Southern Hemisphere. The assessment of past glacier activity remains the most direct method of creating a climatic record for a region, and the comparison of these glacial chronologies tests the synchronicity of climatic change between regions. This study investigates inter-hemispheric synchronicity by developing a detailed glacier history in southern Patagonia for comparison to robust glacier chronologies from the northwestern North America. Five Neoglacial advances of Stoppani Glacier in the Cordillera Darwin of southern Patagonia broadly correspond to the Neoglacial activity documented in northwestern North America. This Stoppani Glacier chronology is based on radiocarbon-dated detrital and in situ plant material contained within the northeastern lateral moraine stratigraphy. The age range from dated plant material records the first Neoglacial expansion of Stoppani Glacier which, overlaps with the end of the '4.2 ka Advance' reported throughout northwestern North America. Stoppani Glacier advanced multiple times between 3500–1900 cal yr BP which overlaps with the 'Peyto-Tiedemann Advance' documented in northwestern North America. The lacustrine record from nearby Lago Roca also suggests that local sea level lowered during the 3500–1900 cal yr BP period, resulting in the isolation of the lake from the Beagle Channel ca. 2300 cal yr BP. Plant material from within till at Stoppani Glacier and lacustrine sediments from Lago Roca yield an age range for the last advance of glaciers in the Cordillera Darwin; the range coincides with the end of the wide-spread 'Little Ice Age Advance' documented throughout northwestern North America. Although the data suggest there is synchronicity over a broad scale between hemispheres, this study demonstrates the limitations inherent in using radiocarbon dating to produce high resolution chronologies of glacier fluctuations. As many Neoglacial advances are separated by retreat intervals shorter than the advance itself, it may be unreasonable to assume radiocarbon dating, with its associated errors, can numerically constrain these advances.

Table of Contents

Abstract ii
Table of Contents iii
List of Tables v
List of Figures vi
List of Appendices ix
Acknowledgements x
1. Introduction 1
2. A 3800-year record of activity of Stoppani Glacier, Cordillera Darwin, Chile 4
  2.1 Introduction 4
  2.2 Study Site 6
  2.3 Methods 9
    2.3.1 Field investigation 9
    2.3.2 Radiocarbon dating 11
  2.4 Results 12
    2.4.1 Moraine stratigraphy 12
    2.4.2 Radiocarbon ages 17
  2.5 Discussion 19
    2.5.1 Interpretation of lateral moraine stratigraphy 19
    2.5.2 Regional comparison 22
  2.6 Conclusion 28
3. A 2700-year record of environmental change at Lago Roca, southern Patagonia 29
  3.1 Introduction 29
  3.2 Study site 30
  3.3 Methods 31
    3.3.1 Core collection and analysis of bulk physical properties 31
    3.3.2 Elemental composition, particle size analysis and diatom analysis 34
    3.3.3 Thin sections and varve chronology 35
  3.4 Results 36

3.4.1 Lithostratigraphy and bulk physical properties 36
3.4.2 Couplet thickness, radiocarbon ages and sedimentation rates 44
3.4.3 Geochemistry 51
3.4.4 Diatom analyses 57
3.5 Discussion 57
3.5.1 Sediment provenance 57
3.5.2 Regional comparison 63
3.6 Conclusion 69
4. Comparison of inter-hemispheric glacier fluctuations 70
4.1 Introduction 70
4.2 Comparison of Neoglacial glacier activity 73
4.2.1 Early-middle Neoglacial (5000–3500 cal yr BP) 73
4.2.2 Middle Neoglacial (3500–1900 cal yr BP) 74
4.2.3 Late Neoglacial (1900 cal yr BP - present) 77
4.2.4 Summary 80
4.3 Limitations to a global comparison of glacier fluctuations 84
5. Conclusions 87
Reference 89
Appendices 100

List of Tables

Table 2.1: Radiocarbon ages and calibrated age ranges. 18

Table 2.2: Maximum and minimum limiting ages of Stoppani Glacier advances.......... 26

Table 3.1: Mean, median, minimum and maximum couplet thickness. 45

Table 3.2: Radiocarbon ages and corresponding calibrated age ranges from Lago Roca. 47

Table 3.3: Calculated average sedimentation rates between marker beds (MB) and calibrated radiocarbon ages (RC) compared to the measured average sedimentation rate for each Lago Roca core.......... 51

Table 3.4: Pearson correlation coefficient matrix for principal components 1, 2 and 3 and percent clay, water density, wet content, organic matter and magnetic susceptibility for samples from 09-LRoca(02). Bold values are significant ($p<0.05$).......... 57

Table A.1: Stratigraphic section at the Main Gully site, northeast lateral moraine of Stoppani Glacier.......... 99

Table D.1: Correlation among principal components 1, 2 and 3, percent clay, water density, water content, organic matter and magnetic susceptibility.......... 106

Table E.1: Calibrated age ranges of in situ fossil plants that span the Neoglacial period in northwestern North America.......... 107

List of Figures

Figure 2.1: Map of southern Patagonia and inset map of the Cordillera Darwin on Tierra del Fuego. Inset map shows the locations of Stoppani Glacier and Lago Roca. Modified from Holmlund and Fuenzalida (1995). 7

Figure 2.2: Landsat7 image of Stoppani Glacier, Dartmoore Glacier and the glaciers in the Lago Roca watershed, Tierra del Fuego (543 band colour composite from February 2001). Red lines denote ice cover in 2011 derived from the Global Land Ice Measurements from Space (GLIMS) Glacier Database. 8

Figure 2.3: Northeastern lateral moraine of Stoppani Glacier valley showing the Main Gully, Middle Section and Stream Gully sites. 10

Figure 2.4: Landsat7 image of the lower part of Stoppani Glacier, showing locations of study sites (543 band colour composite from February 2001). White dashed line denotes the vegetated ridge outside the Little Ice Age moraine that is the focus of this study. 11

Figure 2.5: Northeast lateral moraine of Stoppani Glacier showing the study site. White dashed line delineates the vegetated ridge mentioned in the text. The downvalley direction and toe of the glacier are to the right. 12

Figure 2.6: Stratigraphic sections in the northeast lateral moraine of Stoppani Glacier; contacts between units are delineated with red dashed lines. Numbered yellow circles are units (see text and Figure 2.7). Inset photos are examples of sediments from which samples were collected for radiocarbon dating: a) rhythmically laminated silt and sand containing leaves (unit 5 at the Stream Gully); b) oxidized layer of diamicton with detrital wood (separates units 1 and 2 at the Middle Section); c) diamicton (units 7, 8 and 9 at the Main Gully; red box = detrital wood mat separating units 7 and 8; d) diamicton containing tree stems (Main Gully; lower red box = contact between units 2 and 3; upper red box = unit 3; e) diamicton (unit 2 at the Middle Section); f) silty sand containing wood fragments (unit 6 at the Main Gully) 15

Figure 2.7: Stratigraphic sections in the northeast lateral moraine of Stoppani Glacier and calibrated radiocarbon ages. Age ranges derived from radiocarbon ages on stumps, stems and roots in growth position and a leaf layer within lacustrine sediment are indicated with asterisks 16

Figure 2.8: Subfossil stems partly buried in gravel or diamicton at Southwest Site #2. 18

Figure 2.9: Calibrated radiocarbon ages of advances of outlet glaciers of the Southern Patagonian Icefield, Ema Glacier, glaciers near Bahia Pia, cirque glaciers near Ushuaia and Stoppani Glacier. Bars bracket minimum and maximum limiting ages from in situ woody material, and question marks indicate age ranges of detrital wood. Light blue columns outline advances of Stoppani Glacier. Radiocarbon ages: a - Mercer (1965), b - Mercer (1968), c - Mercer (1970), d - Mercer (1976), e - Röethlisberger (1987), f - Aniya (1995), g - Kuylenstierna et al. (1996), h - Wenzens (1999), i - Strelin et al. (2008), j -Menounos et al. (2013) and k - this study. 27

Figure 3.1: Landsat 7 image showing core locations in Lago Roca (543 band colour composite from February 2001). 32

Figure 3.2: Bathymetry of the eastern half of Lago Roca (5 m isobaths) and sediment core locations. Topography after Hoja Ushuaia 5569-17-1, Gobierno de Tierra del Fuego 2003 by Gustavo Bujalesky (50 m contour interval). 33

Figure 3.3: Lithostratigraphy, calibrated radiocarbon ages and bulk physical properties of core 09-LRoca(01). Calibrated radiocarbon ages are reported in Table 3.2). 38

Figure 3.4: Lithostratigraphy, calibrated radiocarbon ages and bulk physical properties of core 09-LRoca(02). Calibrated radiocarbon age ranges are reported in Table 3.2. 39

Figure 3.5: Lithostratigraphy and bulk physical properties of core 09-LRoca(03). 40

Figure 3.6: Lithostratigraphy, calibrated radiocarbon ages and bulk physical properties of core 09-LRoca(04). Calibrated radiocarbon age ranges are reported in Table 3. 41

Figure 3.7: Lithostratigraphic boundary at 156 cm in 09-LRoca(02) (core top to the left). 42

Figure 3.8: Examples of Lago Roca laminae. a) 09-LRoca(01) core [34-30 cm depth]; b) 09-LRoca(03) core [83.5-80 cm depth]; c) 09-LRoca(04) [22-18 cm] core (core tops upward). Blue lines denote couplet boundaries and red lines measure 1 cm. 42

Figure 3.9: Thick beds (black lines) at 203–197 cm and 214–211 cm in 09-LRoca(02). Core top to the left and red line at top left equals 1 cm. 43

Figure 3.10: Thick bed (black lines) at 12.5–10 cm in wet sediments (top) and partially dried sediments (bottom) of 09-LRoca(01). Core top to the left and red line at top left equals 1 cm. The dark band in the lower photo is a desiccation crack. 43

Figure 3.11: Couplet thickness as a function of depth in the four Lago Roca cores. Marker beds (MB) are shown as dashed red lines. No marker beds were identified in 09-LRoca(04). 46

Figure 3.12: Correlation of cores 09-LRoca(01), (02), (03) and (04). Red lines denote marker beds MB-B through MB-I. Purple lines delineate depth ranges with measured varves and counted couplets; the average sedimentation rate is shown in purple for each of these zones. Calibrated radiocarbon age ranges (cal yr BP) are shown in red. The blue ages and age ranges represent the expected age of the sediment at that specific depth based on the measured average sedimentation rate for the core. 50

Figure 3.13: Concentrations of sodium, boron, phosphorus, arsenic and molybdenum in 09-LRoca(02). 52

Figure 3.14: Elemental composition of sediment in 09-LRoca(02): a) Loading scores of principal component (PC) 1 against PC 2; b) loading scores of PC 3 against PC 1; c) loading scores of PC

3 against PC 2. The numbers 1 through 20 in a, b and c are the 20 sediment samples, with their associated depths in the table at the lower right. The red symbols represent the loading scores of elements on each of the three principal components. The numbered sediment samples denote the principal component loading score for corresponding sample depths. 54

Figure 3.15: Principal component 1, 2 and 3 for 20 geochemistry samples from 09-LRoca(02). 55

Figure 3.16: Locations of raised beaches along the north coast of Beagle Channel documented by Gordillo et al. (1992). (Modified from Gordillo et al., 1992). 65

Figure 3.17: Local sea level relative to the current datum over the past 7000 years. Solid bars represent a range of sea level positions for a calibrated age range. Thin dashed lines above and below calibrated age ranges denote sea level minima and maxima with a 2 m tidal range. The blue dashed line is the elevation of Lago Roca, and the red and green dashed lines show a sea level trend that intersects known sea levels over time, assuming a constant rate of uplift. Sea surface elevations and ages from Gordillo et al. (1992, 1993). 66

Figure 4.1: Major mountain systems and ranges of western Canada. The Cariboo, Purcell, Selkirk and Monashee mountains are referred to in the text as the interior mountain ranges. Blue shading denotes 2009 ice cover. Modified from Menounos et al. (2009). 72

Figure 4.2: (Top) Calibrated radiocarbon ages of advances of outlet glaciers of the Southern Patagonian Icefield, Ema Glacier, glaciers near Bahia Pia, cirque glaciers near Ushuaia and Stoppani Glacier. Bars are minimum and maximum limiting ages from in situ material, and question marks indicate ages from detrital wood (refer to Figure 2.8 for data sources). Light blue columns outline advances of Stoppani Glacier. (Bottom) Calibrated radiocarbon ages of in situ plant material killed by expanding glaciers prior to the late LIA in the Canadian Rocky Mountains, interior mountain ranges, Cascade Range, and Canadian and Alaskan coastal mountains. Late LIA calibrated radiocarbon ages were not included because their ranges commonly span much of the last several hundred years, precluding correlation of individual advances from region to region. Bars are maximum limiting ages and dashed lines are ages derived from a study of lake sediments in the Cariboo Mountains in the interior of British Columbia (refer to Appendix E for sources). Grey line denotes generalized LIA glacier extent in northwestern North America derived from a combination of radiocarbon ages, dendrochronolgy, lichenometry and proglacial lake sedimentation. Modified from Clague et al. (2009). 83

Figure C.1: Elemental concentrations in core 09-LRoca(02). 104

Figure C.2: Total concentration of redox-indicator elements molybdenum, vanadium, zinc and uranium in core 09-LRoca(02). 107

Figure D.1: Principal component 1, 2 and 3 of 20 geochemistry samples from 09-LRoca(02). 108

List of Appendices

Appendix A: Stratigraphy of the northeast lateral moraine of Stoppani Glacier. 99

Appendix B: Sediment analysis procedures. 100

Appendix C: Elemental concentrations determined by Inductively Coupled Plasma Mass Spectrometry (ICP-MS). 102

Appendix D: Principal component analysis of total elemental concentrations after standardization for clay fraction. 106

Appendix E: Northwestern North America Neoglacial in situ ages. 108

Acknowledgements

A Master's you say? Well, that seems like a great idea! Travel to beautiful southern patatgonia! Who can say no to that? Not me, that's for sure. Well it all started with a missed plane, a confisgated Leatherman, a lost bag, and there was snow in the cirques. No lost love there because it turns out, there wasn't enough of a story in those cirques for a Master's anyways. The long and short of it was that the most southern Irish bar was wonderful, we didn't get arrested for drinking in Chile during an election and we didn't go down in the Beagle Channel dispite our skipper's obvious worry of the contrary. After three weeks of great highs and great lows in southern Patagonia I though I had left the drama of my Master's degree behind me, from here on in it would be clear sailing. Right?

If only! Five long, painful, confusing, depressing, and did I mention painful years later it is done. Five years in which I have learned more about myself then I could have ever hope. I know that people everywhere successfully complete Master's degress on a regular basis, but this was my Everest.

And so, I would like to especially thank my long-suffering supervisor, Brian Menounos for struggling through my atrocious spelling throughout the multiple drafts of my thesis. I may not have seen the merit behind every compli-but at the time, but I would not be where or whom I am today without each and every one. Thank you for not giving up on me.

I must also thank my committee members John Clague and Jerry Osborn for sharing their vast knowledge, experience and quadriceps with me. Your time and effort has and always will be much appreciated. In addition to my committee, I thank Paul Sandborn for stepping up to be my external examiner; your quick and informed response to our request was a degree saver.

Research funding was provided by the Natural Sciences and Engineering Research Council of Canada, a University of Northern British Columbia Graduate Research Award and support from all the warm harted people at CADIC-CONICET Ushuaia, without which I would not have been able to even entertain the idea of pursuing a MSc. Thank you.

I would also like to specially thank Natalie Saindon for doing all the time consuming lab work that I could throw at her. Christina Tennant, for always talking my computer down from the suicidial ledge it insisted on living on; and for indulging all my naive R related questions. I am eternially greatful to you both.

Finally, I would like to thank all my family and friends for the support and encouragement through the years. I would specifically like to thank the following: my parents for always thinking I was the best the world could ever ask for; Faye Hirshfield for always being right there with me, wheather it be with a slide hammer, an ice cream cone or just hours upon hours of chat; Vicky Serafini for her perfect balance between undying loyalty and steadfast motivation regardless how far off my rocker I slid.

And the last and forever thank you goes to my B, Brenden McBain, who has been there through every freak out and every tear and every threatened quit. This is as much his Master's as mine and there would have been no hope without him. Thank-you can not begin to cover it.

1. Introduction

In order to understand past climate dynamics, it is necessary to identify internal and external forcing mechanisms (Mitchell, 1976; McCulloch et al., 2000; Licciardi et al., 2009; Schaefer et al., 2009). The importance of each of these mechanisms is dependent on the time scale on which it influences climate (Sugden et al., 2005). Changes in forcing mechanisms that operate on a short timescale, for example, may have less influence on global climate than those operating on long timescales (Sugden et al., 2005). Forcing mechanisms external to the Earth also often occur in cycles of varying duration and can amplify or dampen the influence of other external or internal forcing mechanisms (Mitchell, 1976).

The annual mass balance of a glacier is a function of the amount of snow and ice that has accumulated due to precipitation and the amount lost due to summertime melt and, in some instances, calving (Luckman, 2000; Beedle et al., 2009). Glaciers fluctuate in response to long-term changes in precipitation and temperature, which are the primary drivers of glacier mass balance (Denton and Karlén, 1973; Ariztegui et al., 1997). Studies of past glacier fluctuations can thus identify intervals of notable climate change (Osborn et al., 2007; Menounos and Clague, 2008; Menounos et al., 2009; Winkler and Matthews, 2010). Fluctuations in glaciers driven by climate change are commonly recorded in the landforms and sediments they leave behind (Osborn et al., 2007; Menounos and Clague, 2008).

The most direct method of developing a record of glacier fluctuations is to map and date landforms that record past glacier activity (Menounos et al., 2004, 2009). A less direct method is to document long-term changes in the amount and calibre of sediment carried by glacial meltwater into a proglacial lake (Menounos and Clague, 2008; Schiefer et al., 2010). A combination of terrestrial and lacustrine records often provides a superior chronology of glacier fluctuations (Menounos et al., 2004; Osborn et al., 2007).

The climate of the Holocene Epoch has been much more stable than that of the Pleistocene, but recent studies highlight the substantial global and regional variability of Holocene climate (Mayewski et al., 2004; Clague et al., 2009; Davis et al., 2009). However, the degree to which Holocene climatic events occurred synchronously in the Northern and Southern hemispheres remains uncertain (McCulloch et al., 2000; Mayewski et al., 2004; Sugden et al., 2005; Strelin et al., 2008; Menounos et al., 2009; Rodbell et al., 2009; Schaefer et al., 2009; Winkler and Matthews, 2010). Schaefer et al. (2009) argue that Holocene glacier fluctuations in the Southern Hemisphere were neither in phase nor strictly anti-phased to those in the Northern Hemisphere. Clague et al. (2009) note, however, that many glacier advances in both hemispheres are not well constrained by bracketing ages, which renders direct comparisons difficult at best. In addition, the uncertainties of most radiocarbon ages exceed 50 years ($\pm 1\ \sigma$), which further complicates inter-hemispheric comparisons (Clague et al., 2009).

A difficulty in using glaciers to establish the degree of climatic synchronicity in the two hemispheres is the limited number of well-dated glacier chronologies from the Southern Hemisphere (Porter, 2000; Rodbell et al., 2009). In addition, most studies of inter-hemispheric syncronicity have focused on events of the latest Pleistocene (Glasser et al., 2004). Most research on Holocene glacier fluctuations in southernmost South America to date has focused on outlet glaciers of the Southern and Northern Patagonian icefields (Mercer, 1968, 1976; Röethlisberger, 1987; Aniya, 1995; Wenzens, 1999; Koch and Kilian, 2005) and small glaciers farther south, on the island of Tierra del Fuego in southernmost Patagonia (Kuylenstierna et al., 1996; Rabassa et al., 2000; Strelin and Malagnino, 2000; Strelin et al., 2008; Menounos et al., 2013b). There is a need to extend this research by studying new sites (Rodbell et al., 2009).

My thesis objectives are toexamine Holocene glacier fluctuations in southern Patagonia and to compare past glacier activity between similar areas in both hemispheres, by critically examining published glacier chronologies from northwestern North America. In Chapter 2, I describe a 3800-year record of activity of Stoppani Glacier, established by radiocarbon dating detrital wood and stumps in growth position exposed in one of the glacier's lateral moraines. I compare the chronology of Stoppani Glacier to published glacier chronologies from the Cordillera Darwin and the Southern Patagonian Icefield. In Chapter 3, I examine the sedimentary record of glacier activity in Lago Roca, a proglacial lake east of Stoppani Glacier. In Chapter 4, I compare records of glacier activity in southern Patagonia to established glacier chronologies in northwestern North America. I also illustrate the limitations inherent in an inter-hemispheric comparison of glacier activity. Chapter 5 provides a summary of the significant findings of this study and suggestions for further work.

2. A 3800-year record of activity of Stoppani Glacier, Cordillera Darwin, Chile

2.1 Introduction

Glaciers adjust their thickness, width and length in response to long-term changes in precipitation and temperature (Denton and Karlén, 1973; Ariztegui et al., 1997). Changes in length are typically the most obvious indicators of a glacier's response to past climate change (Osborn et al., 2007; Menounos et al., 2009). In northwestern North America, for example, most glaciers reached their maximum downvalley positions during the past several centuries, at which time they overrode and destroyed most of the evidence of earlier advances (Ryder and Thomson, 1986; Reyes and Clague, 2004; Osborn et al., 2007; Menounos et al., 2009).

Even without such evidence many glacier forefields contain rich stratigraphic records that enable detailed reconstructions of the timing of past glacier activity (Menounos et al., 2004, 2009; Osborn et al., 2007; Davis et al., 2009). Sub-fossil wood from glacier forefields can be dated to constrain an advance or retreat, although an accurate reconstruction depends on a correct interpretation of the origin of the wood (Ryder and Thomson, 1986). Trees that were overrun by a glacier can be dated by dendrochronology or radiocarbon techniques to provide an age for an expansion of the glacier past the sample site (Ryder and Thomson, 1986). Detrital wood is more difficult to interpret because the origin of the wood can be ambiguous (Ryder and Thomson, 1986; Iturrizaga, 2008). For instance, wood fragments in till that originated from vegetated slopes above a glacier may provide no information about glacier activity. If, however, non-glacial sources (e.g. mass wasting of wood from vegetated slopes above the glacier) can be eliminated, detrital wood within till provides a maximum limiting age for glacier activity (Ryder and Thomson, 1986).

Rapid retreat of glaciers during the twentieth century has exposed many sites where the stratigraphy of lateral moraines can be studied (Osborn and Karlstrorn, 1988; Osborn et al., 2007; Harvey et al., 2012). Some lateral moraines comprise multiple tills and may contain sub-fossil wood and tephras that can be studied to establish a chronology of glacier activity (Clague, 1986, 1987; Ryder and Thomson, 1986; Osborn and Karlstrom, 1989; Desloges and Ryder, 1990; Osborn et al., 2001; Reyes and Clague, 2004; Harvey et al., 2012).

The stratigraphy of lateral moraines must be carefully interpreted. Lateral moraines only record advances that produce thicker ice than all earlier glacier advances; the history of lesser advances is commonly absent, and periods of glacier thinning and retreat can only be indirectly constrained (Osborn and Karlstrorn, 1988; Osborn et al., 2007). Stratigraphic sections may also contain unconformities produced by erosion (Clague, 1986). Nevertheless, woody debris, stumps and stems in growth position, paleosols and tephras in lateral moraines yield valuable information on past glacier activity (Ryder and Thomson, 1986; Osborn and Karlstrorn, 1988; Reyes and Clague, 2004; Harvey et al., 2012). These types of information have been widely used to develop chronologies of glacier activity in northwestern North America, but have not yet been widely applied in southern Patagonia.

In this chapter, I describe the stratigraphy of a lateral moraine at Stoppani Glacier near the Chile-Argentina border on Tierra del Fuego. I provide new radiocarbon ages on wood recovered from several horizons in the moraine. I infer the origins of the dated wood using the method outlined by Ryder and Thomson (1986) and generate a glacier chronology for the area. I also compare my chronology to other published glacier chronologies in southern Patagonia.

2.2 Study Site

Tierra del Fuego is a large island in southernmost South America that is shared by Chile and Argentina. The climate of Tierra del Fuego is cool and humid; with a mean annual temperature of 5°C and average annual rainfall of 550 mm in the southwest and less than 300 mm in the northeast (Gordillo et al., 1993). Precipitation arises from frontal activity from the south and southwest and orographic uplift of moisture-laden air masses (Rabassa et al., 2000). Forests of evergreen southern beech and several species of deciduous beech occur below 700 – 800 m above sea level (asl), and peat bogs are common in poorly drained areas (Gordillo et al., 1993).

The southernmost portion of the Andes in Patagonia includes the Cordillera Darwin Range, which consist of schists and intrusive granitic rocks of Mesozoic age and forms part of the Scotia Plate (Rabassa et al., 2000). The Cordillera Darwin contains deep valleys separated by sharp, glacially eroded ridges and peaks (Rabassa et al., 2000). Slightly less than half the area of the range is covered by glacier ice, principally the Cordillera Darwin Icefield with an area of 2300 km^2 (Gordillo et al., 1993; Boyd et al., 2008).

Stoppani Glacier is located 40 km west of the city of Ushuaia, Argentina (Figure 2.1) on the east side of the Cordillera Darwin. It is 11 km long and has an area of about 75 km^2 (Figure 2.2). The glacier flows southeast from the flanks of Pico Frances (2150 m asl) and Pico Italia (2360 m asl) to its terminus at 100 m asl. Meltwater from Stoppani Glacier flows directly into Yendegaia Bay and then into Beagle Channel.

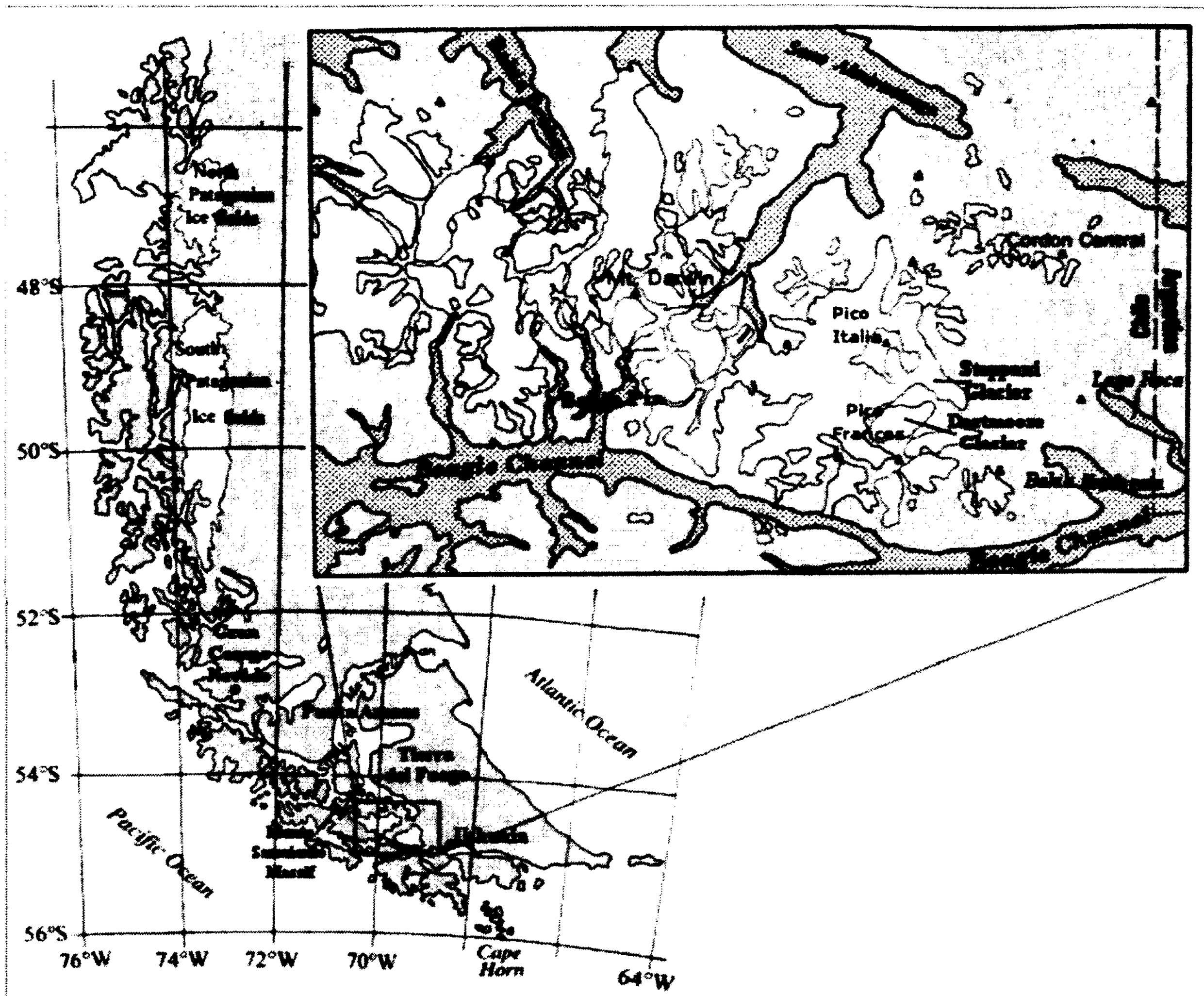

Figure 2.1: Map of southern Patagonia and inset map of the Cordillera Darwin on Tierra del Fuego. Inset map shows the locations of Stoppani Glacier and Lago Roca. Modified from Holmlund and Fuenzalida (1995).

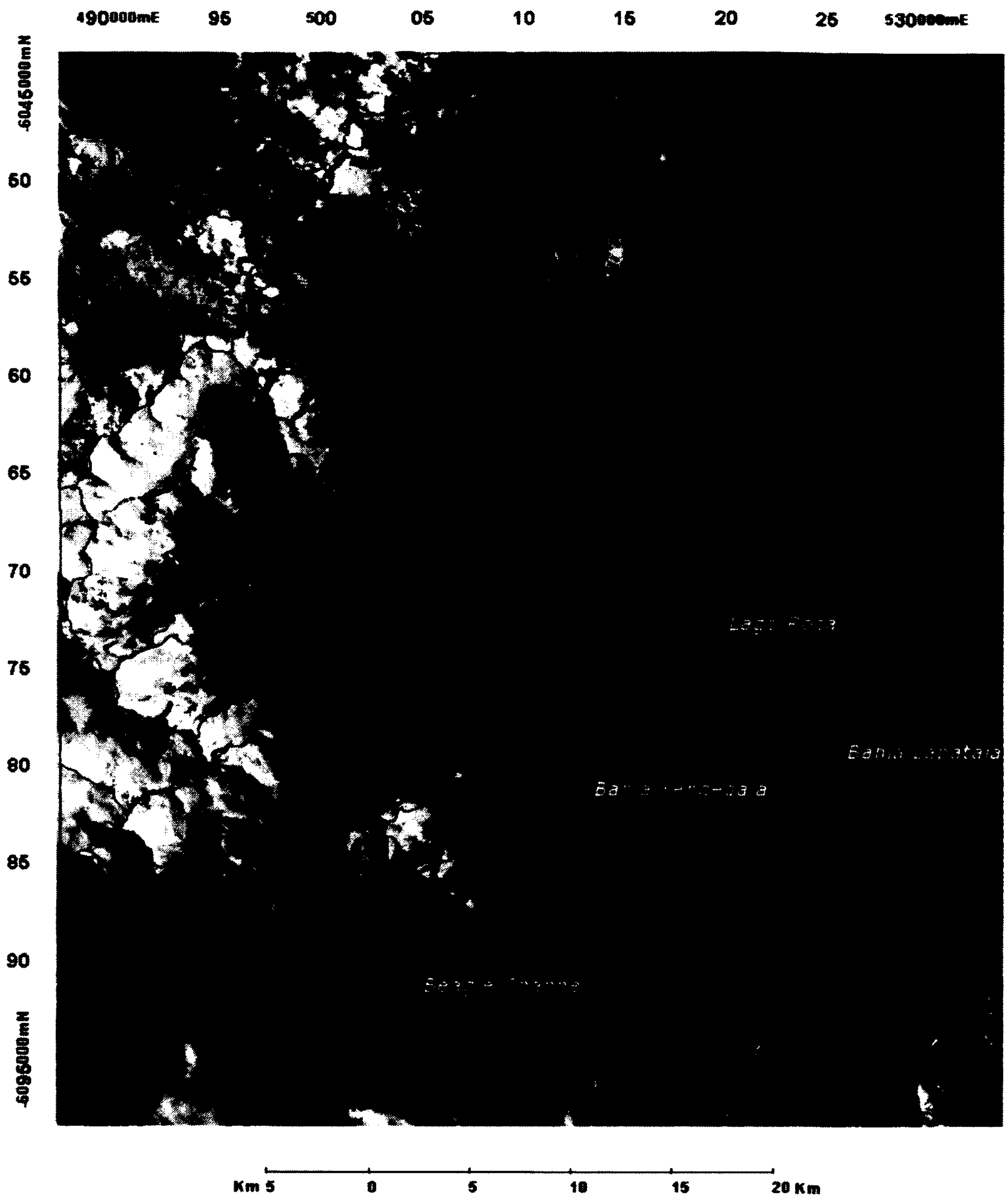

Figure 2.2: Landsat7 image of Stoppani Glacier, Dartmoore Glacier and the glaciers in the Lago Roca watershed, Tierra del Fuego (543 band colour composite from February 2001). Red lines denote ice cover in 2011 derived from the Global Land Ice Measurements from Space (GLIMS) Glacier Database.

2.3 Methods

2.3.1 Field investigation

In December 2009, Brian Menounos, Jerry Osborn, John Clague and I visited the terminus of Stoppani Glacier to document the past activity of the glacier. We searched for subfossil wood within the glacier forefield and lateral moraines. We chose a 100-m-high, 250-m-long section of the northeast (left side as viewed down-valley) lateral moraine for detailed stratigraphic work. We made stratigraphic observations at three sites along the section, which we informally named 'Main Gully',' Middle Section' and 'Stream Gully' (Figure 2.3). The section is 2.5 km from the terminus of the glacier and about 150 m from its edge (Figure 2.4). Beech forest extends from the crest of the moraine to treeline at about 550 m asl. We also searched the southwest side (right side as viewed down-valley) of the glacier and collected wood samples from two sites. Southwest Site #1 is located about 1.1 km from the west margin of Stoppani Glacier, opposite the northeastern lateral moraine exposure and Southwest Site #2 is located about 350 m up-valley from the snout of the glacier (Figure 2.4).

The section was photographed, described in the field and divided into lithostratigraphic zones using the procedure and nomenclature of Eyles et al. (1983). We searched the section for tephras and plant macrofossils. We excavated around the base of stumps to ensure that they were in growth position. If we were unable to find a rooting horizon, we assumed the stump to be detrital. Sample locations were determined using a hand-held GPS, the stratigraphy was logged, and wood samples were bagged, labelled, and transported to the University of Northern British Columbia (UNBC).

Figure 2.3: Northeastern lateral moraine of Stoppani Glacier valley showing the Main Gully, Middle Section and Stream Gully sites.

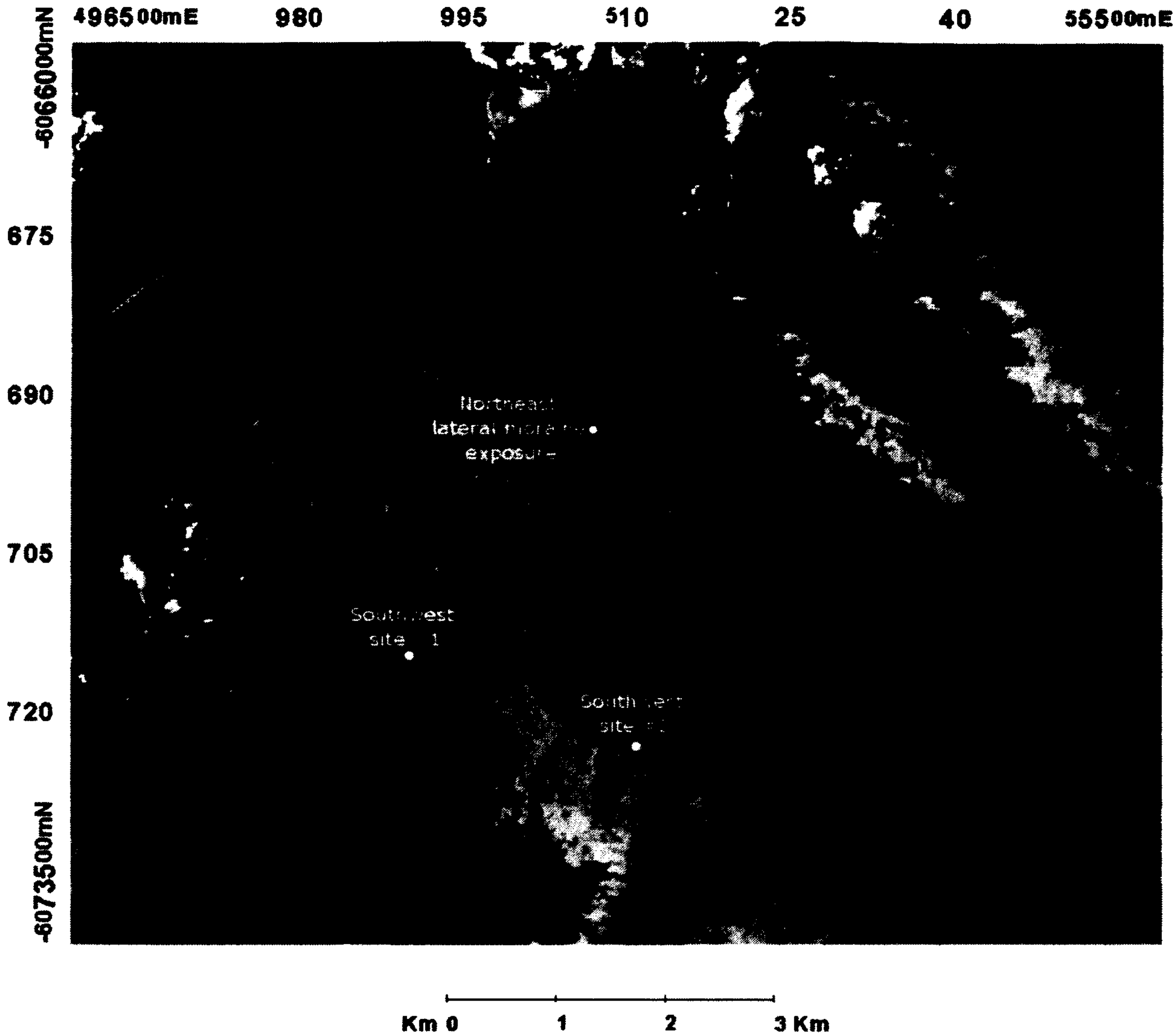

Figure 2.4: Landsat7 image of the lower part of Stoppani Glacier, showing locations of study sites (543 band colour composite from February 2001). White dashed line denotes the vegetated ridge outside the Little Ice Age moraine that is the focus of this study.

2.3.2 Radiocarbon dating

I submitted wood samples to the Keck Carbon Cycle Accelerator Mass Spectrometry (AMS) Facility in the Earth System Science Department, University of California - Irvine for radiocarbon dating. I used the online CALIB 6.0 Radiocarbon Calibration program (Stuiver et al., 2010) to convert radiocarbon ages to calendar age ranges (2 σ) before present (1950) (cal yr

BP) using the Southern Hemisphere Atmospheric Calibration Curve (Stuiver et al., 2010). I report calibrated age ranges to the nearest 10 years.

2.4 Results

2.4.1 Moraine stratigraphy

A 2-km-long, vegetated ridge extends parallel to Stoppani Glacier about 60 m above and 100 m beyond the lateral moraine that is the focus of this chapter (Figure 2.4 andFigure 2.5). We were unable to access this landform and so could not confirm its origin, but it has the characteristics of a moraine. Its age is uncertain.

Figure 2.5: Northeast lateral moraine of Stoppani Glacier showing the study site. White dashed line delineates the vegetated ridge mentioned in the text. The downvalley direction and toe of the glacier are to the right.

I recognize nine units at the Main Gully location and five units at both the Middle Section and Stream Gully sites (Figure 2.6). The lowest 20 m of the section is covered by colluvium. Most of the units could be traced continuously from the Main Gully site upvalley to the Stream Gully site. Of the nine units at the Main Gully location, units 1, 3, 4, 5, 7, 8 and 9 all consist of matrix-supported sandy gravel diamicton with varying degrees of stratification and clast size (Appendix A). At the Main Gully most units are separated by wood layers containing a variety of detrital logs, stems, roots and stumps in growth position (Figure 2.7; Table 2.2). Units 1 and 3 are separated by a unit of horizontally stratified sand and sandy gravel (unit 2), which does not contain any wood fragments and is structurally dissimilar to the surrounding units. Units 5 and 7 are also separated by a distinct unit of silty to sandy gravel which contains lenses of peat and wood fragments (unit 6). Because sediments were best exposed in the Main Gully, I correlate the nine units to units at the Middle Section and Stream Gully (Figure 2.6 and 2.7; Appendix A). Not all unit boundaries at the Middle Section and Stream Gully contain wood fragments (Figure 2.6 and 2.7).

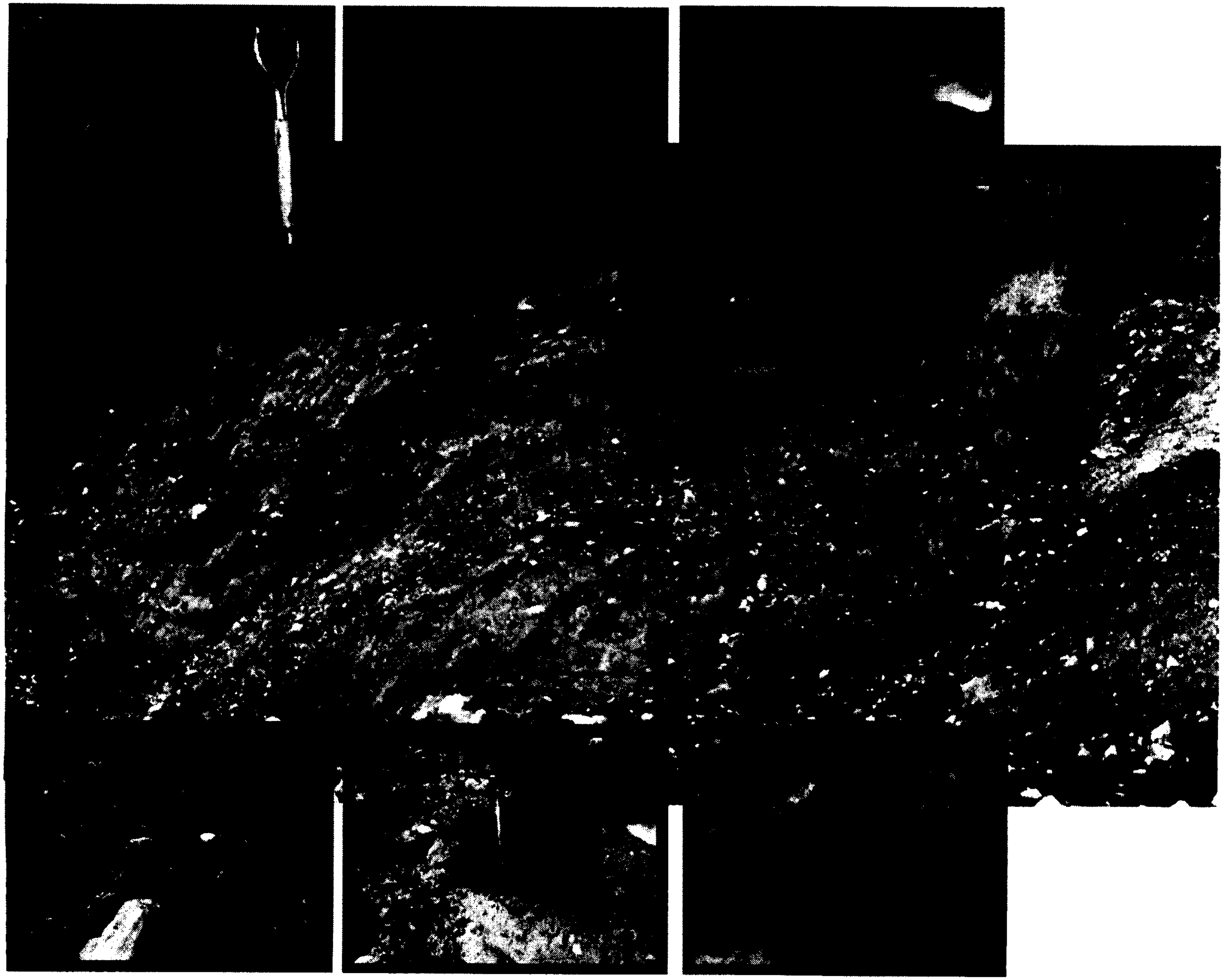

Figure 2.6: Stratigraphic sections in the northeast lateral moraine of Stoppani Glacier; contacts between units are delineated with red dashed lines. Numbered yellow circles are units (see text and Figure 2.7). Inset photos are examples of sediments from which samples were collected for radiocarbon dating: a) rhythmically laminated silt and sand containing leaves (unit 5 at the Stream Gully); b) oxidized layer of diamicton with detrital wood (separates units 1 and 2 at the Middle Section); c) diamicton (units 7, 8 and 9 at the Main Gully; red box = detrital wood mat separating units 7 and 8; d) diamicton containing tree stems (Main Gully; lower red box = contact between units 2 and 3; upper red box = unit 3; e) diamicton (unit 2 at the Middle Section); f) silty sand containing wood fragments (unit 6 at the Main Gully).

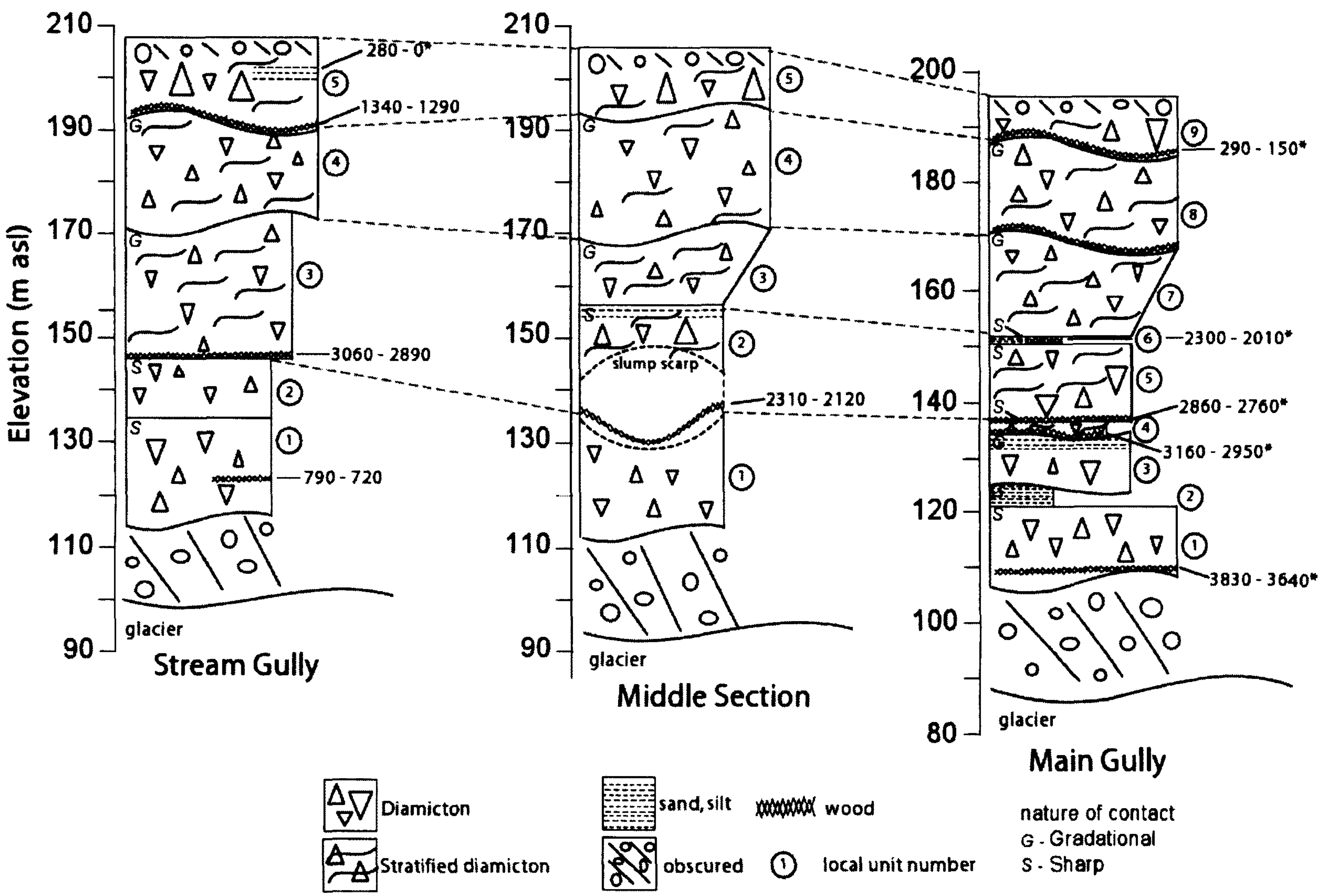

Figure 2.7: Stratigraphic sections in the northeast lateral moraine of Stoppani Glacier and calibrated radiocarbon ages. Age ranges derived from radiocarbon ages on stumps, stems and roots in growth position and a leaf layer within lacustrine sediment are indicated with asterisks

2.4.2 Radiocarbon ages

We collected 20 samples of plant macrofossils from the northeast lateral moraine: eight from the Main Gully and Middle Section and four from the Stream Gully. Due to limited funds, only 10 of the 20 samples were dated (Figure 2.7, Table 2.1): four samples of wood in growth position (two samples from roots, one stem and one stump); one sample of leaves; a branch from a compressed wood and peat mat; and five samples of detrital wood. Each in situ wood fragment was dated and the remaining samples were chosen from the detrital material based on the location and preserved state in which the wood was found. The ages range from 3830–3640 to 280–0 cal yr BP and decrease up-section with one exception at the Stream Gully (Figure 2.7).

We also collected three, and radiocarbon-dated two, wood samples (Figure 2.8) from the glacier forefield southwest of the glacier. A sample from one of three highly weathered wood fragments, lacking bark found partially buried on the crest of the outer moraine at Southwest Site #1 returned a radiocarbon age with a calibrated age range of 250–0 cal yr BP. A sample of the outer rings of one of two steeply inclined stems, 50–60 cm in diameter, at Southwest Site #2 returned a radiocarbon age with a calibrated age range of 300–150 cal yr BP (Table 2.1). We were unable to excavate this stem and thus are uncertain if it is in growth position; therefore I classified it as a detrital wood sample.

Table 2.1: Radiocarbon ages and calibrated age ranges.

Laboratory no [a]	Field no.	Location	Elevation (m asl)	Material	^{14}C age (yr BP)	Calendar age [b]
Stoppani Glacier: northeast lateral						
UCIAMS-72637	09-STO(B)	54°46'12.7" S 68°59'15.0" W	200	Leaf layer below till	185 ± 15	280 – 0
UCIAMS-72642	09-Sto(03)E	54°46'24.3" S 68°59'5.8" W	185	Root in growth position	210 ± 15	290 – 150
UCIAMS-72645	LPSW(VIII)	54°46'.19.8" S 68°59'15.27" W	123	Detrital log	885 ± 15	790 – 720
UCIAMS-72636	09-STO(A)	54°46'12.0" S 68°59'15.5" W	190	Detrital log	1450 ± 15	1340 – 1290
UCIAMS-72643	09-Sto(03)F	54°46'24.3" S 68°59'5.8" W	152	Root in growth position	2185 ± 15	2300 – 2010
UCIAMS-72644	LPSW(I)	54°46'23.2" S 68°59'10.5" W	137	Detrital log	2230 ± 15	2310 – 2120
UCIAMS-72640	09-Sto(03)B	54°46'24.3" S 68°59'5.8" W	138	Stump in growth position	2775 ± 15	2860 – 2760
UCIAMS-72638	09-STO(D)	54°46'16.4" S 68°59'16.7" W	147	Detrital log	2890 ± 15	3060 – 2890
UCIAMS-72641	09-Sto(03)C	54°46'24.3" S 68°59'5.8" W	137	Stem in growth position	2950 ± 15	3160 – 2950
UCIAMS-72639	09-Sto(03)	54°46'24.3" S 68°59'5.8" W	110	Branch in wood and peat mat	3510 ± 15	3830 – 3640
Stoppani Glacier: southwest side						
UCIAMS-79273	09-STO(02)B	54°47'54.6" S 68°58'41.1" W	80	Detrital log	135 ± 15	250 – 0
UCIAMS-79275	09-STO(01)	54°47'24.7" S 69°00'58.4" W	150	Detrital log	250 ± 15	300 – 150

[a] Radiocarbon laboratory: UCIAMS-University of California at Irvine.
[b] Calendar ages ranges before present (AD 1950) converted from radiocarbon ages using CALIB 6.0 (Stuiver et al., 2010) with 2σ uncertainties.

Figure 2.8: Subfossil stems partly buried in gravel or diamicton at Southwest Site #2.

2.5 Discussion

2.5.1 Interpretation of lateral moraine stratigraphy

Based on the stratigraphy and radiocarbon ages, I infer that Stoppani Glacier advanced many times during the past 3800 years. If the vegetated ridge outside the composite moraine I studied is also a lateral moraine, it marks the outermost known limit of Stoppani Glacier. If it is a moraine, however, its age is unknown. The position of this feature outboard of the stratigraphic section I studied does not ensure that it is older than any but the uppermost unit in the section. At Tiedemann Glacier in the Coast Mountains of British Columbia, for example, a till associated with the outermost lateral moraine is exposed tens of meters below the crest of a younger, inner moraine (Ryder and Thomson, 1986; Menounos et al., 2013a).

The massive sandy gravel diamicton (unit 1) overlying peat with roots in growth position in the Main Gully (Figures 2.6 and 2.7, Table 2.1) records the first advance of Stoppani Glacier for which there is stratigraphic evidence. I interpret the massive compact diamicton above the wood mat to be till deposited when Stoppani Glacier advanced over a vegetated surface. A branch within peat mat yielded an age of 3830–3640 cal yr BP, which is a maximum for an advance during which Stoppani Glacier reached at least 20 m above its 2009 surface.

I interpret unit 2 in the Main Gully to be glaciofluvial sediments deposited by a meltwater stream flowing along the margin of Stoppani Glacier. The presence of cobbles within the sand implies ice-proximal deposition at a time when the glacier reached the elevation of unit 2 at the Main Gully. It is unclear whether unit 2 was deposited during the 3830–3640 cal yr BP advance or during a later advance. The unit is overlain by matrix-supported diamicton with striated clasts (unit 3), indicating that Stoppani Glacier later advanced to at least 45 m above its 2009 level.

After Stoppani Glacier deposited unit 3, it thinned and retreated enough for a forest to become established on top of the unit. Correlative diamicton units (unit 4 at the Main Gully, unit 1 at the Middle Section and unit 2 at the Stream Gully) were later deposited on the remnants of that forest. Unit 4 at the Main Gully is similar to unit 3, from which I infer that it also is till deposited when Stoppani Glacier advanced into a forest shortly after 3160–2950 cal yr BP (Figures 2.6 and 2.7, Table 2.1). A similar age on the detrital wood mat at the top of unit 2 at the Stream Gully (3060–2890 cal yr BP) supports the argument that Stoppani Glacier was advancing about 3100–2950 cal yr BP.

A stump in growth position in the wood mat between units 4 and 5 at the Main Gully has a calibrated age of 2860–2760 cal yr BP. Unit 5 diamicton in the Main Gully resembles underlying unit 4, as well as unit 2 at the Middle Section, and is therefore interpreted to be till deposited when Stoppani Glacier advanced shortly after 2860–2760 cal yr BP. The stratification of unit 5 suggest that the till was deposited in a dump moraine as Stoppani Glacier advanced to at least 50 m above its 2009 elevation.

Roots in growth position within unit 6 at the Main Gully yielded a calibrated age of 2300–2010 cal yr BP age, which is a maximum age for a fourth advance of Stoppani Glacier. During this advance, Stoppani Glacier deposited unit 7 in the Main Gully and unit 3 at the Middle Section and Stream Gully (Figures 2.6 and 2.7, Table 2.1). These units are stratified and resemble units 4 and 5 at the Main Gully, thus I infer that they were deposited by Stoppani Glacier as it advanced into forest shortly after 2300–2010 cal yr BP. Wood from unit 2 at the Middle Section returned a similar age of 2320–2120 cal yr BP. Because unit 2 at the Middle Section slumped from higher in the moraine, there is doubt about the relation of this age to a glacier advance; however, the equivalence of the age to the age of the in situ wood sample from the Main Gully suggests that the detrital wood was also killed when Stoppani Glacier expanded to about 60 m above the 2009 ice margin at 2300–2010 cal yr BP.

The presence of a wood mat at the contact between units 7 and 8 at the Main Gully implies that the glacier advanced into a forest sometime after 2300–2010 cal yr BP, but before 290–150 cal yr BP (Figure 2.7, Table 2.1). The age of a piece of detrital wood at the top of unit 4 at the Stream Gully suggests that this advance happened sometime after 1340–1290 cal yr BP. It is also possible that after 2300–2010 cal yr BP, Stoppani Glacier advanced in stages, with short periods of stability during which a forest became established on the moraine, until Stoppani Glacier reached its most recent maximum extent.

The detrital wood in unit 1 at the Stream Gully, which returned a calibrated age of 790–720 cal yr BP (Figures 2.6 and 2.7, Table 2.1), may have been deposited as an inset into the northeast lateral moraine during a minor advance early during the Little Ice Age. Although vertical stacking of tills is the most common way that composite lateral moraines are created, there are documented cases in northwestern North America of tills inset into the proximal flank of a lateral moraine that subsequently have been overridden by the glacier that deposited them (Osborn, 1986; Samolczyk, 2011).

Although it is not known when the most recent advance of Stoppani Glacier commenced, the radiocarbon age on a stump at the contact between units 8 and 9 in the Main Gully indicates that the glacier achieved its maximum extent of the past 4000 years shortly after 290–150 cal yr BP (Figures 2.6 and 2.7, Table 2.1). Units 8 and 9 were also stratified, which implies that Stoppani Glacier continued to thicken 50 m between 2300–2010 and 290–150 cal yr BP. A similar age of 280–0 cal yr BP from leaves within rhythmically laminated silt below till at the

Stream Gully (unit 5) confirms that the glacier thickened and reached at least 100 m above the 2009 ice level and deposited till shortly after that time. The inclined tree stem and piece of detrital wood in the glacier forefield on the southwest side of the glacier returned ages of 300–150 and 250–150 cal yr BP, which are similar to the age of the in situ stump at the contact between units 8 and 9 at the Main Gully (Figure 2.4, Table 2.1). The similarity in ages of these samples and that of the stump at the Main Gully suggests that the trees from which the dated samples came were all killed during the final advance of Stoppani Glacier. The time of the retreat of Stoppani Glacier from its most recent maximum limit is unknown; it is also uncertain whether retreat occurred in stages or was more-or-less continuous.

2.5.2 Regional comparison

The onset of the Neoglaciation in southern Patagonia is marked by the widespread advance of glaciers about 5000 years ago (Mercer, 1968; Wenzens, 1999; Rodbell et al., 2009). It is possible that the outermost vegetated lateral moraine on the northeast side of Stoppani Glacier is a product of this event, although it could equally likely have been deposited during Late Glacial time. Regardless of the age of this landform, there is no stratigraphic evidence for a 5000-year-old advance in the northeast lateral moraine of Stoppani Glacier. There could be glacial deposits of this age in the covered portion of the moraine, but if so, they would record only a minor advance with glacier thickening limited to no more than 15 m above the 2009 level of the glacier. Prior to the onset of the Neoglaciation, most glaciers in southern Patagonia had retreated to less than half their maximum Late-Glacial lengths (Wenzens, 1999). Some studies suggest advances at 8500–8400, 8000–7500 and 6300 cal yr BP (Clapperton and Sugden, 1988; Wenzens, 1999). Clapperton and Sugden (1988) note, however, that any pre-5000 cal yr BP advances, if they occurred, were minor. This inference is supported by the record from the northeast lateral moraine of Stoppani Glacier. Evidence from cirques near Ushuaia, Argentina (Figure 2.1) suggest one or perhaps two advances centered at 7960–7340 and 5290–5050 cal yr BP (Menounos et al., 2013b), but glaciers only reached positions tens of meters beyond those achieved during the past 250 years.

The lowermost exposed till in the northeast lateral moraine records the earliest evidence of Neoglacial activity at Stoppani Glacier. The maximum limiting age of this advance (3830–3640 cal yr BP) coincides with the time of expansion of outlet glaciers of the Southern Patagonian Icefield just before ca. 3600 cal yr BP (Figure 2.9, Table 2.2; Mercer, 1968, 1970, 1976; Aniya, 1995; Wenzens, 1999). This advance of Stoppani Glacier occurred during an interval of cooler-than-average air temperatures in the vicinity of the Beagle Channel (Kuylenstierna et al., 1996; Strelin et al., 2008).

According to Strelin et al. (2008), glaciers in the Cordillera Darwin were retreating ca. 3200 cal yr BP. Stoppani Glacier retreated between 3830–3640 and 3160–2950 cal yr BP, allowing a forest to become established on the moraine (Figure 2.9, Table 2.2). An advance of Ema Glacier on Monte Sarmeinto, west of the Cordillera Darwin (Figure 2.1), occurred between 3460 and 3070 cal yr BP, at about the same time as the second advance of Stoppani Glacier (3160–2950 cal yr BP). According to Strelin et al. (2008), this advance was the second most extensive advance of the Neoglacial period (Strelin et al., 2008). A comparable advance of glaciers in Bahia Pia on the south side of the Cordillera Darwin (Figure 2.1) commenced before 3390–3080 cal yr BP (Kuylenstierna et al., 1996). The maximum limiting age of the Ema Glacier advance and the minimum limiting age of the glaciers in Bahia Pia overlap the age of the second advance of Stoppani Glacier. No evidence has been presented for advances of outlet glaciers of the Southern Patagonian Icefield at this time (Mercer, 1965, 1968; Aniya, 1995).

Stoppani Glacier advanced a third time soon after 2860–2760 cal yr BP (Figure 2.9, Table 2.2). No evidence has been presented that Ema Glacier advanced at this time, but a minimum limiting age (2770–2360 cal yr BP) suggests glacier expansion in the Bahia Pia area at about this time (Kuylenstierna et al., 1996). Again, no evidence has been presented for an advance of outlet glaciers of the Southern Patagonian Icefield at the time of the third advance of Stoppani Glacier (Mercer, 1968; Aniya, 1995; Wenzens, 1999). It is possible that evidence of glacier activity at the Southern Patagonian Icefield just before ca. 2700 cal yr BP was destroyed by more extensive advances between 2700–2070 and 2120–1610 cal yr BP (Mercer, 1968; Aniya, 1995).

Work to date in the Cordillera Darwin does not indicate glacier expansion during the fourth advance of Stoppani Glacier, which commenced about 2300–2010 cal yr BP (Figure 2.9; Kuylenstierna et al., 1996; Strelin et al., 2008). Kuylenstierna et al. (1996) infer a warm period at Bahia Pia between 2770–2360 and 2000– 1620 cal yr BP, which may indicate that increased precipitation rather than decreased temperatures caused Stoppani Glacier to advance at about 2300–2010 cal yr BP. Alternatively, the inference of Kuylenstierna et al. (1996) might be incorrect. Kaplan et al. (2011) report ^{10}Be ages of 2360–1610 cal yr BP from boulders on moraines left by outlet glaciers of the Southern Patagonian Icefield; these ages correspond to the time of the fourth advance of Stoppani Glacier. Minimum limiting ages on peat indicate that glaciers on the east side of the Southern Patagonian Icefield advanced around 2340–1880 cal yr BP and retreated by 2120–1610 cal yr BP (Figure 2.9; Mercer, 1968). This advance has not been previously identified in the Cordillera Darwin.

Stoppani Glacier may have advanced shortly after 1340–1290 cal yr BP, although this interpretation is not certain because the radiocarbon age that constrains the advance is derived from detrital wood (Figures 2.7 and 2.9, Table 2.2). Two units of till at the Main Gully (unit 7 and 8) are above the 1340–1290 cal yr BP detrital wood sample, indicating that the glacier advanced twice between 1340–1290 and 290–150 cal yr BP. Ema Glacier advanced to within meters of its 3460–3066 cal yr BP limit around 1290–980 cal yr BP (Strelin et al., 2008), and outlet glaciers of the Southern Patagonian Icefield advanced between 1370–1060 and 1330–990 cal yr BP (Clapperton and Sugden, 1988; Aniya, 1995); therefore, it is plausible that Stoppani Glacier likewise advanced around 1340–1290 cal yr BP.

A detrital log with a calibrated age of 790–720 cal yr BP in till (Figures 2.7 and 2.9) may be associated with expansion of Stoppani Glacier, although because the wood is detrital, its age must be considered a maximum limiting age; the wood could have been delivered to the glacier as trees today grow above the site. Several sites in southern Patagonia experienced glacier expansion during the past millennium. Bahia Pia glaciers, for example, expanded sometime between 930–680 and 730–540 cal yr BP (Kuylenstierna et al., 1996). Two units of till in the forefield of Ema Glacier are younger than 730–500 cal yr BP (Strelin et al., 2008), and outlet glaciers of the Southern Patagonian Icefield were advancing between 1120–650 and 930–670 cal yr BP (Mercer, 1968; Aniya, 1995).

The age on a stump 10 m below the crest of the northeast lateral moraine (290–150 cal yr BP) and the two ages on the southwest side of the glacier (250–150 and 300–150 cal yr BP) date the final Neoglacial advance of Stoppani Glacier. Most glaciers in the Cordillera Darwin were advancing by 500–00 cal yr BP (Strelin et al., 2008). Ema Glacier expanded after 520–150 cal yr BP and remained near its limit until AD 1890 (Figure 2.9; Strelin et al., 2008). Glaciers on Gran Campo Nevado (Figure 2.1) were expanding by 330 cal yr BP and reached their maximum Holocene extents during this advance (Koch and Kilian, 2005). In other areas of southern

Patagonia, glaciers expanded from 670–480 to 440–0 cal yr BP, reaching positions near those achieved during the 1330–1060 cal yr BP advance (Mercer, 1968; Clapperton and Sudgen, 1988; Aniya, 1995; Wenzens, 1999). An advance of Tyndall Glacier in the Southern Patagonia Icefield culminated about AD 1700, within meters of the terminal moraine it built sometime between 1120 and 670 cal yr BP (Mercer, 1968; Aniya, 1995).

Warm dry conditions triggered widespread glacier retreat on Tierra del Fuego starting at the beginning of the twentieth century (Strelin and Iturraspe, 2007; Strelin et al., 2008). Glaciers elsewhere in southern Patagonia retreated most rapidly between AD 1930 and 1960 (Clapperton and Sugden, 1988). Glacier recession slowed between AD 1960 and 1970, with continued retreat thereafter (Strelin and Iturraspe, 2007). I have no evidence for the timing of retreat of Stoppani Glacier during the past century, but the glacier thinned 100 m between 280 cal yr BP and today.

Table 2.2: Maximum and minimum limiting ages of Stoppani Glacier advances.

Stoppani advance	Maximum limiting age (cal yr BP)	Minimum limiting age (cal yr BP)
1st	3830 – 3640	3160 – 2950
2nd	3160 – 2950	2860 – 2760
3rd	2860 – 2760	2300 – 2010
4th	2300 – 2010	290 – 150
5th	290 – 150	–

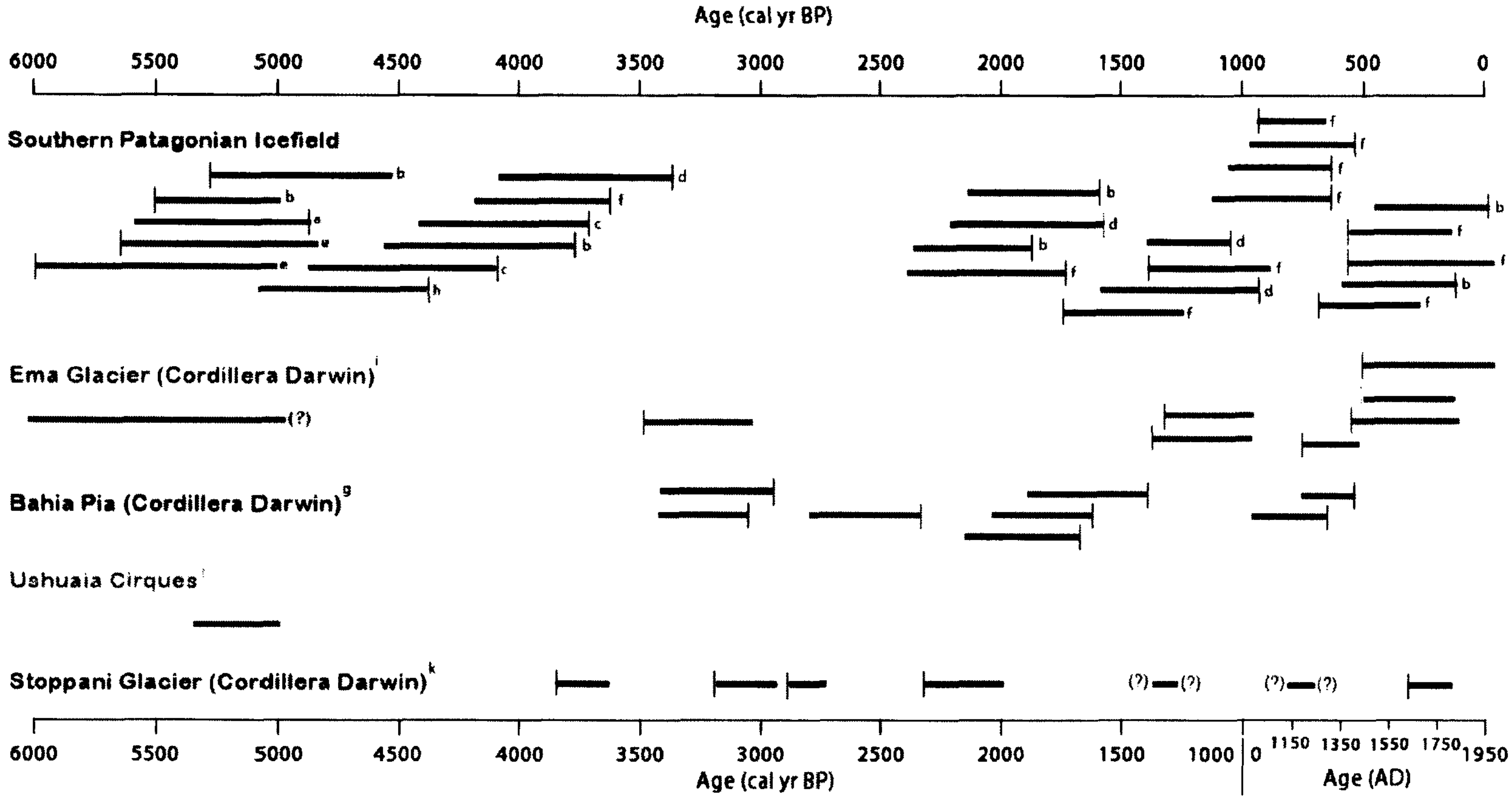

Figure 2.9: Calibrated radiocarbon ages of advances of outlet glaciers of the Southern Patagonian Icefield, Ema Glacier, glaciers near Bahia Pia, cirque glaciers near Ushuaia and Stoppani Glacier. Bars bracket minimum and maximum limiting ages from in situ woody material, and question marks indicate age ranges of detrital wood. Light blue columns outline advances of Stoppani Glacier. Radiocarbon ages: a - Mercer (1965), b - Mercer (1968), c - Mercer (1970), d - Mercer (1976), e - Röethlisberger (1987), f - Aniya (1995), g - Kuylenstierna et al. (1996), h - Wenzens (1999), i - Strelin et al. (2008), j - Menounos et al. (2013) and k - this study.

2.6 Conclusion

I used lateral moraine stratigraphy and radiocarbon ages on wood samples to determine the history of Stoppani Glacier over the past 3800 years. Stoppani Glacier advanced at least five times over this period. Although Neoglaciation in southern Patagonia began before 5000 years ago, evidence for glacier activity at Stoppani Glacier before 3800 cal yr BP is lacking. The lack of evidence suggests that: 1) the glacier behaved differently than other glaciers in southern Patagonia, 2) pre-3800 cal yr BP glacier deposits have been destroyed, or, most likely, 3) evidence for older advances has not yet been exposed in the glacier forefield. Assuming that the third explanation is correct, pre-3800 cal yr BP advances of Stoppani Glacier were minor, with no more than 15 m of thickening of the glacier at the study site.

The first recorded advance at Stoppani Glacier commenced soon after 3830–3640 cal yr BP. The second advance was underway by 3160–2950 cal yr BP, and the third occurred shortly after 2860–2760 cal yr BP. The fourth advance began by 2300–2010 cal yr BP and was followed by a final advance that culminated shortly after 290–150 cal yr BP. Detrital wood returned ages for two additional possible advances at 1340–1290 and 790–720 cal yr BP, but the origin of the wood fragments remains ambiguous. Two of the five advances (3830–3640 and 2300–2010 cal yr BP) have not been previously recognized in the Cordillera Darwin, but likely were times when outlet glaciers elsewhere in the Cordillera Darwin advanced. The outermost vegetated ridge outside the prominent northeast lateral moraine is likely also a moraine, but its age is unknown.

3. A 2700-year record of environmental change at Lago Roca, southern Patagonia

3.1 Introduction

Terrestrial evidence provides the most direct record of glacier fluctuations, but the fragmentary nature of these records limits their use (Leonard and Reasoner, 1999; Loso et al., 2006; Osborn et al., 2007; Menounos and Clague, 2008). Proglacial lake sediments, in contrast, can provide a continuous, although indirect record of past glacier activity (Karlén, 1976; Souch, 1994; Leonard and Reasoner, 1999; Miller et al., 2005; Osborn et al., 2007; Bakke et al., 2010; Larsen et al., 2011). The sensitivity and resolution of lake sediment records are partly a function of the location and size of the lake relative to its catchment (Souch, 1994; Leonard and Reasoner, 1999; Snowball et al., 1999). Although lake sediment records cannot be used to infer the magnitude of a glacier advance, their timing and duration commonly can be constrained (Leemann and Niessen, 1994; Souch, 1994; Menounos, 2006; Bakke et al., 2010; Larsen et al., 2011).

A general assumption when using proglacial lake sediments as a proxy of glacier activity is that an increase in glacier area increases subglacial erosion because a greater fraction of substrate is beneath ice (Hallet et al., 1996; Leonard, 1997; Larsen et al., 2011). Erosion over a greater area increases sediment delivery flux to a proglacial lake and thus increases the rate of clastic sedimentation in the lake (Leemann and Niessen, 1994; Leonard and Reasoner, 1999). In contrast, low clastic sedimentation rates are thought to indicate times when glaciers in the contributing catchment are relatively small (Karlén, 1981; Souch, 1994).

In the case of temperate glaciers, erosion is also controlled by the rate of sliding of the glacier over its bed, which in turn is a function of basal water pressures (Boyd et al., 2008).

Erosion is greater when a glacier slides faster over its bed than when it slides more slowly (Hallet et al., 1996). Souch (1994) asserts that more sediment is available for transport during the period of initial retreat of a glacier due to exposure of unvegetated glacial deposits. Because high sedimentation can arise during times of both glacier advance and retreat, the use of proglacial lake sediment records to constrain period of glacier expansion is difficult (Leonard and Reasoner, 1999).

Sediments can also be deposited in proglacial lakes during landslides, floods and other extreme events (Hodder et al., 2007). Any non-glacial sediment sources should thus be identified and accounted for before lake sediments are used to infer glacier activity (Souch, 1994). Given the limitations of both terrestrial and lacustrine proxies, a combination of both proxies provides the most robust record of past glacier activity (Osborn et al., 2007).

Although I was able to construct a well constrained history of glacier activity from the data gathered at Stoppani Glacier, it is possible that evidence of additional glacier activity was not captured within the lateral moraine stratigraphy. It is also likely that any minor advance between the five documented advance of Stoppani Glacier were not recorded, producing a fragmented chronology. In this chapter, I describe lake cores obtained from proglacial Lago Roca (Figure 2.2) and interpret them in the context of late Holocene glacier activity in the catchment. I also assess the role that changes in local sea level may have had on sedimentation in the lake.

3.2 Study site

Lago Roca straddles the Chile-Argentina border in southernmost Tierra del Fuego (Figure 2.1). The lake is 4 m above sea level (asl), has an area of approximately 22 km^2, and lies

20 km east of Stoppani Glacier (Figures 2.1 and 2.2). Lago Roca is separated from Bahia Lapataia and Beagle Channel by 2 km of low-lying hummocky land. The Lago Roca watershed has an area of about 470 km^2, of which approximately 16% is glacier-covered. Meltwater from small glaciers of the Condon Central and glaciers on the northeast side of Pico Italia flows into Lago Roca (Figure 2.2). The peaks of the Fuegian Andes surrounding Lago Roca reach 1200 – 1400 m asl. The climate at Lago Roca is cool and humid (Section 2.2). The Fuegian Andes consist of granitic gneiss and amphibolite. The Cordillera Darwin Range consists of a basement complex of Late Paleozoic greenschist, amphibolite, phyllite, schist, metaquartzite and metachert. Post-tectonic intrusions of tonalite and quartz monzonite form the high peaks of the Cordillera Darwin (Nelson et al., 1978).

Local sea level in the Beagle Channel rose during the mid-Holocene (6000 cal yr BP), connecting Lago Roca and Bahia Lapataia forming a fjord (Gordillo et al., 1993). Between 5440–4630 and 4420–3980 cal yr BP, sea level was 6 m higher than present, but it later fell, isolating Lago Roca from Beagle Channel (Gordillo et al., 1993). Once isolated, Lago Roca was no longer influenced by the sea and sedimentation was strictly lacustrine.

3.3 Methods

3.3.1 Core collection and analysis of bulk physical properties

In early 2009, Brian Menounos and Jorge Rabassa recovered four sediment cores from Lago Roca using a percussion coring system (Figures 3.1 and 3.2; Reasoner, 1993). They collected the cores along the central axis of the lake in water depths of 35 to 75 m to maximize the temporal resolution of the sediment records and reduce input of shallow-water sediments (Figure 3.2). Cores 09-LRoca(02) and the 09-LRoca(04) were overdriven to recover the oldest sediments possible. In contrast, an attempt was made to recover surface sediments in cores 09-LRoca(01) and 09-LRoca(03). The four cores were capped and labeled in the field and shipped to UNBC. Once at the University of Northern British Columbia, I stored the cores at 4°C prior to and after analysis.

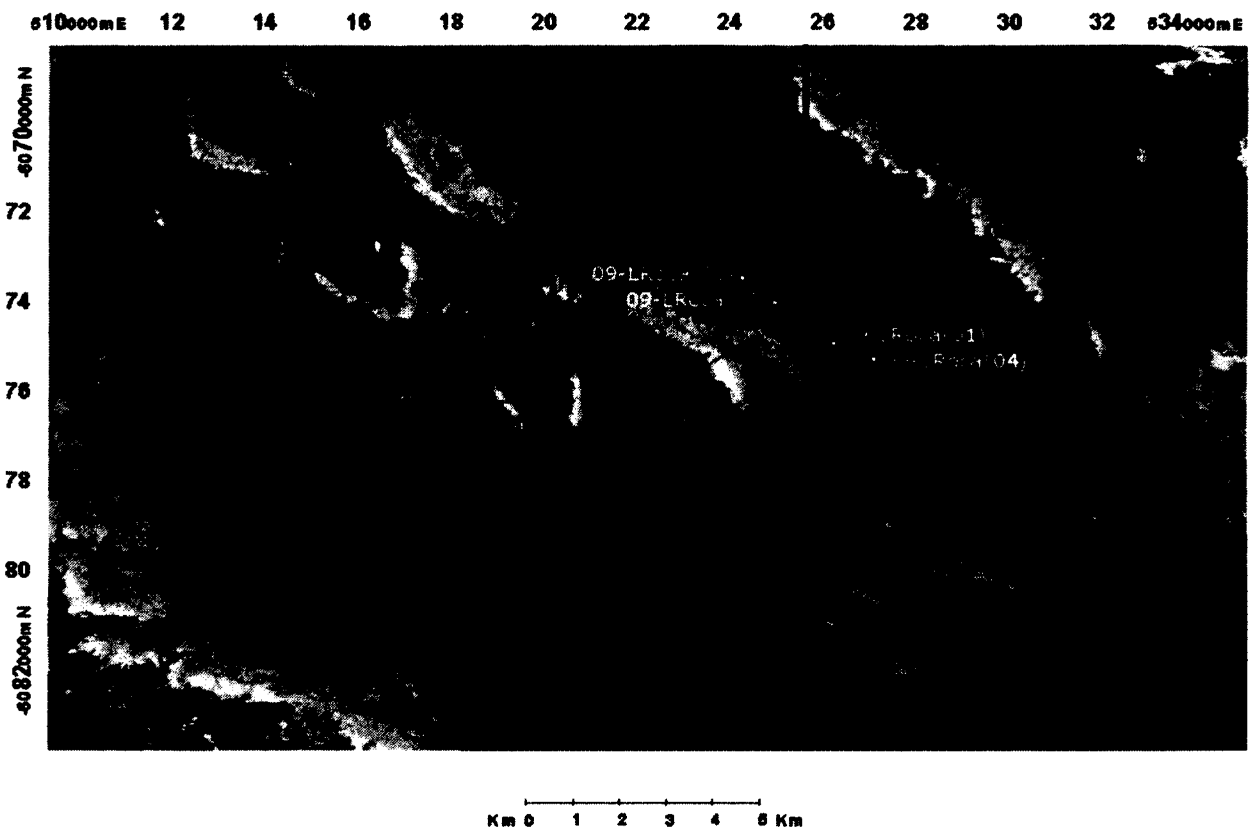

Figure 3.1: Landsat 7 image showing core locations in Lago Roca (543 band colour composite from February 2001).

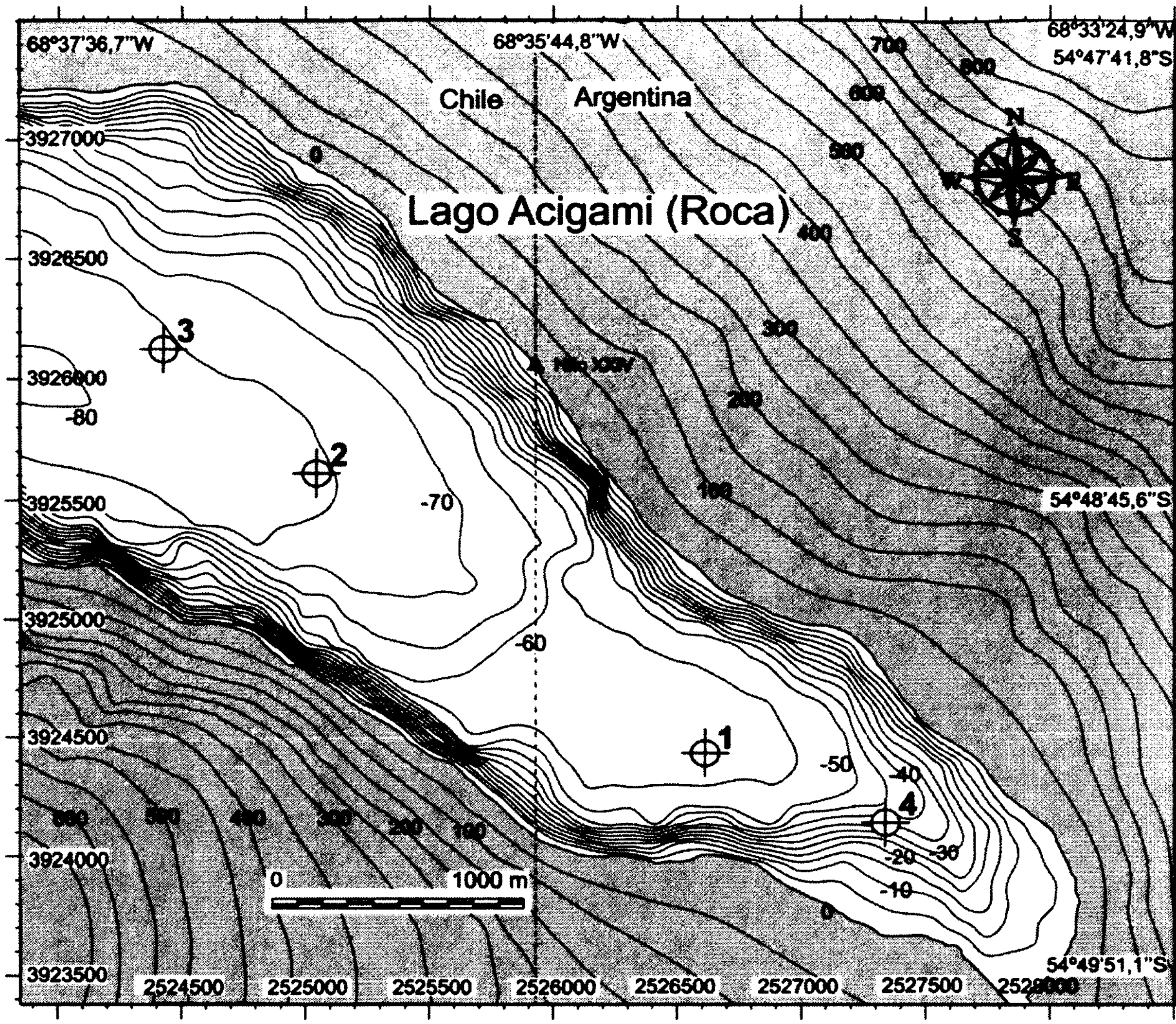

Figure 3.2: Bathymetry of the eastern half of Lago Roca (5 m isobaths) and sediment core locations. Topography after Hoja Ushuaia 5569-17-1, Gobierno de Tierra del Fuego 2003 by Gustavo Bujalesky (50 m contour interval).

I split, logged and photographed the four cores. I sampled each core at a 1 cm interval for magnetic susceptibility, water content, wet and dry density and organic matter (bulk physical properties). I used a Bartington MS2 magnetic susceptibility meter to measure the magnetic susceptibility of the sediments. Magnetic susceptibility provides a measure of the ferromagnetic mineral content of the sediments (Leemann and Niessen, 1994). Ferromagnetic minerals in lake sediments are mainly derived from erosion of bedrock and soils (Snowball et al., 1999). In watersheds with glaciers and rocks or soils containing ferromagnetic minerals, an increase of freshly eroded ferromagnetic material within lake sediments can indicate increased ice cover (Matthews et al., 2000).

To determine the clastic content of the sediments, I calculated the percent water content, organic matter and wet and dry density from the weight loss-on-ignition (LOI) using standard analysis procedures outlined by Heiri et al. (2001) (Appendix B). The weight loss after combustion is directly related to the amount of organic matter in the sample (Heiri et al., 2001; Santisteban et al., 2004).

3.3.2 Elemental composition, particle size analysis and diatom analysis

The elemental composition of lake sediments may indicate the source of the sediments and the composition of the water at the time of deposition (Gibson et al., 2002). I sampled 09-LRoca(02) at 20 evenly-spaced intervals and submitted the samples to the Central Equipment Lab at UNBC for determination of total elemental composition by inductively coupled plasma mass spectrometry (ICP-MS) after digestion in nitric and hydrochloric acid. I performed a principal component analysis using singular value decomposition on the covariance matrix of the total elemental composition of the elemental data to identify changes in sediment sources over time (Rubio et al., 2000; Brahney et al., 2007). Principal component analysis can identify common groups of elements that are associated with specific sediment sources and sedimentary processes, as well as changes that could be the result of environmental changes (Rubio et al., 2000).

The grain size of glacial lake sediments depends on the genesis and transportation and deposition processes. Sediment particles deposited in the deeper portions of proglacial lakes are typically silt and silty clay (Leonard and Reasoner, 1999; Matthews et al., 2000). I performed particle size analyses using a Malvern Mastersizer 2000 at Simon Fraser University in accordance with the method outlined by Sperazza et al. (2004) on the same 20 samples submitted for total elemental composition analysis (Appendix B).

I submitted two sediment samples from the 09-LRoca(02) to Dr. Janice Brahney (UBC Okanagan) for diatom analysis. The species of diatoms and their concentrations in lake sediments provide information on the aquatic environment (Westman and Hedenström, 2002).

3.3.3 Thin sections and varve chronology

Overlapping 7-cm-long sections of each sediment core were sectioned to provide additional details on Lago Roca stratigraphy and to develop a varve chronology (Kemp et al., 2001). I flash-froze the slabs with liquid nitrogen before freeze-drying them to remove all moisture from the sediments (Lamoureux, 1994). I embedded the sediment slabs in a low viscosity resin and oven-dried the resin until it had completely hardened (Kemp et al., 2001). I then used a rock saw to separate the slabs from each other and sandpaper to remove excess resin from the bottom side of the slabs. Once the resin slabs were ground flat, I mounted them on a frosted glass microscope slide with quick-set epoxy. I then used a Petrothin machine to grind each mounted slab down to 40-50 μm or until laminae were clearly visible through transmitted light. I then scanned each slide at 600 dpi to provide a digital record of each slab.

Due to bioturbation of the sediments and cracking induced by the thin section process, I was unable to identify marker horizons in the four cores solely from the thin sections. I thus re-examined the wet sediments from the archived halves of each of the four cores for marker horizons and allowed the sediments to slowly dry while continuously photographing them

(Gilbert, 1975; Menounos, 2006; Schiefer et al., 2010). Using the photographs of partially dried sediments, I counted and measured individual laminae in each of the four cores. I only counted and measured laminae if they were well preserved and undistorted.

To constrain the ages determined by counting laminae, I collected 11 macrofossils from the cores for radiocarbon dating. Of the 11 macrofossils, I submitted eight to the Keck Carbon Cycle AMS Facility at the Department of Earth System Science at the University of California - Irvine for AMS radiocarbon dating. I used the Southern Hemisphere Calibration Curve from the online CALIB 6.0 Radiocarbon Calibration program (Stuiver et al., 2010) to convert the radiocarbon ages to calibrated age ranges (2 σ) before present (1950) (cal yr BP). All calibrated age ranges from radiocarbon ages have been rounded to the nearest 10 years.

3.4 Results

3.4.1 Lithostratigraphy and bulk physical properties

The four sediment cores range in length from 159 cm (09-LRoca(03)) to 289 cm (09-LRoca(04)). The sediments consist of rhythmically laminated, inorganic silt and clay (Figures 3.3–3.6). I subdivided the sediments in the cores into two lithostratigraphic units based on sediment colour and lamina thickness. Unit 1 consists of dark grey, rhythmically laminated, inorganic silt and clay. Unit 2 comprises light grey, rhythmically laminated, inorganic silt and clay. Unit 2 is denser and contains less organic matter than unit 1 (Figure 3.4). Laminae are also generally thinner in unit 2 than unit 1. The contact between unit 1 and 2 is gradational. Cores 09-LRoca(01) and 09-LRoca(02) contain both unit 1 and unit 2; 09-LRoca(03) contains only unit 2; and the 09-LRoca(04) contains only unit 1 (Figures 3.3–3.6). All four cores display 'coning', which is indicative of coring-induced disturbance and is responsible for the curved contact between units 1 and 2 (Figure 3.7).

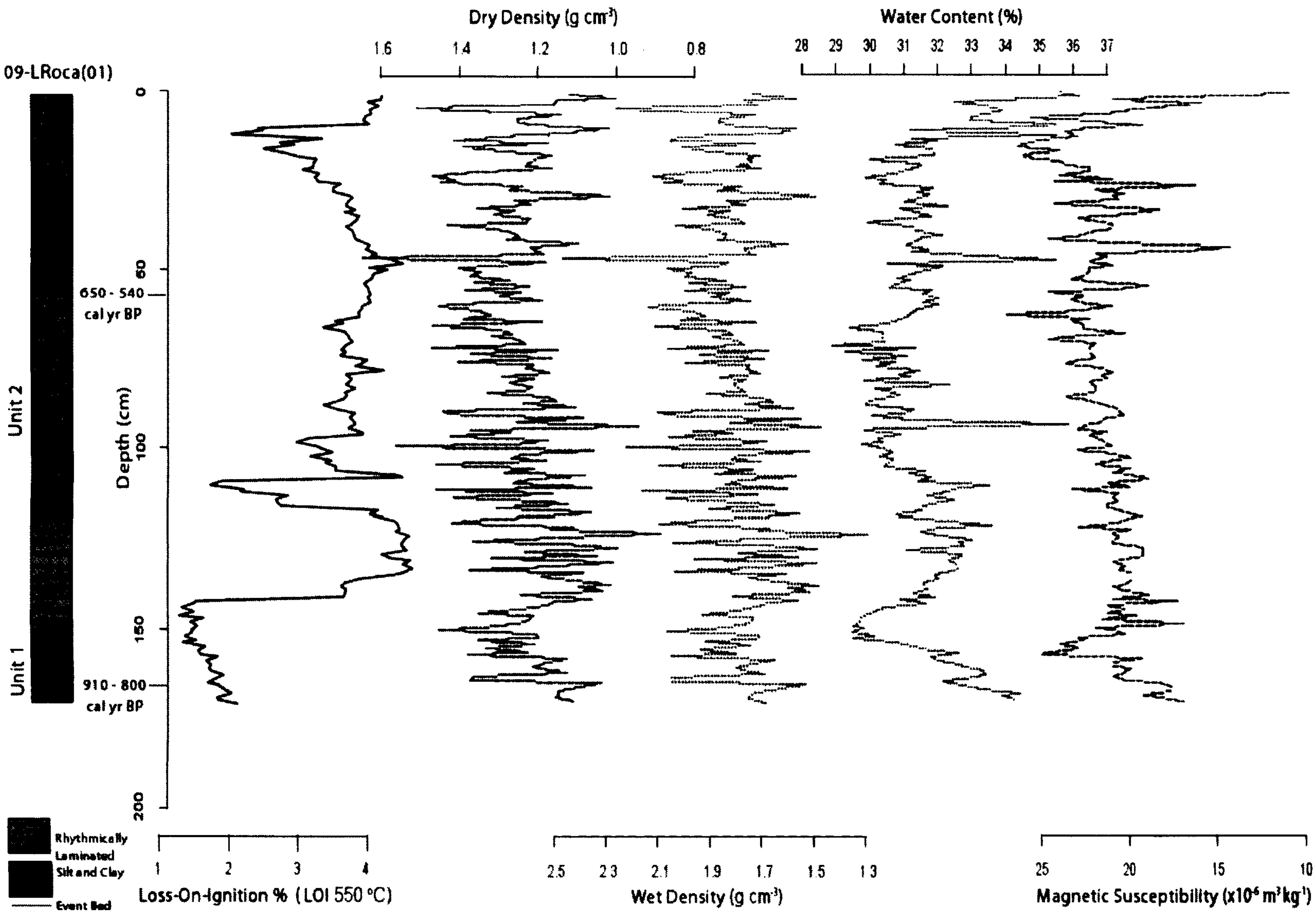

Figure 3.3: Lithostratigraphy, calibrated radiocarbon ages and bulk physical properties of core 09-LRoca(01). Calibrated radiocarbon ages are reported in Table 3.2).

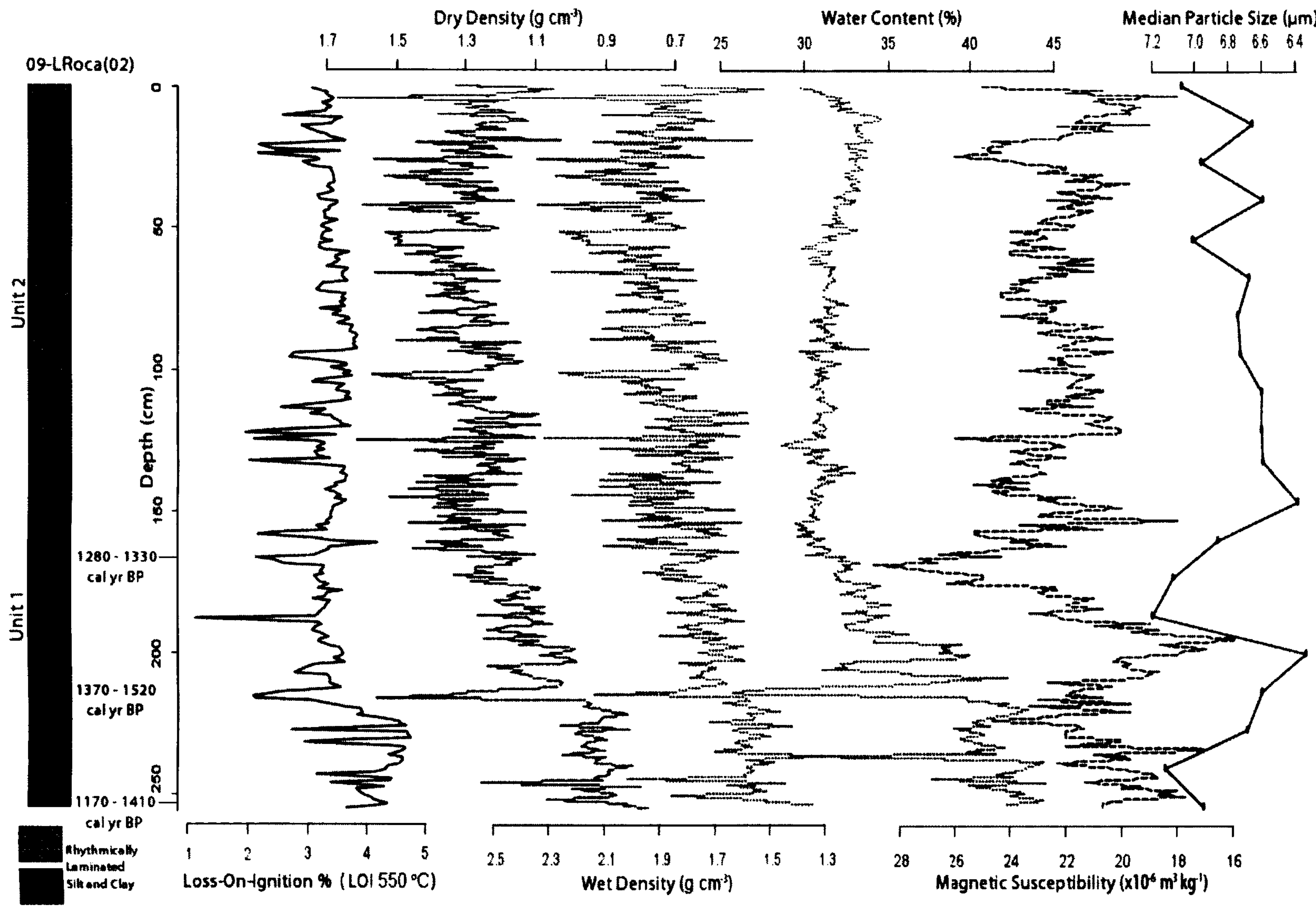

Figure 3.4: Lithostratigraphy, calibrated radiocarbon ages and bulk physical properties of core 09-LRoca(02). Calibrated radiocarbon age ranges are reported in Table 3.2.

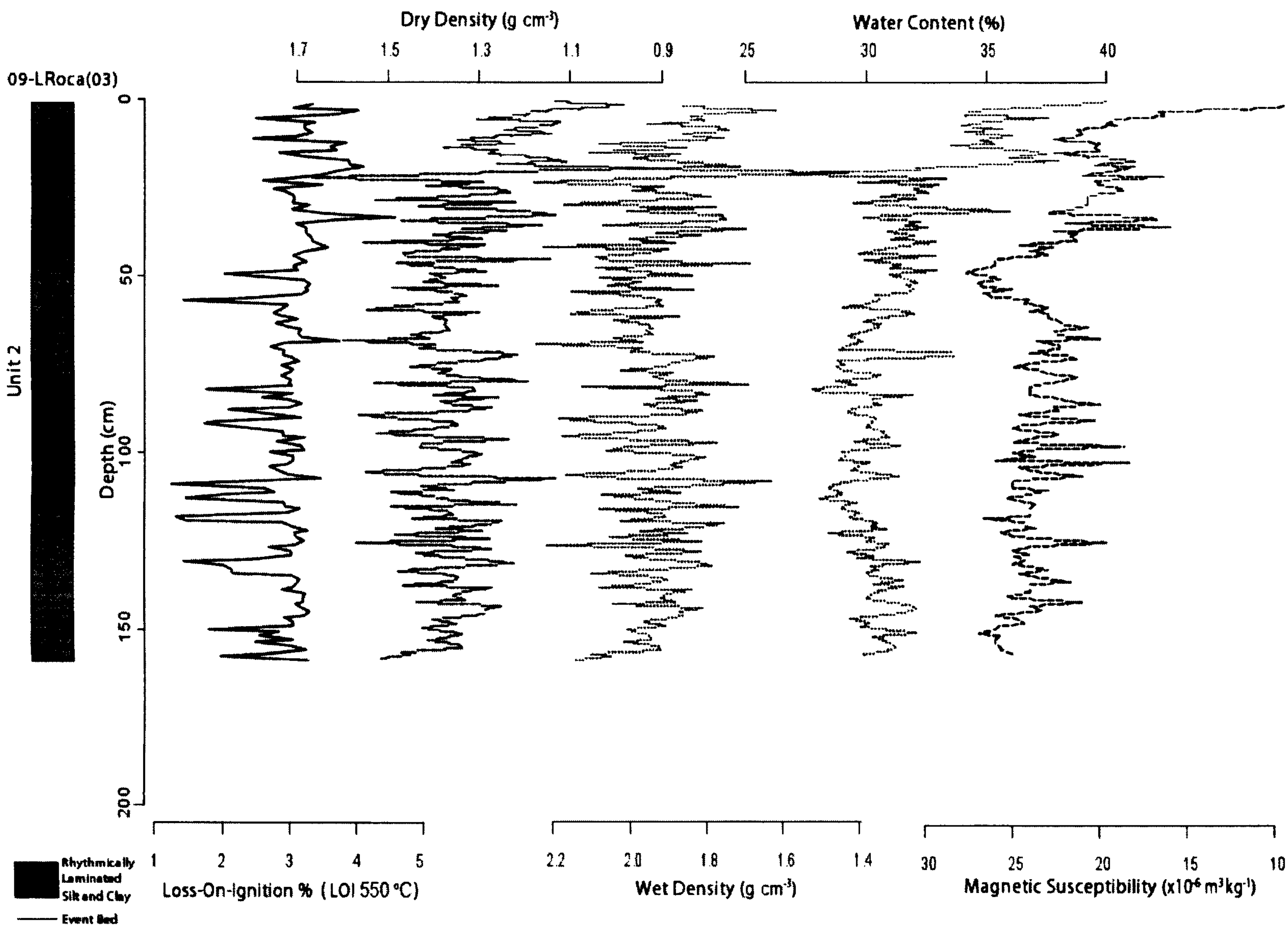

Figure 3.5: Lithostratigraphy and bulk physical properties of core 09-LRoca(03).

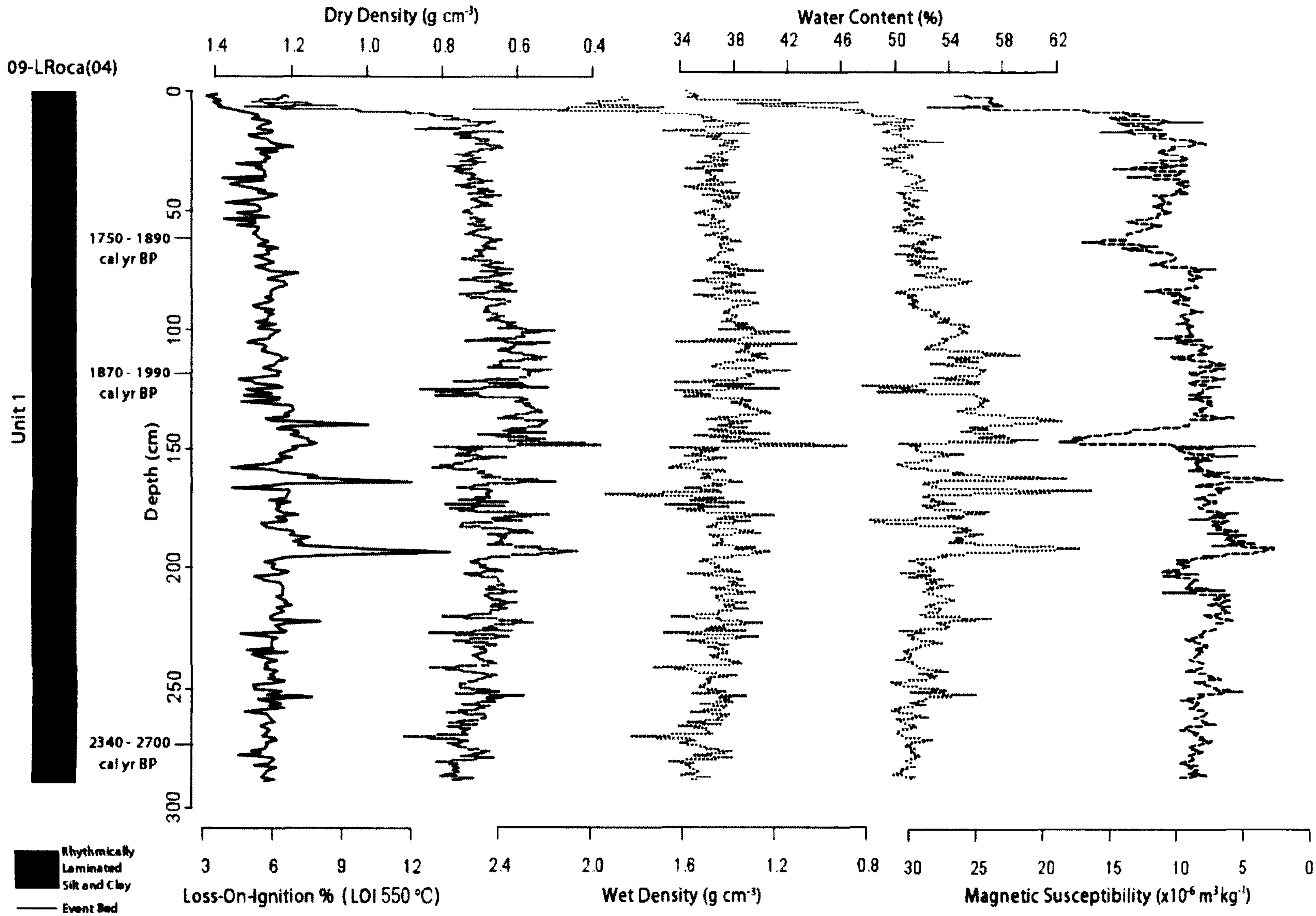

Figure 3.6: Lithostratigraphy, calibrated radiocarbon ages and bulk physical properties of core 09-LRoca(04). Calibrated radiocarbon age ranges are reported in Table 3.

Figure 3.7: Lithostratigraphic boundary at 156 cm in 09-LRoca(02) (core top to the left).

Laminae in all four cores consist of normally graded, silt-clay couplets (Figure 3.8). Each couplet consists of coarse silt, in some cases very fine sand, grading upward into clay (Figure 3.8). Most of the contacts between clay caps and silt of the overlying couplet are sharp (Figure 3.8 a and b). Some couplets in 09-LRoca(03) have a clay cap that grades into the overlying silt lamina (Figure 3.8 b). Many of the thick couplets in 09-LRoca(03) contain multiple sub-annual laminae (Figure. 3.8 b) that are not evident in the thinner couplets of the other three cores.

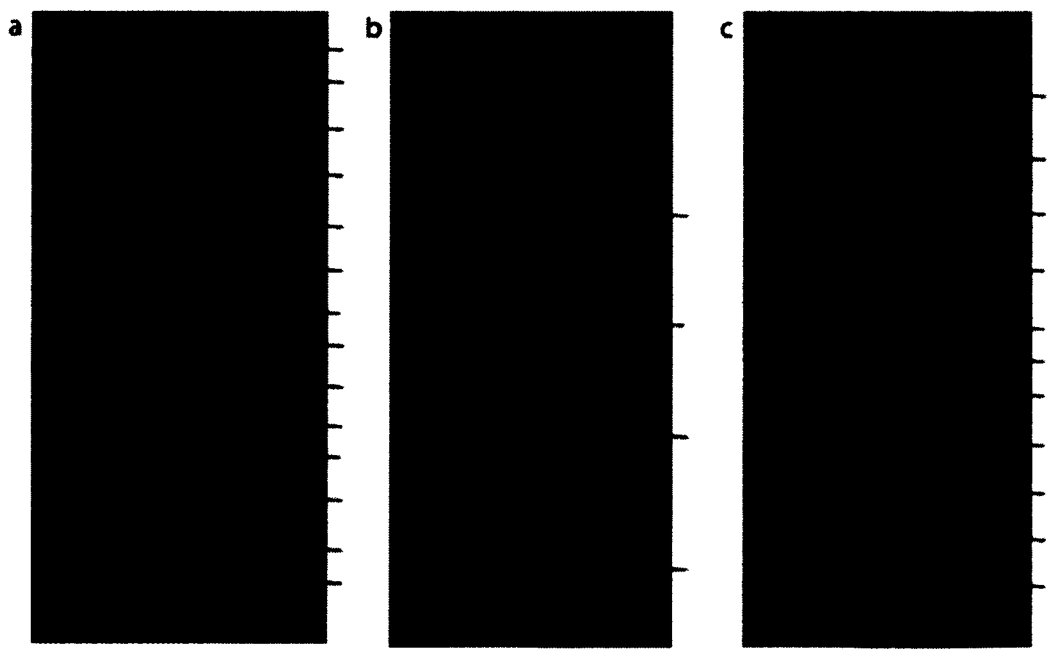

Figure 3.8: Examples of Lago Roca laminae. a) 09-LRoca(01) core [34-30 cm depth]; b) 09-LRoca(03) core [83.5-80 cm depth]; c) 09-LRoca(04) [22-18 cm] core (core tops upward). Blue lines denote couplet boundaries and red lines equal 1 cm.

Thick, massive silt-sand beds occur in the sediment cores. The beds range from 2.5 to 6 cm in thickness and are generally coarser than adjacent sediments. Thick massive silt-sand beds occurs at 214–211 and 203–197 cm in unit 1 in 09-LRoca(02), for example (Figure 3.9), and a laminated silt-sand bed occurs at 12.5–10 cm in unit 2 in 09-LRoca(01) (Figure 3.10).

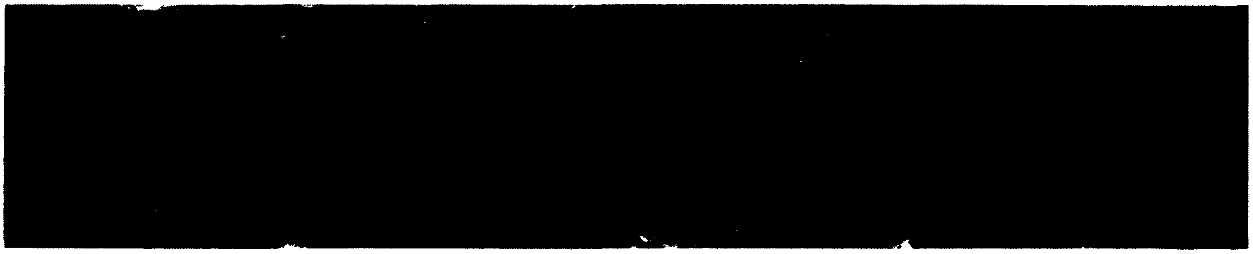

Figure 3.9: Thick beds (black lines) at 203–197 cm and 214–211 cm in 09-LRoca(02). Core top to the left and red line at top left equals 1 cm.

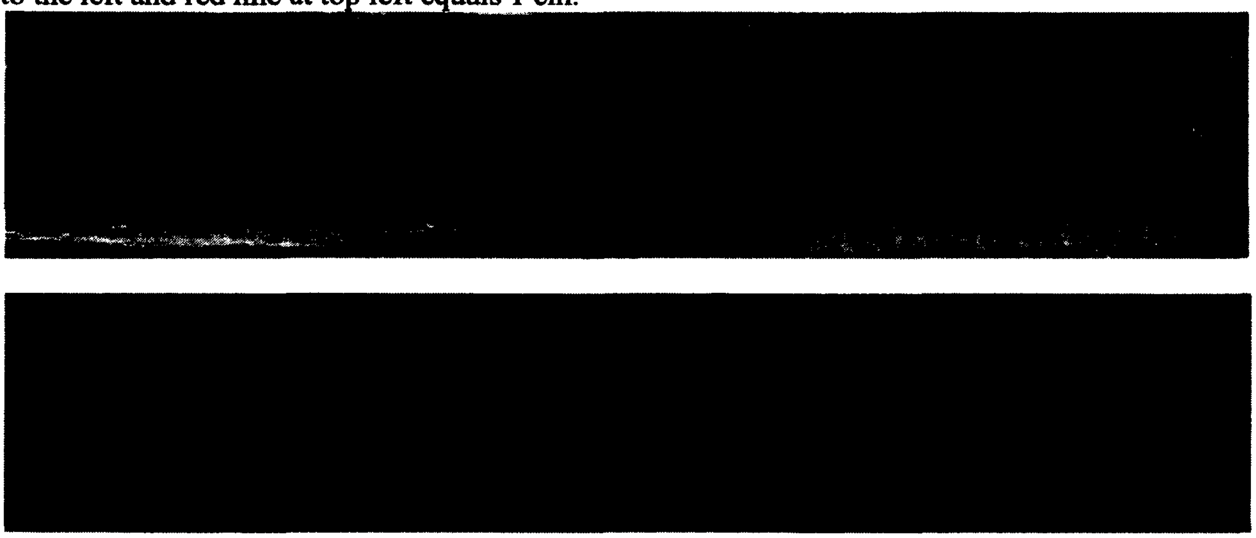

Figure 3.10: Thick bed (black lines) at 12.5–10 cm in wet sediments (top) and partially dried sediments (bottom) of 09-LRoca(01). Core top to the left and red line at top left equals 1 cm. The dark band in the lower photo is a desiccation crack.

The bulk physical properties of the Lago Roca sediment cores vary with depth (Figures 3.3–3.6). Loss-on-ignition (LOI), dry and wet densities, water content and magnetic susceptibility in 09-LRoca(04) show no significant trends between 289 and 10 cm depth (Figure 3.6), but LOI and water content decrease above 10 cm.

Dry density, wet density and magnetic susceptibility increase in 09-LRoca(02) to the boundary between units 1 and 2 at 156 cm depth (Figures 3.4). Wet density and water content respectively reach maxima and minima at the unit boundary. Magnetic susceptibility peaks just below the unit boundary in 09-LRoca(02) (Figure 3.4). Median grain size generally decreases gradually upcore in 09-LRoca(02) with a local maximum at 187 cm. Above this depth, median grain size is more variable (Figure 3.4). Water content increases above the boundary between units 1 and 2 in both the 09-LRoca(01) and 09-LRoca(02) cores, whereas wet and dry density do not significantly change (Figures 3.3 and 3.4). Magnetic susceptibility initially decreases in unit 2, but does not reach the minimum value recorded in unit 1. Above the unit boundary, LOI is relatively constant in both the 09-LRoca(01) and 09-LRoca(02) cores (Figures 3.3 and 3.4). Similarly, the LOI, dry and wet densities, water content and magnetic susceptibility change little in unit 2 of the 09-LRoca(03) core (Figure 3.5).

3.4.2 Couplet thickness, radiocarbon ages and sedimentation rates

I identified eight beds in 09-LRoca(01) that, based on their colour, thickness, and unusual lithology, are potential markers that might be traceable among the cores (Figures 3.11 and 3.12). Because 09-LRoca(01) and 09-LRoca(03) are least likely to have been overdriven in the coring process, their tops may preserve sediments close to the water-sediment interface. The couplets at the top of 09-LRoca(01) are well preserved; I thus assigned a count value of one to the topmost couplet in that core (Figure 3.12). 09-LRoca(01) also contains the least disturbed couplets of the four cores; the couplets in 09-LRoca(03) have the greatest disturbance (Table 3.1).

Couplet thickness in 09-LRoca(01) differs little through the core, except near 85 cm, between 50 and 30 cm depth, and above 10 cm, where the couplets are thicker than average

(Figure 3.11) Couplet thickness in 09-LRoca(02) core averages 3 mm and shows no trend with depth, with the exception of the uppermost 25 cm where couplet thickness increases upward, but then sharply decreases near the top of the core. Average couplet thickness in 09-LRoca(03) is greater near 120 and 75 cm depth than elsewhere. Much of the uppermost 40 cm of sediment in 09-LRoca(03) is too disturbed to measure or count couplets. Couplets in the bottom half of 09-LRoca(02) are too disturbed to measure or count couplets. In 09-LRoca(04) couplet thickness decreases upcore, except for increases in thickness at 30 cm and above 15 cm. Coring-induced disturbance precludes measurements of couplets between 289 and 200 cm and 150 and 100 cm in this core.

Table 3.1: Mean, median, minimum and maximum couplet thickness.

	09-LRoca(01)	**09-LRoca(02)**	**09-LRoca(03)**	**09-LRoca(04)**
Number of couplets measured	545*	422	245*	454
Depth range (cm)	0 – 150	0 – 117	4 – 158	0 – 198
Mean thickness (mm)	1.8	2.7	5.2	2.9
Standard deviation (mm)	0.5	1.1	2.0	1.3
Median thickness (mm)	1.7	2.5	5.0	2.6
Minimum thickness (mm)	0.8	0.7	1.6	0.9
Maximum thickness (mm)	4.5	7.9	13.5	13.7

* Thicknesses of large event beds are excluded .

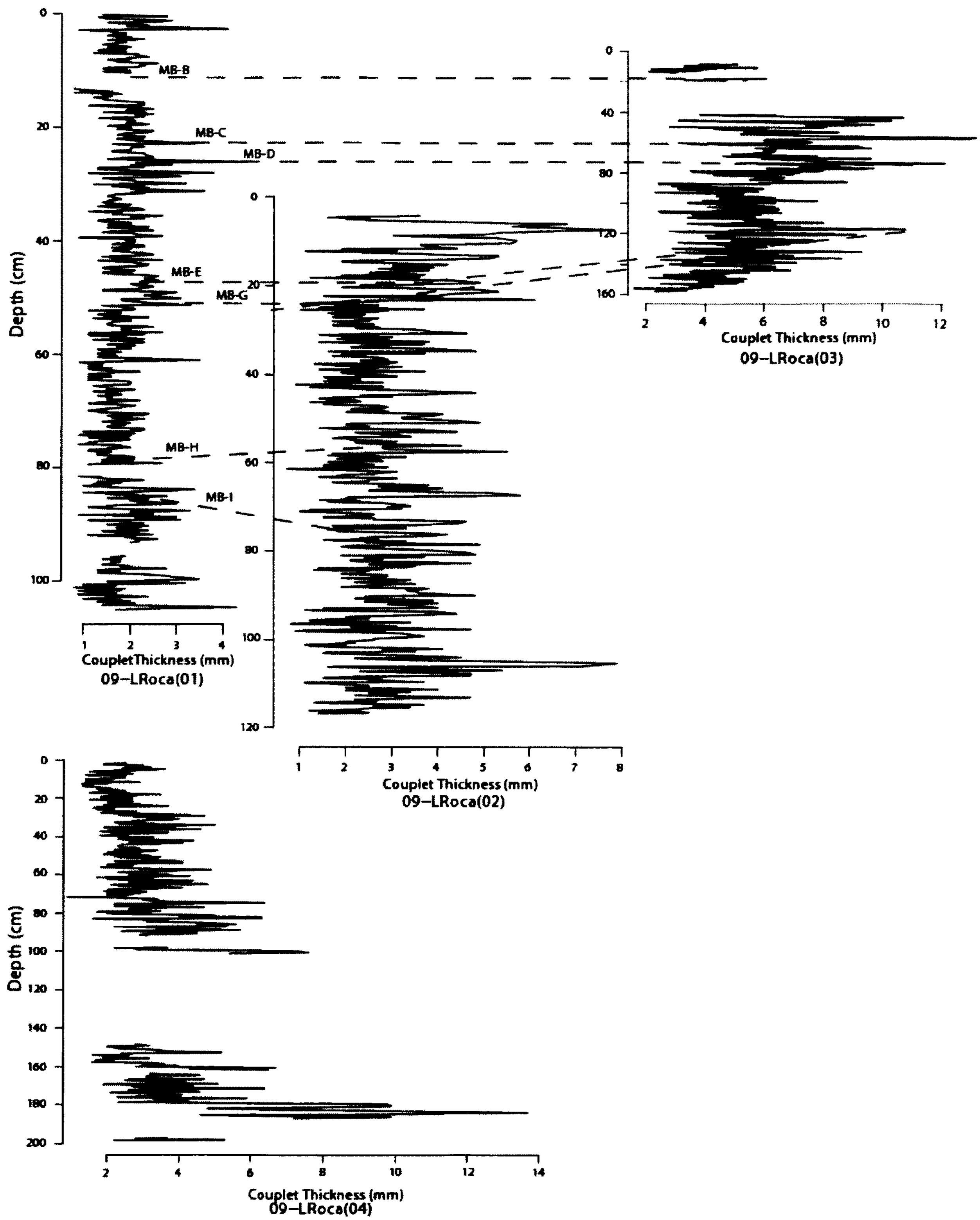

Figure 3.11: Couplet thickness as a function of depth in the four Lago Roca cores. Marker beds (MB) are shown as dashed red lines. No marker beds were identified in 09-LRoca(04).

The eight macrofossil samples include twigs, twigs with leaves and leafy plant material (Table 3.2). All radiocarbon ages decrease upcore, with the exception of one at 257 cm in 09-LRoca(02) (1410–1170 cal yr BP). The calibrated age range of this sample spans those of the two other radiocarbon samples farther upcore, at 225 and 170 cm (Figures 3.3–3.6, Table 3.2). The oldest radiocarbon age in 09-LRoca(04) was obtained on a twig 33 cm above the base of the core (Figure 3.6, Table 3.2). The leafy twig at 170 cm in 09-LRoca(02) is 14 cm below the boundary between units 1 and 2 in 09-LRoca(02) (Figure 3.4, Table 3.2).

Table 3.2: Radiocarbon ages and corresponding calibrated age ranges from Lago Roca.

Laboratory no [a]	Field no.	Location	Material	^{14}C age (yr BP)	Calendar years before present (1950) (cal yr BP) [b]
UCIAMS-101779	09-LRoca(01); 57cm	54°49'20.50" S 68°35'9.80" W	Twig	620 ± 45	650 –540
UCIAMS-90373	09-LRoca(01); 170cm	54°49'20.50" S 68°35'9.80" W	Twig	980 ± 20	920 – 800
UCIAMS-90374	09-LRoca(02)2/2; 45cm (170cm) [c]	54°48'42.80" S 68°36'38.21" W	Leafy twig	1435 ±15	1330 –1280
UCIAMS-90375	09-LRoca(02)2/2; 100cm (225cm) [c]	54°48'42.80" S68°36'38.21" W	Twig	1585 ± 20	1520 –1370
UCIAMS-90376	09-LRoca(02)2/2; 132cm (257cm) [c]	54°48'42.80" S68°36'38.21" W	Leafy twig	1400 ± 90	1410 – 1170
UCIAMS-101780	09-LRoca(04); 64cm	54°49'29.70" S 68°34'29.90" W	Leafy twig	1940 ± 20	1890 –1750
UCIAMS-83751	09-LRoca(04)1/2; 125cm	54°49'29.70" S 68°34'29.90" W	Leafy twig	2025 ± 20	1990 – 1870
UCIAMS-83752	09-Lroca(04)2/2; 131cm (256cm) [c]	54°49'29.70" S 68°34'29.90" W	Twig	2445 ± 40	2700 – 2340

[a] Radiocarbon laboratory: UCIAMS-University of California at Irvine.
[b] Calendar ages determined using CALIB 6.0 (Stuiver et al., 2010).
[c] Depth below the lake floor in parentheses when sample was taken from the second half of a long core.

The structure of the sedimentary couplets in the Lago Roca sediment cores is comparable to that of clastic varves. Each couplet consists of a silt lamina capped by a clay lamina (Figure 3.8). The contact between the top of the clay laminae and overlying silt is sharp in most Lago Roca sediment cores, which is characteristic of clastic varves deposited in proglacial lakes (Menounos and Clague, 2008). Because each couplet is interpreted to be a clastic varve, and a varve represents one year of sedimentation in Lago Roca, the average sedimentation rate for each core should equal the mean couplet thickness (excluding the event beds in 09-LRoca(01) and 09-LRoca(03); Table 3.1). Because substantial portions of the cores are disturbed, I was unable to measure each varve and it is thus possible that the mean varve thickness does not represent the true average sedimentation rate for the core. For the purpose of this study, however, I assume that the average measurable varve thickness in each core is the sedimentation rate for the entire core (Table 3.1). Assuming that this assumption is valid, I calculated the expected age of the sediment at each radiocarbon-dated level. I also determined the average sedimentation rate between each marker bed and the closest radiocarbon age, which would be required for the calibrated radiocarbon ages to represent maximum limiting ages for those sediments.

Because neither 09-LRoca(01) nor 09-LRoca(03) were overdriven during collection, it is probable that they include sediment deposited in 2009 (Figure 3.12). I counted varves in 09-LRoca(01) back to the AD 1950 (corresponding to 0 cal yr BP) at 13.2 cm depth. Using the observed average sedimentation rate of 1.8 mm/yr in 09-LRoca(01) and the depth below 13.2 cm, I calculated the expected ages of the sediment at the depths of marker bed MB-E, radiocarbon-dated level 650–40 and radiocarbon-dated level 910–800 cal yr BP to be, respectively, 190, 243 and 871 cal yr BP (Figure 3.12). The age of the radiocarbon-dated sample at 57 cm depth (650–540 cal yr BP) is 407–297 years younger than expected. The average sedimentation rate based on this sample is 0.8–0.6 mm/yr, which is one-half to one-third the average varve thickness estimate of 1.8 mm/yr for the entire core (Table 3.3). On the other hand, the average rate of 1.8 mm/yr is consistent with the depth of the sample that yielded the calibrated radiocarbon age range of 910 –800 cal yr BP (170 cm) (Figure 3.12, Table 3.3).

There are no radiocarbon ages from 09-LRoca(03), but the average sedimentation rate between marker beds MB-B and MB-E is similar to the average sedimentation rate determined from measured varves (Table 3.3).

Using the average sedimentation rate in 09-LRoca(02) and the position of marker bed MB-E (190 cal yr BP), I calculated the expected age of the unit 1-unit 2 boundary in that core (156 cm) be 700 cal yr BP (Figure 3.12). Similarly, using average sedimentation rates, I estimated the ages of the dated samples in unit 1 with calibrated age ranges of 1330–1280, 1520–1370 and 1410–1170 cal yr BP to be, respectively, 749, 952 and 1071 cal yr BP (Figure 3.12). None of the ages from unit 1 calculated on the basis of average sedimentation rates falls within the calibrated age range of the sample at that depth. Sedimentation rates required for the radiocarbon ages to be maximum limiting ages are much lower than the average sedimentation assumed for 09-LRoca(02) (Table 3.3).

09-LRoca(04) does not overlap any of the other cores (Figures 3.11 and 3.12). Using the average sedimentation rate and the depth distance from the 1890–1750 cal yr BP radiocarbon sample, I calculated the age of the sediment at the top of 09-LRoca(04) to be 1653–1513 cal yr BP (Figure 3.12). The calculated average sedimentation rates between the three radiocarbon samples in 09-LRoca(04) are similar to the sedimentation rate based on measured varves in that core (Table 3.3).

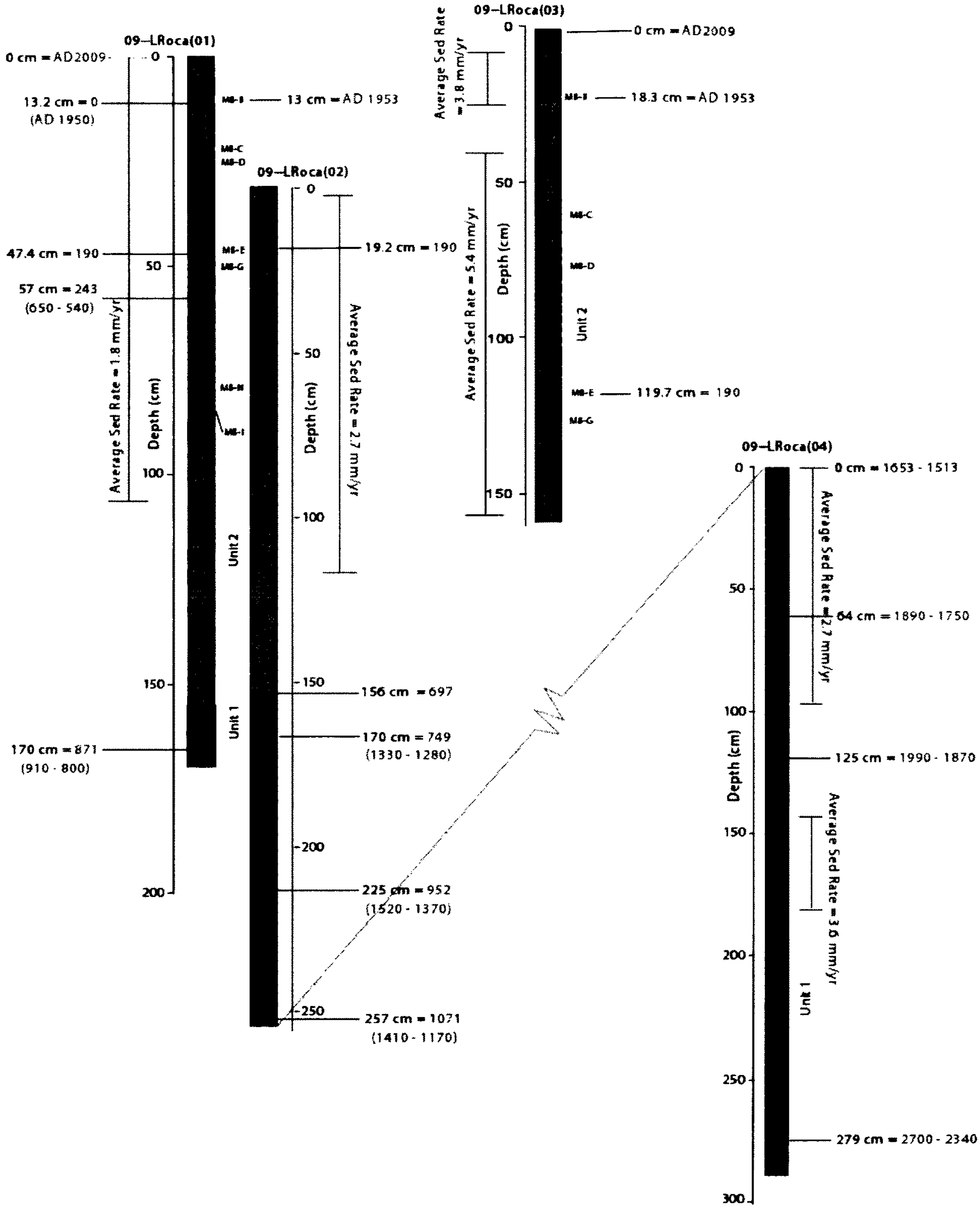

Figure 3.12: Correlation of cores 09-LRoca(01), (02), (03) and (04). Red lines denote marker beds MB-B through MB-I. Purple lines delineate depth ranges with measured varves and

counted couplets; the average sedimentation rate is shown in purple for each of these zones. Calibrated radiocarbon age ranges (cal yr BP) are shown in red. The blue ages and age ranges represent the expected age of the sediment at that specific depth based on the measured average sedimentation rate for the core.

Table 3.3: Calculated average sedimentation rates between marker beds (MB) and calibrated radiocarbon ages (RC) compared to the measured average sedimentation rate for each Lago Roca core.

Core ID	Depth (cm)	Calibrated age (cal yr BP)	Sedimentation rate (mm/yr)	Average sedimentation rate (mm/yr)
09-LRoca(01)				**1.8**
MB-B	13	AD 1953		
MB-E	47.4	190	1.8	
RC:650-540	57	650-540	0.8 – 0.6	
RC:910-800	170	910-800	2.0 – 1.7	
09-LRoca(03)				**5.2**
MB-B	18.3	AD 1953		
MB-E	119.7	190	5.2	
09-LRoca(02)				**2.7**
MB-E	19.2	190		
RC:1330-1280	170	1330-1280	1.4 - 1.3	
RC:1520-1370	225	1520-1370	1.7 - 1.5	
RC:1410-1170	257	1410-1170	2.4 – 1.9	
09-LRoca(04)				**2.9**
RC:1890-1750	64	1890-1750		
RC:1990-1870	135	1990-1870	7.1 - 3.0	
RC:2700-2340	279	2700-2340	4.1 - 1.7	

3.4.3 Geochemistry

The concentration of 49 elements were identified in the 20 geochemistry samples from core 09-LRoca(02) (Appendix C). Concentrations of only five of the 49 elements changed markedly at the boundary between units 1 and 2 (Appendix C). Concentrations of sodium, boron, phosphorus, arsenic and molybdenum decrease above the lithostratigraphy unit boundary at 156 cm (Figure 3.13). Sodium decreases from over 3000 mg/kg below the unit boundary to about 1250 mg/kg above the boundary and remains at this low level throughout unit 2. Boron concentrations likewise decrease from more than 20 mg/kg below the unit boundary to around 15 mg/kg above the boundary. Phosphorus concentrations decrease steadily upward from over 800 mg/kg at the bottom of the core to 500 mg/kg at the base of unit 2 and remain at about that level through the remainder of the core. Arsenic follows a similar pattern to phosphorus, with values of over 20 mg/kg below the unit boundary to less than 10 mg/kg above it. Similarly, the concentration of molybdenum decreases from as high as 0.97 mg/kg below the unit boundary to approximately 0.2 mg/kg above the boundary.

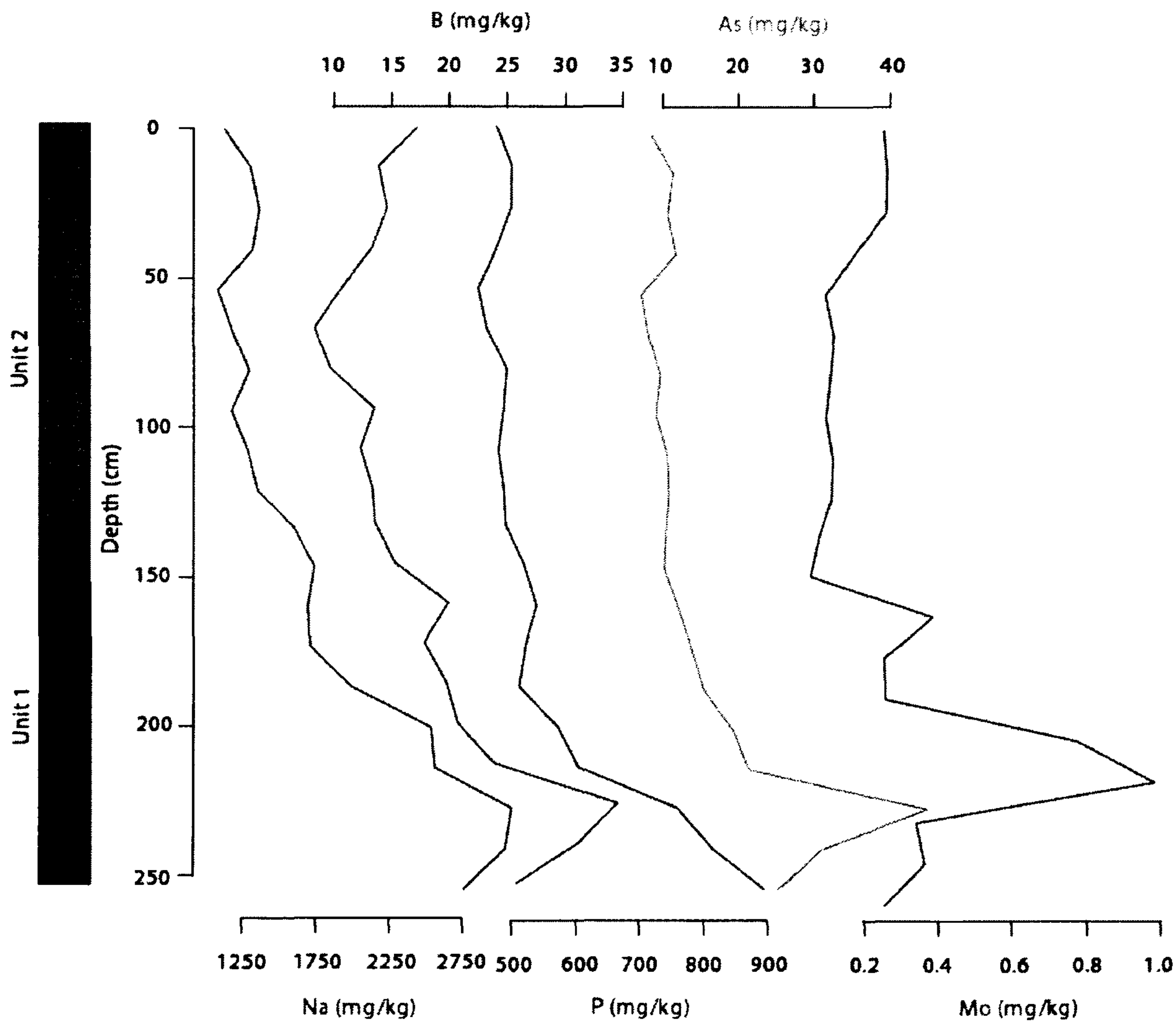

Figure 3.13: Concentrations of sodium, boron, phosphorus, arsenic and molybdenum in 09-LRoca(02).

Principal component (PC) analysis on the 49 sets of elemental data from the 09-LRoca(02) core demonstrate that principal components 1, 2 and 3 explain 77% of the total variance (PC1 = 42%, PC2 = 18%, PC3 = 17%). All element concentrations are positively loaded on PC 1 except phosphorus, molybdenum, arsenic, boron and sodium (Figure 3.14 a). Sodium, boron, arsenic and phosphorus are strongly loaded positively on PC 2, whereas the rest of the elements are loaded on both PC 1 and PC 3 (Figure 3.14 a – c).

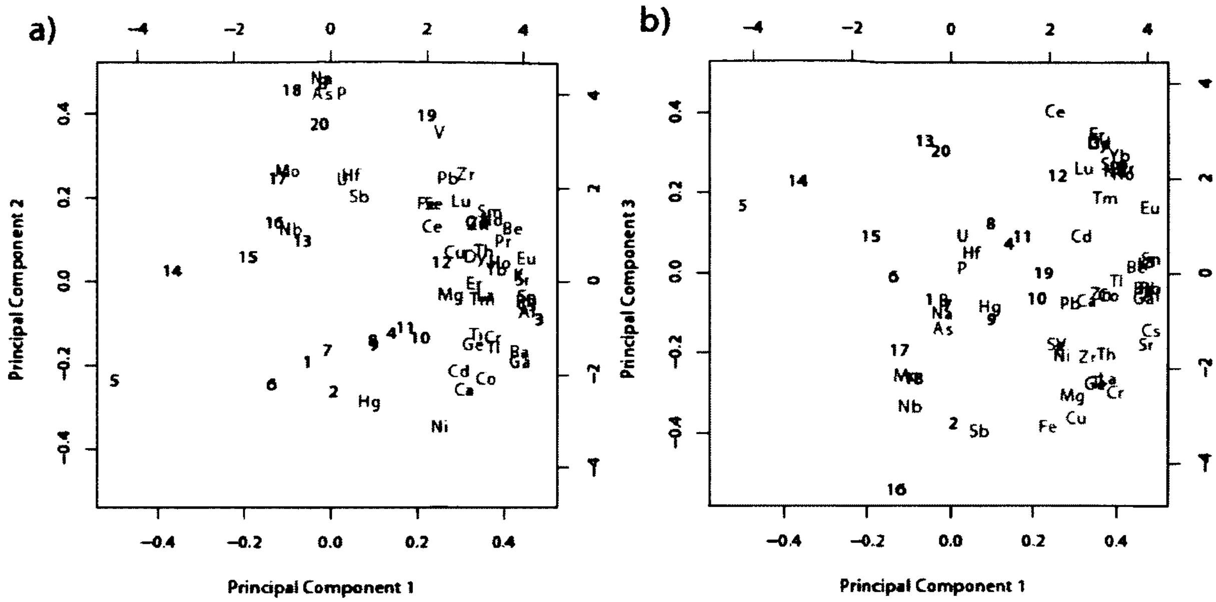

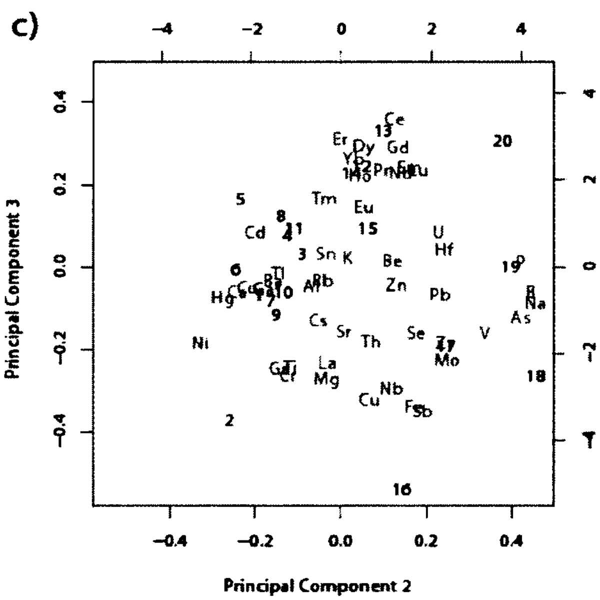

Sample ID #	Core Depth (cm)
1	0
2	13
3	27
4	40.5
5	54
6	67.5
7	81
8	94.5
9	108
10	121.5
11	133
12	146.5
13	160
14	173.5
15	187
16	200.5
17	214
18	227.5
19	241
20	254.5

Figure 3.14: Elemental composition of sediment in 09-LRoca(02): a) Loading scores of principal component (PC) 1 against PC 2; b) loading scores of PC 3 against PC 1; c) loading scores of PC 3 against PC 2. The numbers 1 through 20 in a, b and c are the 20 sediment samples, with their associated depths in the table at the lower right. The red symbols represent the loading scores of elements on each of the three principal components. The numbered sediment samples denote the principal component loading score for corresponding sample depths.

The total elemental composition of 09-LRoca(02) samples is positively loaded on PC1 at 241 cm, between 146.5 cm and 81 cm, and between 40.5 and 13 cm (Figure 3.15). It is positively loaded on PC 2 between 254.5 and 146.5 cm, and is positively loaded on PC3 from 254.5 to 241.5 cm, between 187 and 133 cm, at 94.5 cm and between 67.5 and 27 cm.

I also standardized the total elemental composition data against the percent clay for each sample and then performed principal component analysis again on the standardized data. Standardizing for the percent clay minimizes any influence that grain size may have on elemental composition. The standardization procedure did not significantly change the result (Appendix D).

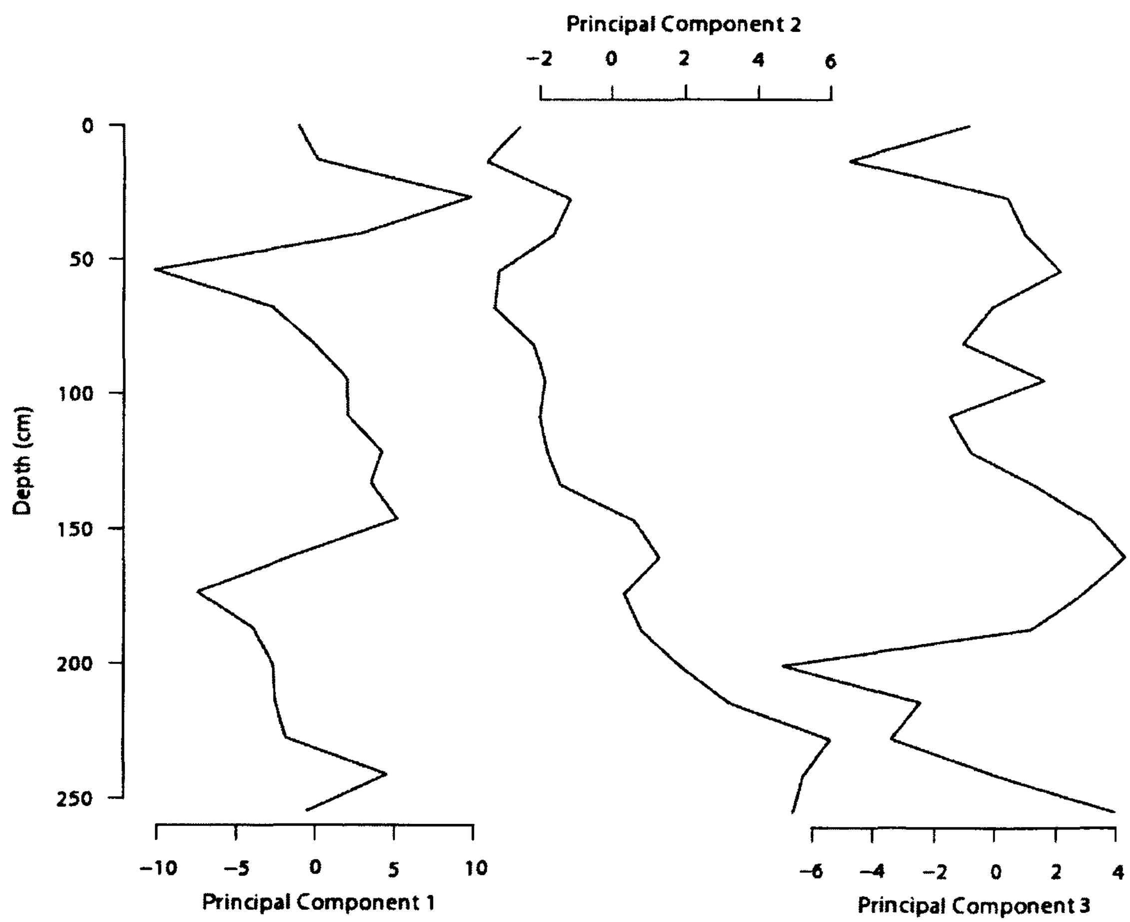

Figure 3.15: Principal component 1, 2 and 3 for 20 geochemistry samples from 09-LRoca(02).

There is a significant correlation between principal component 1 and percent clay content ($r = 0.34$) in each of the 20 samples from core 09-LRoca(02) (Table 3.4). Principal component 2 strongly correlates with water content ($r = 0.79$) and dry density ($r = -0.68$). Principal component 3 correlates with percent clay ($r = -0.44$) and magnetic susceptibility ($r = 0.55$) of the sediments.

Table 3.4: Pearson correlation coefficient matrix for principal components 1, 2 and 3 and percent clay, water density, wet content, organic matter and magnetic susceptibility for samples from 09-LRoca(02). Bold values are significant ($p<0.05$).

	PC1	PC2	PC3	% clay	Wet density	Dry density	Water content	Organic matter	Magnetic susceptibility
PC1	1	-5.0E-16	-1.0E-16	0.34	0.075	0.039	0.059	-0.054	-0.15
PC2	-5.0E-16	1	2.9E-16	0.30	-0.54	-0.68	0.79	0.60	-0.24
PC3	-1.0E-16	2.9E-16	1	-0.44	0.14	0.18	-0.17	-0.16	0.55
% Clay	**0.34**	0.30	**-0.44**	1	-0.06	-0.11	0.20	0.18	-0.61
Wet density	0.075	-0.54	0.14	-0.06	1	0.96	-0.51	-0.25	0.26
Dry density	0.039	**-0.68**	0.18	-0.11	0.96	1	-0.72	-0.43	0.35
Water content	0.059	**0.79**	-0.17	0.20	-0.51	-0.72	1	0.73	-0.43
Organic matter	-0.054	0.60	-0.16	0.18	-0.25	-0.43	0.73	1	-0.37
Magnetic susceptibility	-0.15	-0.24	**0.55**	-0.61	0.26	0.35	-0.43	-0.37	1

3.4.4 Diatom analyses

No whole diatoms were present in the two samples collected for diatom analysis, one at 81 cm in unit 2 and the other at 214 cm in unit1 (J. Brahney, personal communication, 2012). A fragment of a pinnate raphid diatom (a freshwater diatom) was present in the sample at 214 cm, but no diatom fragments were found in the sample at 81 cm (J. Brahney, personal communication, 2012).

3.5 Discussion

3.5.1 Sediment provenance

There is evidence at Lago Roca for both marine and lacustrine environments in the past 2700 years. I interpret changes in bulk physical properties, sedimentation rate and geochemistry to be the result of changes in sediment input. Because Lago Roca is located downvalley from glaciers in the Fuegian Andes, glaciers are likely an important source of sediment to the lake.

Lago Roca was once a fjord opening into the Beagle Channel (Gordillo et al., 1993) and at that time sediment deposited within Lago Roca was influenced by the marine or brackish environment. Below, I interpret the environments in which the sediments were deposited based on observed physical changes in the sediment cores.

3.5.1.1 Marine environment sediment deposition

The colour, geochemical and bulk physical properties of lithostratigraphic units 1 and 2 differ. Given the high clastic content and the rhythmically laminated nature of Lago Roca sediments, it is likely that sediments derived from glaciers accumulated in the lake throughout its history. However, sediment deposited between 2700–2340 and ca. 700 cal yr BP contains more organic matter than sediment deposited after 700 cal yr BP. In many proglacial lake environments organic input is less variable than mineral sediment input and, therefore, any change in organic matter content is inversely related to a change in clastic content (Souch, 1994). Because Lago Roca was open to the ocean until sometime after 4420–3980 cal yr BP (Gordillo et al., 1993), it is possible that the higher organic matter content in unit 1 does not reflect an increase in organic matter input, but rather a diluted mineral sediment input, as a result of additional marine influences. The sediment history of this study does not extend beyond 2700–2340 cal yr BP; therefore, the date of isolation of Lago Roca from the Beagle Channel remains uncertain. Whether a saline layer of water remained in the lake after isolation from the ocean, or the lake continuously received marine water inputs until the last millenium, the influence of marine water is evident from the elemental composition of the sediments in unit 1 of the Lago Roca sediments, which is discussed below.

There is a gradual change in total elemental composition of the sediments in core 09-LRoca(02) near the unit 1-unit 2 boundary. Principal component analysis of the core shows that samples below the boundary are positively loaded on PC 2 (Figure 3.15), which suggests a unique elemental composition of the dominant sediment deposited in Lago Roca at that time. Sodium, boron, phosphorus, arsenic and molybdenum are all heavily loaded on PC 2 (Figure 3.13), which indicates that these elements are common and covary in the sediments of unit 1.

Frederickson and Reynolds (1981) note that the concentration of boron in sediments is linearly related to the salinity of the water in which the sediments were deposited and can be used to detect changes in past water composition. Boron is held in clay minerals, and marine clays tend to contain a higher concentration of boron than clays deposited in freshwater lakes (Frederickson and Reynolds, 1981; Dominik and Stanley, 1993). The highest levels of boron in 09-LRoca(02) occur in sediments of the lower unit (Figure 3.13), which may imply a saline water influence between 2700–2340 and ca. 700 cal yr BP. The gradual decrease in boron levels starting prior to the unit boundary may also suggest that the influence of the marine water slowly diminished, rather than ceased dramatically.

Concentrations of phosphorus and sodium are also higher in sediments below the unit boundary in 09-LRoca(02) and gradually decrease to stable levels in unit 2 (Figure 3.13). According to Smith (1984), phosphorus is the limiting element for organic production in freshwater environments, resulting in diminished levels in those environments. Lower levels of phosphorus in unit 2 of 09-LRoca(02) could indicate organic production in a freshwater environment and higher levels in unit 1 may point to an abundance of phosphorus in a marine environment (Smith, 1984). Sodium is the most abundant cation in seawater (Land and Hoops, 1973), thus the higher concentrations of sodium in unit 1 in the 09-LRoca(02) core supports the argument that the sediment was deposited in a marine environment.

Similarly, arsenic is more abundant (5 to 40 mg/kg) in marine than freshwater environments (Lunde, 1977; Neff, 1997) and, therefore, will have higher concentrations in marine sediments. The concentration of arsenic in 09-LRoca(02) is between 5 and 40 mg/kg throughout the core, but is up to four times as high in unit 1 as in unit 2 (Figure 3.13). The slightly elevated concentrations of arsenic below the unit boundary are not conclusive alone, but taken with the concentration of the other indicator elements support the hypothesis that the sediment in the lower half of 09-LRoca(02) and sediment in the 09-LRoca(04) core were deposited in a marine environment.

Concentrations of molybdenum are higher in unit 1 of 09-LRoca(02) than unit 2 (Figure 3.13). Molybdenum is an indicator of reducing conditions (Algeo and Maynard, 2004; Brahney et al., 2007). Uranium, zinc and vanadium are also indicators of reducing conditions. At least two of the above four 'redox-indicator' elements should be enriched within sediments to argue for reducing conditions (Algeo and Maynard, 2004). Although molybdenum is enriched in unit 1 relative to unit 2, uranium, zinc and vanadium show no trend through the core (Appendix C). It is, therefore, unlikely that the changes in sodium, boron, phosphorus and arsenic are the result of changes in the redox state within the aqueous environment.

The bulk physical properties, lithostratigraphy and geochemistry, taken together, suggest that glacigenic sediment have been a dominant sediment source to Lago Roca since 2700–2340; until ca. 700 cal yr BP, the lake was also influenced by marine conditions. Gordillo et al. (1993) proposed the marine regression at Lago Roca occurred after 4500–4000 cal yr BP; given the gradual change in the geochemical and bulk physical properties of the lake sediments, it is likely that isolation took place over an extend period. It is also possible that following the isolation of Lago Roca from Beagle Channel after 4500–4000 cal yr BP, there remained a layer of saline anoxic bottom water in the lake for some time. The presence of anoxic bottom water in a lake can enhance the release of phosphorus from organic matter (Ingall et al., 2005) and could also account for the higher levels of phosphorus below the unit boundary in the Lago Roca sediments. Although the marine water input to Lago Roca likely ceased sometime after 4500–4000 cal yr BP, the influence of the marine water diminished slowly until ca. 700 cal yr BP.

3.5.1.2 Freshwater environment sediment deposition

The bulk physical properties of unit 2 in 09-LRoca(02) are similar to those of sediments in 09-LRoca(01) and (03) (Figures 3.3– 3.6). The inorganic nature of these sediments of unit 2 compared to those of unit 1 indicates that concentration of clastic sediment in the lake increased after 700 cal yr BP.

Given the rhythmically laminated nature of the clastic sediments, Lago Roca received sediments from glacier meltwater throughout the period spanned by the cores. Prior to the isolation of Lago Roca from the Beagle Channel, the relative contribution of marine and terrestrial sediment to the lake is unknown. I am thus unable to distinguish a change in flux due to marine or freshwater influences and, therefore cannot definitively identify periods of glacier expansion and contraction in the lake sediments between 2700–2340 and 700 cal yr BP.

The bulk physical properties of the lake sediments vary little following the isolation of Lago Roca from the sea and the flushing of saline bottom water from the lake (Figures 3.3–3.6). The uniform properties of the sediments of unit 2 make it impossible to discern glacier fluctuations in the Fuegian Andes. They may indicate that: 1) glaciers did not substantially fluctuate during that period; or 2) the catchment-to-lake ratio is unfavourable for recording changes in ice extent in the sediments. Because I was unable to accurately measure varves below 123.5 cm (580 cal yr BP) in 09-LRoca(02) (Figure 3.11), I do not have a complete high-resolution record of sediment input into Lago Roca following the time when the marine water influence ceased.

There is little variation in varve thickness within 09-LRoca(01), (02) and (03), other than a slight increase between 60 and 40 cm, 38 and 10 cm and 155 and 103 cm in cores 09-LRoca(01), (02) and (03) cores, respectively (Figure 3.11). Using the average sedimentation rate of 1.8 mm/yr for 09-LRoca(01), I conclude that sediment flux into Lago Roca increased between 260 and 150 cal yr BP (60–40 cm). Given the age of 290–150 cal yr BP for the most recent Holocene advance of nearby Stoppani Glacier, it is probable that increased clastic sedimentation between 260 and 150 cal yr BP in 09-LRoca(01) is due to glacier expansion in the Lago Roca watershed.

3.5.1.3 Episodically derived sediment inputs

Unusually thick sandy beds are present within the Lago Roca sediment cores (Figures 3.9 and 3.10). They likely originate from high-energy events such as floods, subaerial landslides or subaqueous slope failures (Desloges and Gilbert, 1994). When the catchment-to-lake ratio is large, anomalously coarse sediments can be produced by major changes in sediment delivery to the fluvial system, caused for example by heavy precipitation. When this ratio is small, coarse event beds are commonly the result of glacier fluctuations and mass movements events (Desloges and Gilbert, 1994). The thickness of event beds is also dependent on of other factors including the proximity of the source of the event bed to the sample site.

A possible source for the thick sand beds at 214–211 and 203–197 cm in core 09-LRoca(04) and at 12.5–10 cm in core 09-LRoca(01) (Figures 3.9 and 3.10) is subaqueous or subaerial mass wasting events (Desloges and Gilbert, 1994; Schnellmann et al., 2002; Moernaut et al., 2007). Landslides and debris flows are most often triggered by intense rain, but can also result from earthquakes (Jibson, 1996; Moernaut et al., 2007). Seismic activity can liquefy lake sediments, induce soft-sediment deformation or cause subaqueous slopes to fail (Shilts and Clague, 1992; Leroy et al., 2002; Moernaut et al., 2007). Seismically induced subaqueous slope failures can produce turbidity currents that affect a large area of the lake floor. There are, however, no diagnostic criteria for distinguishing seismically induced turbidites from nonseismic ones (Jibson, 1996; Leroy et al., 2002; Schnellmann et al., 2002).

The lower two event beds in 09-LRoca(04) are older than the sediments in all other cores, thus their extent within the lake basin is uncertain. The coarse event bed in 09-LRoca(01) and 09-LRoca(03) that dates to about AD 1953 contains graded fine sand and silt characteristic of a turbidity current deposit (Bouma, 1962). Liquefaction or subaqueous slope failure triggered by earthquakes can produce turbidity currents (Jibson, 1996; Schnellmann et al., 2002). The event bed thickens toward the lake outlet (Figure 3.10), suggesting that the source of the sediment within the beds was introduced closest to the 09-LRoca(01) core location. This event bed may have been deposited by a turbidity current triggered by a subaqueous slope failure during one of two $M_l = 7.8$ earthquakes on Tierra del Fuego on December 17, 1949 (Costa et al., 2006). Although the earthquakes occurred three to four years before the assumed AD 1953 event bed in Lago Roca, it is possible that four varves were lost either in core recovery or that there were varve counting errors; in either case, the event bed could date to AD 1949.

3.5.2 Regional comparison

Studies of past sea level change in Beagle Channel area indicate that the local shoreline was 8-10 m higher than today at 6880–6410 cal yr BP (Figure 3.17; Rabassa et al., 1986, in

Gordillo et al., 1993; Bujalesky, 2011). Because Lago Roca today is 4 m asl, sea level was at least 4–6 m above the present level of Lago Roca at that time. Local sea level gradually fell over the next ca. 6500 years (Gordillo et al., 1993).

According to Gordillo et al. (1993), sea level in Bahia Lapataia was still 6 ± 1 m asl or about 2 m above the surface of Lago Roca between 5440–4630 and 4420–3980 cal yr BP (Figure 3.17). At this time Lago Roca changed from a marine fjord to an estuary. The Beagle Channel is microtidal and has a tidal range of up to 2 m, thus sea water would reach up to 3 m above the current elevation of Lago Roca between 5440–4630 and 4420–3980 cal yr BP. In order for Lago Roca to become completely isolated from tidal effects, sea level would have to drop at least 3 m below the 5440–4630 to 4420–3980 cal yr BP level (i.e., to less than 3 m above present sea level).

At Playa Larga (Figure 3.16), sea level was 3.5 ± 0.5 m above the current datum (the same elevation as Lago Roca today) about 3350–2890 cal yr BP (Figure 3.17; Gordillo et al., 1992). A mean sea level position of 3.5 m asl with a tidal range of 2 m would allow marine waters from the Beagle Channel to enter Lago Roca. By 2110–1730 cal yr BP, sea level had dropped to 2.0 ± 0.5 m asl in Bahia Ensenada (Figure 3.16; Gordillo et al., 1992), which implies that Lago Roca was completely separated from the Beagle Channel by this time. Therefore, Lago Roca was isolated from the Beagle Channel sometime between 3350–2890 and 2110–1730 cal yr BP and the transition was likely gradual.

The visual characteristics, geochemistry and bulk physical properties of the Lago Roca sediments suggest that any marine influence to the lake subsided before ca. 700 cal yr BP and thus sea level had fallen to less than 3 m above the current datum before that time (Figure 3.17).

Raised beaches along the Beagle Channel indicate that local sea level was 1.8 m above the present datum at 1220–670 cal yr BP and 1.7 m at 500–0 cal yr BP (Figure 3.16; Gordillo et al., 1992), which supports the assumption that Lago Roca was completely isolated from the Beagle Channel long before the marine water influence on the sediment ceased in the lake.

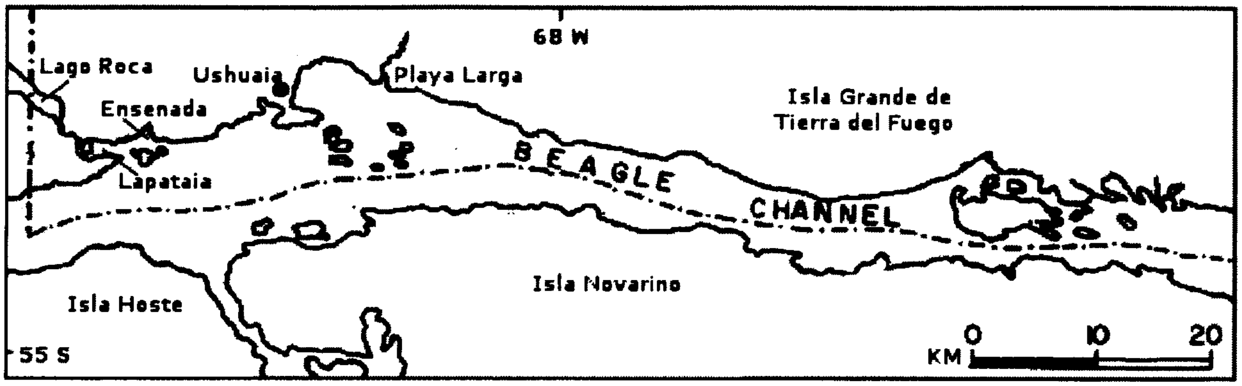

Figure 3.16: Locations of raised beaches along the north coast of Beagle Channel documented by Gordillo et al. (1992). (Modified from Gordillo et al., 1992).

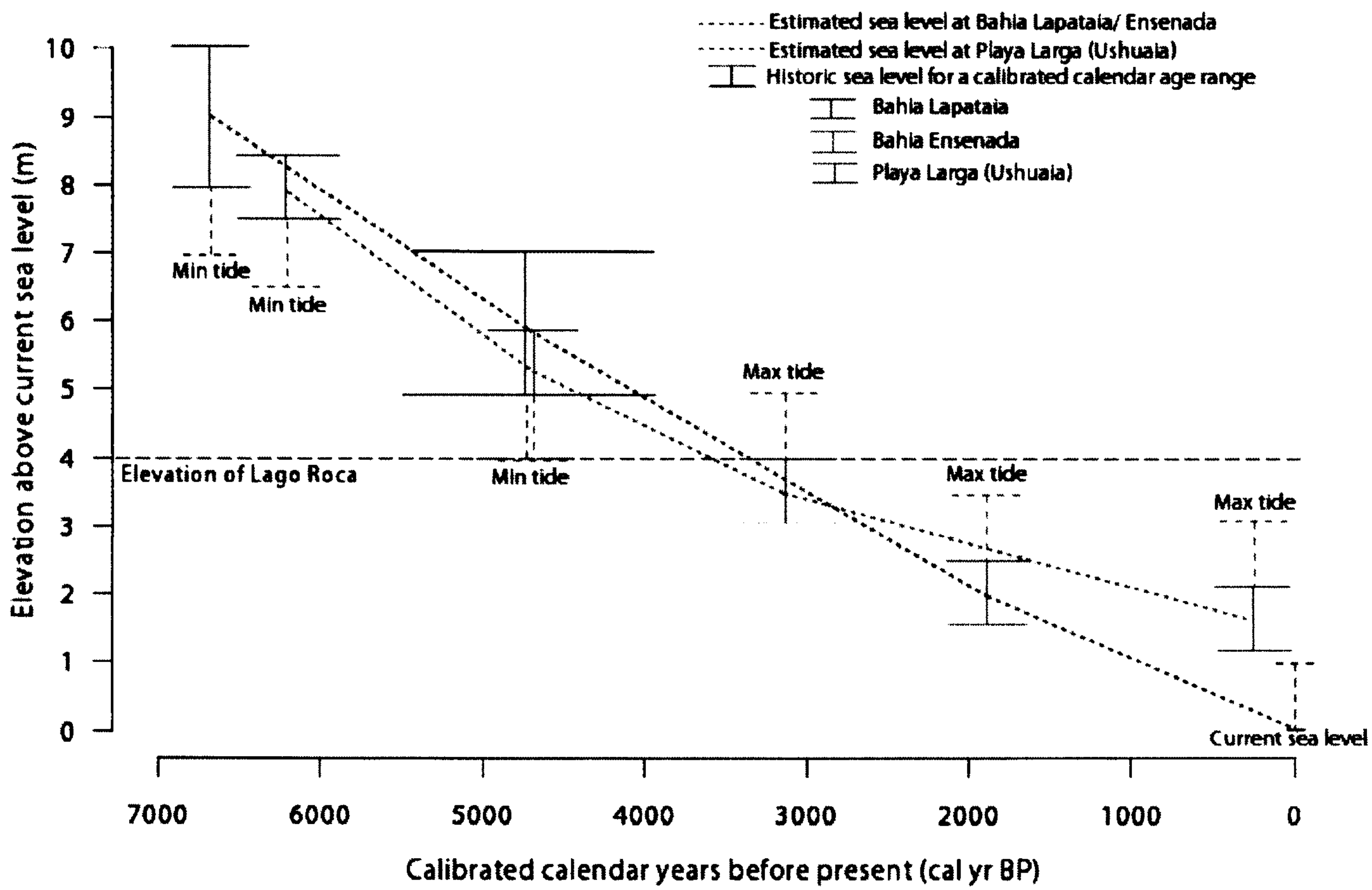

Figure 3.17: Local sea level relative to the current datum over the past 7000 years. Solid bars represent a range of sea level positions for a calibrated age range. Thin dashed lines above and below calibrated age ranges denote sea level minima and maxima with a 2 m tidal range. The blue dashed line is the elevation of Lago Roca, and the red and green dashed lines show a sea level trend that intersects known sea levels over time, assuming a constant rate of uplift. Sea surface elevations and ages from Gordillo et al. (1992, 1993).

Recent sea level change on Tierra del Fuego is the result of glacioisostatic, neotectonic and eustatic processes (Gordillo et al., 1993). Based on a recent study of plate movement along the Magallanes-Fagnano Fault system on Tierra del Fuego, Mendoza et al. (2011) estimate that the current rate of uplift just north of Lago Roca is 3.1 ± 0.4 mm yr^{-1}. Other studies of raised beaches along the Beagle Channel suggest that uplift rates during the Holocene are between 1 and 5 mm yr^{-1} with an average of 1.3 mm yr^{-1} (Costa et al., 2006; Bujalesky, 2011). Given an average rate of uplift of 1.3 mm yr^{-1}, sea level would have been 3 m above the current datum, isolating Loga Roca from the Beagle Channel ca. 2300 years ago. The isolation of Lago Roca millennia earlier than ca. 700 cal yr BP supports the hypothesis that the elemental concentration of the lake sediments was influenced by trapped saline water within the lake long after the marine input terminated.

Following the diminished influence of trapped marine water within Lago Roca around 700 cal yr BP, changes in the sediment signal from the glacial input became more distinct. It is likely that the glaciers in Cordon Central were advancing as the marine water influence subsided in Lago Roca; Ema Glacier on the west side of the Cordillera Darwin advanced 1290–980 cal yr BP (Strelin et al., 2008) and glaciers in Bahia Pia advanced between 2000–1620 and 1860–1420 cal yr BP (Figure 2.8; Kuylenstierna et al., 1996).

An increase in sedimentation derived from thick varves between 260–150 cal yr BP may arise from glacier expansion and coincides with the last advance of Stoppani Glacier (Figure 2.8). Ema Glacier advanced again after 520–150 cal yr BP (Figure 2.8; Strelin et al., 2008). Glaciers of the Gran Campo Nevado also advanced at approximately 330 cal yr BP (Koch and

Kilian, 2005), and outlet glaciers in the Southern Patagonia Icefield expanded for the last time 360–260 cal yr BP (Figure 2.8; Mercer, 1965; Aniya, 1995).

Summer temperature reconstructions imply that glaciers in southern Patagonia advanced from around AD 1300 until sometime between the late 1600s and the early 1800s, depending on the region (Villalba, 1994; Neukom et al., 2011). Retreat of Cordillera Darwin glaciers from their most recent maximum positions was caused by an increase in temperature and a decrease in precipitation (Holmlund and Fuenzalida, 1995). In general, most Cordillera Darwin glaciers studied by Holmlund and Fuenzalida (1995) began to retreat prior to the AD 1940, with the largest rate of recession after AD 1960. Many south-facing glaciers advanced short distances between about AD 1940 and AD 1960, whereas most north-facing glaciers retreated many hundreds of meters to their present positions during this period (Holmlund and Fuenzalida, 1995). Stoppani Glacier retreated 300 m and Dartmoore Glacier (Figure 2.1) retreated 100 m between AD 1960 and 1993 (Holmlund and Fuenzalida, 1995). Three recessional moraines of Lengua Glacier on Gran Camp Nevado were abandoned between 330 cal yr BP and AD 1941; they are separated by approximately 300 m (Koch and Kilian, 2005). Lengua Glacier retreated another 250 m from AD 1941 to the present. Glaciers near Ushuaia retreated slowly until AD 1960, at which time the rate of recession increased and the glaciers thinned considerably (Strelin and Iturraspe, 2007)..

Although the increase in varve thickness between 10 and 0 cm in 09-LRoca(01) is most likely due to increased glacier runoff, the two $M_I = 7.8$ earthquakes on December 17, 1949, may have triggered landslides in the watershed (Moernaut et al., 2007), which would have increased sediment delivery to Lago Roca.

3.6 Conclusion

I collected sediment cores from Lago Roca to reconstruct environmental changes in the watershed. The physical properties of the lowermost recovered sediments imply a marine or a trapped saline bottom water influence from before 2700–2340 cal yr BP until 700 cal yr BP. A previous study of sea level in the Bahia Lapataia concluded that Lago Roca became isolated from Beagle Channel sometime after 4500–4000 cal yr BP. A radiocarbon age from core 09-LRoca(02) supported by other ages from raised beaches along the Beagle Channel suggest that the lake separated from Beagle Channel more recently than previously thought (ca. 2300 cal yr BP) and the isolation left a layer of saline water that influenced the bulk physical properties of the sediment until 700 cal yr BP. I was unable to infer periods of glacier advance in the Lago Roca watershed from sediments deposited prior to declined influence of the saline water, but there is evidence that glaciers were expanding by 260–150 cal yr BP. Two thick sandy beds in core 09-LRoca(02) and one in core 09-LRoca(01) may record floods, landslides or subaqueous slope failures. Unfortunately, due to the lack of historical records and dating uncertainties the origins of these beds remain uncertain.

4. Comparison of inter-hemispheric glacier fluctuations

4.1 Introduction

Reliable glacier chronologies are required to evaluate past climate change (Schaefer et al., 2009; Winkler and Matthews, 2010). With suitable precision and accuracy, these records can identify the amplitude, spatial scale and duration of past climate change events (McCulloch et al., 2000).

Inter-hemispheric comparisons of glacier activity must be sufficiently resolved to discriminate relatively short-lived advances or recession (Winkler and Matthews, 2010). Comparison of records must also consider the nature of the chronological control; that is, whether dates are minima, maxima or closely bracketing ages for a glacier advance. I have documented five advances of Stoppani Glacier during the Neoglacial period. The presence of multiple wood mats and wood in growth position in the northeast lateral moraine and forefield of Stoppani Glacier allows me to compare the behaviour of Stoppani Glacier to that of other well studied glaciers. Each wood mat or in situ stump within the lateral moraine at Stoppani Glacier provides a maximum limiting age for a subsequent expansion of the glacier. Possible unconformities within the lateral moraine, however, may result in some Neoglacial advances going unrecorded.

To facilitate my discussion of inter-hemispheric events, I examine the distribution of maximum limiting ages from material overrun by expanding glaciers. Some inferences can be drawn regarding the duration of each Stoppani advance by assuming that the glacier must have retreated prior to the maximum limiting age of each subsequent advance.

In the following sections, I compare the chronology of Stoppani Glacier and those of other glaciers in southern Patagonia to well-dated glacier chronologies from northwestern North America (Figure 4.1). The purpose of this comparison is to address the question of glacier fluctuation synchronicity between the two hemispheres during the Neoglacial period.

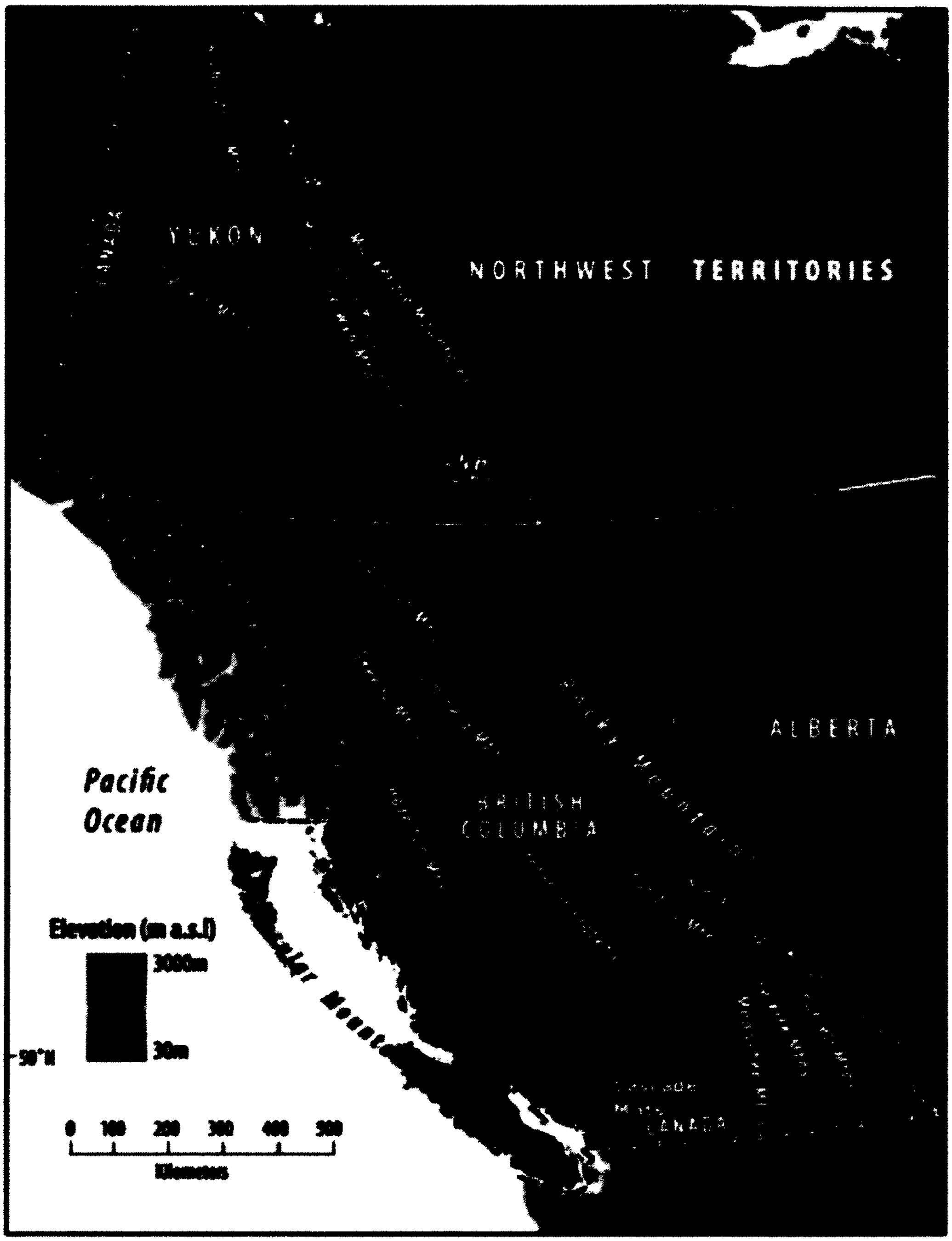

Figure 4.1: Major mountain systems and ranges of western Canada. The Cariboo, Purcell, Selkirk and Monashee mountains are referred to in the text as the interior mountain ranges. Blue shading denotes 2009 ice cover. Modified from Menounos et al. (2009).

4.2 Comparison of Neoglacial glacier activity

4.2.1 Early-middle Neoglacial (5000–3500 cal yr BP)

Stoppani Glacier was advancing by 3830–3640 cal yr BP. A number of maximum and minimum limiting radiocarbon ages from the Southern Patagonian Icefield also indicate that outlet glaciers in that area advanced after ca. 5500 cal yr BP and before ca. 3600 cal yr BP (Section 2.5). The calibrated age range for the first documented Neoglacial advance of Stoppani Glacier corresponds with the end of the age range of an advance of glaciers in western Canada and Alaska between 4530 and 3830 cal yr BP known as the '4.2 ka Advance' (Figure 4.2; Menounos et al., 2008, 2009). The 4.2 ka Advance was inferred from dated in situ stumps in glacier forefields throughout British Columbia and from dated detrital wood samples in southeast Alaska (Figures 4.1 and 4.2; Gardner and Jones, 1985; Luckman, 1995; Wood and Smith, 2004; Menounos et al., 2008, 2009; Barclay et al., 2009). The peak of the 4.2 ka Advance in western Canada is centered on the period 4400–4000 cal yr BP. These glaciers, however, were expanding as early as 4900 cal yr BP and continued to grow until as late as ca. 3800 cal yr BP (Gardner and Jones, 1985; Luckman, 1995; Menounos et al., 2008). The inception of the first advance at Stoppani Glacier is based on only one radiocarbon age and its calibrated range overlaps only the younger end of the multi-century age range for the 4.2 ka Advance, thus additional radiocarbon ages are needed to confirm that the two events are coeval.

The 4.2 ka Advance has not been recognized elsewhere in southern Patagonia. Similar radiocarbon ages from the Southern Patagonia Icefield are minimum limiting ages and may be associated with an older advance (Mercer, 1968, 1970, 1976; Aniya, 1995; Wenzens, 1999). The lack of evidence elsewhere in southern Patagonia for glacier activity at this time may indicate that these glaciers have not yet retreated past positions reached during the early-middle Neoglacial period. It is also possible that the advance at Stoppani Glacier was a local event caused by cool and/or wet condition in the far south. However, climatic conditions favouring glacier expansion 4700–4200 cal yr BP have been inferred on South Georgia Island near Antarctica (Clapperton and Sugden, 1988). It is probable that this advance also occurred over a multi-century age range throughout southern Patagonia and that the evidence has yet to be discovered at other sites due to the limited number of studies that focus on glacier activity during this period.

4.2.2 Middle Neoglacial (3500–1900 cal yr BP)

The second, third and fourth advances at Stoppani Glacier occurred during the North American 'Tiedemann – Peyto Advance' [3500 to 1900 cal yr BP] (Figue 4.2; Ryder and Thomson, 1986; Clague et al., 2009; Osborn et al., 2012). Originally, this interval was believed to record a single long-lived expansion of glaciers. Later work, however, has revealed multiple advances during this period (Osborn and Karlstrom, 1989; Reyes and Clague, 2004; Koch et al., 2007a; Osborn et al., 2007, 2012; Clague et al., 2009; Menounos et al., 2009; Maurer et al., 2012). The centennial-scale pacing of the second, third and fourth advances of Stoppani Glacier allows for the development of a detailed chronology; however, it also hampers a direct comparison to glacier activity in northwestern North America because periods of retreat are short and difficult to identify. The same problem exists when comparing glacier fluctuations within northwestern North America during the Tiedemann – Peyto Advance interval (Clague et al., 2009). Uncertainties exist in the number, ages and durations of the advances (Menounos et al., 2009). I will test inter-hemispheric synchronicity of the Tiedemann-Peyto Advances by comparing each known expansion of Stoppani Glacier to calibrated age ranges of radiocarbon-dated in situ wood killed by an expanding glacier in northwestern North America.

Stoppani Glacier began to thicken and advance for the second time shortly after 3160–2950 cal yr BP; and ended before 2860–2760 cal yr BP. This advance overlaps in time with an advance of Ema Glacier (a maximum limiting age) and an advance of glaciers in the Bahia Pia area (two minimum limiting ages; Section 2.5). There is no published evidence for correlative advances of outlet glaciers of the Southern Patagonian Icefield, which may imply that the advance was restricted in scope or that evidence of it has not been preserved in the Southern Patagonian Icefield. In northwestern North America, glaciers expanded as early as ca. 3600 cal yr BP; an advance centered around 3000 cal yr BP and culminating before 2800 cal yr BP is common throughout the Coast Mountains and the Canadian Rocky Mountains (Figures 4.1 and 4.2; Ryder and Thomson, 1986; Wood and Smith, 2004; Osborn et al., 2007; Barclay et al., 2009; Menounos et al., 2009).

The third and fourth advances of Stoppani Glacier (2860–2760 until sometime before 2300–2010 cal yr BP; and shortly after 2300–2010 cal yr BP) coincide with periods of glacier growth in the Cordillera Darwin and Southern Patagonian Icefield. The ages from the Southern Patagonian Icefield are, however, minimum limiting ages and may be associated with an older advance (Section 2.5). Glaciers in northwestern North America expanded during these times; in most areas there is evidence for two advances between 3000 and 2000 cal yr BP (Figures 4.1 and 4.2; Ryder and Thomson, 1986; Reyes and Clague, 2004; Osborn et al., 2007; Menounos et al., 2009). The reported onset and duration of these advances are different in different regions of northwestern North America.

Following the culmination of the earliest Tiedemann – Peyto Advance, glaciers in the British Columbia Coast Mountains advanced between 2800 and 2400 cal yr BP (Figure 4.1; Osborn et al., 2007; Menounos et al., 2009). Numerous ages from detrital wood samples obtained from glacier forefields in the Rocky Mountains and the interior mountain ranges date to the period 2700–2400 cal yr BP. Strong supporting evidence for this advance is found in the Cariboo Mountains (Maurer et al., 2012). Deming Glacier in the Washington Cascade Range advanced into forest between 2500–2200 and 2350–2010 cal yr BP (Easterbrook and Donnell, 2007; Osborn et al., 2012). An advance between 2800 and 2400 cal yr BP has not yet been documented in Alaska (Barclay et al., 2009).

The fourth advance of Stoppani Glacier, at 2300–2010 cal yr BP, appears to coincide with a period of glacier retreat in the interior mountain ranges and Rocky Mountains of northwestern North America (Figure 4.2). An earlier advance in these areas culminated ca. 2400 cal yr BP, and glaciers were in retreat between 2400 and 1800 cal yr BP (Osborn et al., 2007; Menounos et al., 2009; Maurer et al., 2012). There is, however, evidence for an advance of one glacier in the Washington Cascade Range and two glaciers in the British Columbia Coast Mountains at ca. 2300 cal yr BP, which may support detrital wood ages for a possible widespread advance in the Coast Mountains at this time (Reyes and Clague, 2004; Koch et al., 2007a; Barclay et al., 2009; Koehler and Smith, 2011; Osborn et al., 2012). The duration of the fourth advance of Stoppani Glacier is uncertain, because the age of the fifth advance (290–150 cal yr BP) does not provide a close minimum constraint. As there is evidence for glacier retreat in the interior mountain ranges and Rocky Mountains, but expansion in the Coast and Cascade mountains at the time of the fourth advance of Stoppani Glacier, an inter-hemispheric comparison may be unwarranted at this time.

Although Stoppani Glacier and glaciers in northwestern North American advanced at least three times during the Tiedemann – Peyto Advance interval, the timing and duration of each advance may or may not be in phase with its hemispheric counterpart. Due to the close temporal spacing of the advances during this interval, advances in different regions that are within a few hundred calibrated radiocarbon years of one another commonly are grouped. The point was made by Clague et al. (2009), who stated that comparisons at this temporal scale may not be possible given the uncertainties associated with radiocarbon ages. I conclude that, although the chronology at Stoppani Glacier provides useful information about glacier expansion between ca. 3100 and 2000 cal yr BP, assessing the synchronicity of advances between the Northern and Southern hemispheres during this period is not yet possible. My data do imply that glaciers in southern Patagonia underwent a general expansion between 3100 and 2000 cal yr BP, similar to the general expansion of northwestern North American glaciers and that on a centennial timescale there is synchronicity between hemispheres, but more data are required to assess inter-hemispheric synchronicity at a decadal timescale.

4.2.3 Late Neoglacial (1900 cal yr BP - present)

Between the fourth and fifth advance of Stoppani Glacier (2300–2010 and 290–50 cal yr BP), glaciers elsewhere in southern Patagonia advanced several times (Section 2.5). Clapperton and Sugden (1988) reported an advance of glaciers on the subantarctic islands around 1300 cal yr BP. Additional evidence for an advance of glaciers at high latitudes in the Southern Hemisphere at about this time includes a maximum limiting age of 1690–1300 cal yr BP from Upsala Glacier, numerous minimum limiting ages from Tyndall Glacier in the Southern Patagonian Icefield (Aniya, 1995), and an advance of Ema Glacier at 1290–980 cal yr BP (Strelin et al., 2008). The period between 1800 and 1100 cal yr BP was marked by glacier expansion in northwestern North America and termed the 'First Millennium A.D. Glacier Advance' (Figure 4.2; Reyes and Clague, 2004; Wiles et al., 2004; Reyes et al., 2006; Koch et al., 2007b; Barclay et al., 2009; Menounos et al., 2009). Many northwestern North American glaciers advanced at least twice during the First Millennium A.D. Glacier Advance.

No evidence has yet been found for the First Millennium A.D. Glacier Advance in the Canadian Rocky Mountains; however, two glaciers, one in the Cariboo Mountains and South Cascade Glacier in the Washington Cascade Range, advanced at 1870–1720 cal yr BP and again at 1540–1420 cal yr BP (Maurer et al., 2012; Osborn et al., 2012). The ages from southern Patagonia broadly relate to glacier activity during the First Millennium A.D. Glacier Advance, but there is no evidence to support multiple advances similar to the two documented in the Cariboo Mountains and Cascade Range. The limited evidence in southern Patagonia for one or more advances at this time may indicate that addition work is needed. The 1340–1290 cal yr BP age of a fragment of detrital wood at Stoppani Glacier may indicate glacier expansion during the First Millennium A.D. Glacier Advance, but the origin of the wood is unclear and, therefore, its relation to glacier activity is uncertain.

Elsewhere in southern Patagonia, there is evidence for glacier expansion from shortly after 1000 cal yr BP until the late 1800s. Outlet glaciers of the Southern Patagonian Icefield advanced between 1120–650 and 930–670 cal yr BP, and again from 670–480 until 440–0 cal yr BP (Mercer, 1968; Villalba, 1994; Aniya, 1995). Ema Glacier expanded at 730–500 cal yr BP and again at 520–150 cal yr BP (Strelin et al., 2008), and glaciers at Bahia Pia grew between 930–680 and 730–540 cal yr BP (Kuylenstierna et al., 1996). The sediment record at Lago Roca suggests that glaciers in the Lago Roca basin were expanding by 260–150 cal yr BP and probably earlier. The number and timing of advances between 1000 cal yr BP and present are not well constrained in southern Patagonia; therefore, it is difficult to accurately compare glacier activity within the region during this period.

In the Coast Mountains and Cascade Range, glaciers began to advance towards maximum Holocene positions as early as the 11^{th} century. Expansion continued between AD 1200 and 1300 and again around AD 1500, then culminated in the late AD 1600s and early AD 1700s depending on the locality (Figure 4.2; Ryder and Thomson, 1986; Clague and Mathews, 1992; Reyes and Clague, 2004; Koch et al., 2007a; Jackson et al., 2008; Barclay et al., 2009; Menounos et al., 2009; Osborn et al., 2012). In the Canadian Rocky Mountains and interior mountain ranges, the Little Ice Age (LIA) started between the 11^{th} and 14^{th} centuries. Glaciers likely retreated before commencing their climactic LIA advances, which culminated with construction of outermost Holocene moraines in the AD 1700s and 1800s (Luckman, 1986, 1995, 2000; Menounos et al., 2009; Maurer et al., 2012).

The timing of moraine construction between the early AD 1700s and AD 1800s in northwestern North America coincides with the last expansion of Stoppani Glacier, which was underway before 290–150 cal yr BP (AD 1660 – 1800) and the last advance of Ema Glacier at 520–150 cal yr BP (AD 1430–1800). Glaciers in both hemispheres advanced during the classical LIA interval, and the time of the LIA maximum is the same in both northwestern North America and southern Patagonia.

Glaciers in northwestern North America responded to an increase in temperature in the early 1900s and retreated rapidly from about AD 1920 until AD 1945; retreat then slowed, with minor advances in the AD 1960s and 1970s, until about AD 1980 (Luckman et al., 1987; Menounos, 2006; Beedle et al., 2009). Holmlund and Fuenzalida (1995) reported that retreat of glaciers in the Cordillera Darwin started between AD 1910 and 1953, with the rate of retreat dependent on the aspects of glacier; north-facing glaciers experienced greater ice loss than south-facing glaciers. From AD 1980 until the present, glaciers in both northwestern North America and southern Patagonia have retreated. Temperatures around the Antarctic Peninsula have also been rising rapidly since the AD 1920s (Mulvaney et al., 2012).

4.2.4 Summary

The five intervals of expansion of Stoppani Glacier during the late Holocene improve our understanding of Holocene glacier activity in southern Patagonia. Each interval broadly coincides with well-documented glacier advances in northwestern North America.

Stoppani Glacier and outlet glaciers of the Southern Patagonian Icefield expanded during the 4.2 ka Advance in northwestern North America. The second, third and fourth advances of Stoppani Glacier correspond with several glacier advances between 3500 and 1900 cal yr BP in northwestern North America. Although my data cannot demonstrate synchronicity between the two hemispheres on a decadal scale, there is inter-hemispheric synchronicity on a centennial scale between 3500 and 1900 cal yr BP. I found no definitive evidence for expansion of Stoppani Glacier between 1800 and 1000 cal yr BP, when glaciers in northwestern North America grew, but other glaciers in southern Patagonia advanced during this period. There is no convincing data for an advance of Stoppani Glacier early during the LIA, but glaciers elsewhere in southern Patagonia expanded at that time. Stoppani Glacier and glaciers elsewhere in southern Patagonia and in northwestern North America advanced synchronously during the late LIA. The rate and extent of retreat of glaciers northwestern North America and southern

Patagonia from maximum LIA positions differ depending on topography and aspect, but are broadly similar in the two hemispheres.

Dispite the uncertainties and limitations inherent in this study, it appears that glaciers underwent a general expansion in the mid- to late-Holocene in both southern Patagonia and northwestern North America. I am unable to determine if glacier activity was synchronous in both hemispheres on a decadal-to-century scale, but I conclude that glaciers collectively responded to millennial multi-century climate variability. There are a number of forcing mechanisms that could have caused the general expansion of global glaciers in the mid- to late-holocene: reduced solar insolation due to the overlap of Milankovitch cycle minimums, decreased solar production, dampening or complete break down of the thermohaline circulation, variations in the El Niño Southern Oscillation (ENSO) phenomena or the eruption of large volcanoes. It is probable that the combination of the above forcing mechanisms drove the general cooling and expansion of glaciers in both hemispheres in the mid- to late-Holocene.

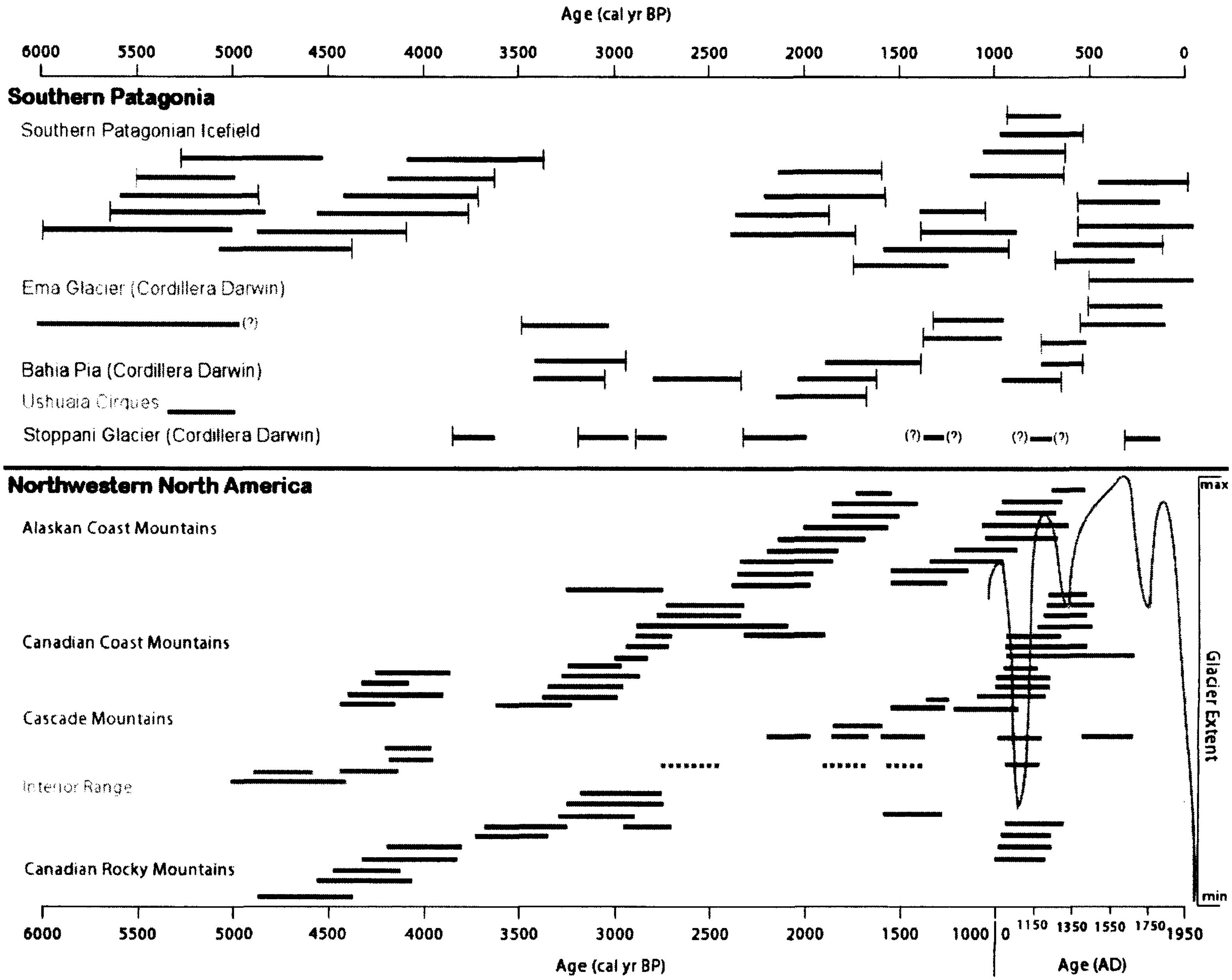

Age (cal yr BP)
6000 5500 5000 4500 4000 3500 3000 2500 2000 1500 1000 500 0
Southern Patagonia
Southern Patagonian Icefield
Ema Glacier (Cordillera Darwin)
(?)
Bahia Pia (Cordillera Darwin)
Ushuaia Cirques
Stoppani Glacier (Cordillera Darwin)
(?) (?) (?) (?)
Northwestern North America
Alaskan Coast Mountains
Canadian Coast Mountains
Cascade Mountains
Interior Range
Canadian Rocky Mountains
max
Glacier Extent
min
6000 5500 5000 4500 4000 3500 3000 2500 2000 1500 1000
0 1150 1350 1550 1750 1950
Age (cal yr BP)
Age (AD)

Figure 4.2: (Top) Calibrated radiocarbon ages of advances of outlet glaciers of the Southern Patagonian Icefield, Ema Glacier, glaciers near Bahia Pia, cirque glaciers near Ushuaia and Stoppani Glacier. Bars are minimum and maximum limiting ages from in situ material, and question marks indicate ages from detrital wood (refer to Figure 2.8 for data sources). Light blue columns outline advances of Stoppani Glacier. (Bottom) Calibrated radiocarbon ages of in situ plant material killed by expanding glaciers prior to the late LIA in the Canadian Rocky Mountains, interior mountain ranges, Cascade Range, and Canadian and Alaskan coastal mountains. Late LIA calibrated radiocarbon ages were not included because their ranges commonly span much of the last several hundred years, precluding correlation of individual advances from region to region. Bars are maximum limiting ages and dashed lines are ages derived from a study of lake sediments in the Cariboo Mountains in the interior of British Columbia (refer to Appendix E for sources). Grey line denotes generalized LIA glacier extent in northwestern North America derived from a combination of radiocarbon ages, dendrochronolgy, lichenometry and proglacial lake sedimentation. Modified from Clague et al. (2009).

4.3 Limitations to a global comparison of glacier fluctuations

My comparison of glacier advances in the Cordillera Darwin to glacier activity elsewhere in southern Patagonia and in northwestern North America highlights several inherent limitations with this type of evaluation. Although each documented increase in glacier size in the Cordillera Darwin corresponds to a period of glacier advance in northwestern North America, a comparison of synchronicity between the hemispheres is hampered by limited high-resolution chronological data, especially in southern Patagonia.

A comparison of glacier chronologies cannot be considered robust until it is based on well constrained chronologies (Winkler and Matthews, 2010), and a chronology cannot be considered well constrained until both the onset and culmination of glaciers advances are dated. Poorly constrained maximum and minimum limiting ages of even the best documented glacier advances can confound comparisons. Clague et al. (2009) discuss the problems in defining the time of a glacier advance and assert that it must be bracketed by periods of significant retreat. In many cases, especially in northwestern North America, it is difficult to define retreat based on landforms and stratigraphy in glacier forefields because the last Holocene advance was the most extensive and obscured or destroyed evidence of earlier glacier activity (Osborn et al., 2007; Clague et al., 2009). In any case, more data are needed from southern Patagonia to better constrain the onset, duration and termination of each Neoglacial advance before hemispheric synchronicity issues can be resolved.

Another significant limitation encountered when comparing glacier chronologies is the unavoidable error associated with radiocarbon ages. Despite recent refinements in the technique, which have significantly reduced the errors associated with the method, the calibrated age range from a single radiocarbon age can span a period longer than the advance itself. A radiocarbon age from a glacially overridden stump can yield a calibrated age range that spans a period of both advance and retreat. Notable short advances separated by a short, but significant retreat during the LIA in northwestern North America are good examples of glacier fluctuations that occur on a shorter time scale than the error associated with radiocarbon dating.

It may only be possible to acquire a single radiocarbon sample from a site, which limits the ability to closely constrain the age of glacier advance (Winkler and Matthews, 2010). Calculating a weighted mean of multiple samples from a site yields a more accurate representation of the age of an advance, provided one can assume that each age is a "kill" date. On the other hand, in some cases the researcher may choose only the oldest age from a cluster of samples to date an advance (Winkler and Matthews, 2010). According to Porter (2000), a minimum of six radiocarbon ages are needed to represent the true age of an advance, but he also suggests that current methods are only capable of distinguishing between advances that differ by 500–1000 cal yr. The absence of a standard methodology leads to differences in interpreting past chronologies, which can lead to errors in comparisons of these chronologies.

Radiocarbon dating of organic material within glacial deposits is the most direct way of establishing a glacier chronology, but the origin of the organic material may be uncertain (Ryder and Thomson, 1986). Even in the case of buried soils in lateral moraines, there may be more than a 500-year lag between moraine construction and soil establishment (Porter, 2000).

Porter (2000) also cautions that glacier fluctuations many not solely reflect changes in climate. Changes in calving glaciers are difficult to interpret because they are influenced by factors other than changes in temperature and precipitation; therefore, direct comparison of chronologies of calving glaciers and alpine glaciers might not be warranted. Landslides onto glaciers can also affect the mass balance of the glacier and cause it to respond to changes in climate differently than other glaciers in the same area (Porter, 2000; Menounos et al., 2013a).

Even if the exact times of onset and termination of an advance can be determined, comparisons between regions can still be problematic, because not all glaciers react to changes in climate in the same way. The response of a glacier to a change in climate depends on topography, glacier size and hypsometry and elevation (Clague et al., 2009). One significant factor is the aspect of glaciers: south-facing glaciers of the Cordillera Darwin remained stable or even advanced in the past 50 years while all other glaciers in the Cordillera Darwin retreated (Holmlund and Fuenzalida, 1995). Regardless of the aspect of a glacier, the lag time between changes in glacier mass balance and the response of the glacier terminus can often exceed a decade (Beedle et al., 2009). Furthermore, global changes in climate do not always occur concurrently in space and time (Clague et al., 2009). Winkler and Matthews (2010) point out these problems and question whether local and regional differences in glacier responses are large enough that hemispheric or global comparisons are possible.

Although there are many issues in comparing inter-hemispheric glacier synchronicity, incomplete comparisons can still provide useful information about past climate. More detailed glacier chronologies in southern Patagonia are needed to accurately constrain the times of glacier advances. This chronology of Stoppani Glacier and its comparison to northwestern North America identified previously unrecognized periods of glacier expansion in the Cordillera Darwin that are similar to those of northwestern North America.

5. Conclusions

A comparison of past glacier fluctuations between hemispheres provides insight into climate forcing mechanisms. As the number of detailed glacier chronologies increases throughout the world, our ability to identify inter-hemispheric connectivity improves. This study provides a record of past glacier expansion in southern Patagonia for comparison to the well documented glacial history of northwestern North America. The lateral moraine stratigraphy at Stoppani Glacier provides evidence of multiple periods of glacier expansion that have not previously been documented in the Cordillera Darwin. Sediment cores recovered from Lago Roca also indicate that the lake may have been isolated from the Beagle Channel more recently than previously thought. This study demonstrates the limitations inherent in any inter-hemispheric comparison of past glacier fluctuations, as well as the sparse research that has been done to date in southern Patagonia. The significant findings of this study and my suggestions for further work are as follows:

- Stoppani Glacier expanded at least five times in the past 3800 years. Each advance coincides with documented increases in glacier cover elsewhere in the Cordillera Darwin and/or the Southern Patagonian Icefield. The record of glacier expansion from southern South America broadly corresponds with the glacial record from northwestern North America. Although the evidence from Stoppani Glacier provides a detailed chronology, there are few other well constrained chronologies in southern Patagonia. More well bracketed chronologies of glacier advances in southern Patagonia are needed to better evaluate inter-hemispheric synchronicity of glacier advances.

- Comparison of inter-hemispheric Holocene glacier fluctuations is hampered by the limitations inherent in radiocarbon dating. Calibrated radiocarbon age ranges may span a period greater than the duration of an advance. As research on past glacier activity has increased and improved, it has become apparent that climate, and the glacier responses to it, during the Holocene were significantly variable. Additional work is needed to constrain the onset and termination of glacier advances, especially in southern Patagonia.

- The bulk physical properties of Lago Roca sediments suggest that the lake was separated from the Beagle Channel more recently than previously thought (ca. 2300 cal yr BP) and saline marine water trapped within the lake influenced the composition of the lake sediments until 700 cal yr BP. A more detailed study of Lago Roca sediments and stratigraphy would help determine the time when Lago Roca became isolated from the Beagle Channel.

- The marine water influence in Lago Roca made it difficult to identify changes in glacier activity in the watershed. Other lakes in the area may provide a better record of glacial fluctuations in the Fuegian Andes and Cordillera Darwin. I recommend that both lateral moraine stratigraphy and proglacial lake lithostratigraphy be utilized in more studies in southern Patagonia.

Reference

Algeo, T.J., and Maynard, J.B., 2004. Trace-element behavior and redox facies in core shales of Upper Pennsylvanian Kansas-type cyclothems. Chemical Geology 206, 289–318, doi: 10.1016/j.chemgeo.2003.12.009.

Allen, S.M., and Smith, D.J., 2007. Late Holocene glacial activity of Bridge Glacier, British Columbia Coast Mountains. Canadian Journal of Earth Sciences 44, 1753–1773.

Aniya, M., 1995. Holocene Glacier chronology in Patagonia: Tyndall and Upsala Glaciers. Arctic and Alpine Research 27, 311–322.

Ariztegui, D., Bianchi, M.M., Masaferro, J., LaFargue, E., and Niessan, F., 1997. Interhemispheric synchrony of late-glacial climatic instability as recorded in proglacial Lake Mascardi, Argentina. Journal of Quaternary Science 12, 133–138.

Bakke, J., Dahl, S.O., Paasche, Ø., Riis Simonsen, J., Kvisvik, B., Bakke, K., and Nesje, A., 2010. A complete record of Holocene glacier variability at Austre Okstindbreen, northern Norway: An integrated approach. Quaternary Science Reviews 29, 1246–1262, doi: 10.1016/j.quascirev.2010.02.012.

Barclay, D.J., Wiles, G.C., and Calkin, P.E., 2009. Holocene glacier fluctuations in Alaska. Quaternary Science Reviews 28, 2034–2048, doi: 10.1016/j.quascirev.2009.01.016.

Beedle, M.J., Menounos, B., Luckman, B.H., and Wheate, R., 2009. Annual push moraines as climate proxy. Geophysical Research Letters 36, 2–6, doi: 10.1029/2009GL039533.

Bouma, A.H., 1962. Sedimentology of some Flysch deposits: A graphic approach to facies interpretation. Elsevier, Amterdam, 168 pp.

Boyd, B.L., Anderson, J.B., Wellner, J.S., and Fernandez, R.A., 2008. The sedimentary record of glacial retreat, Marinelli Fjord, Patagonia: Regional correlations and climate ties. Marine Geology 255, 165–178, doi: 10.1016/j.margeo.2008.09.001.

Brahney, J., Clague, J.J., Menounos, B., and Edwards, T.W.D., 2007. Geochemical reconstruction of late Holocene drainage and mixing in Kluane Lake, Yukon Territory. Journal of Paleolimnology 40, 489–505, doi: 10.1007/s10933-007-9177-z.

Briner, J.P., Stewart, H.A.M., Young, N.E., Philipps, W., and Losee, S., 2010. Using proglacial-threshold lakes to constrain fluctuations of the Jakobshavn Isbræ ice margin, western Greenland, during the Holocene. Quaternary Science Reviews 29, 3861–3874.

Bujalesky, G.G., 2011. The flood of the Beagle Valley (11,000 yr BP), Tierra del Fuego. Anales Instituto Patagonia (Chile) 39, 5–21.

Clague, J.J., 1986. The Quaternary stratigraphic record of British Columbia - Evidence for episodic sedimentation and erosion controlled by glaciation. Canadian Journal of Earth Sciences 23, 885–894.

Clague, J.J., 1987. Quaternary stratigraphy and history, Williams Lake, British Columbia. Canadian Journal of Earth Sciences 23, 147–158.

Clague, J.J., and Mathews, W.H., 1992. The sedimentary record and Neoglacial history of Tide Lake, northwestern British Columbia. Canadian Journal of Earth Sciences, 29, 2383–2396, doi: 10.1139/e92-186.

Clague, J.J., Menounos, B., Osborn, G., Luckman, B.H., and Koch, J., 2009. Nomenclature and resolution in Holocene glacial chronologies. Quaternary Science Reviews 28, 2231–2238. doi: 10.1016/j.quascirev.2008.11.016.

Clapperton, C.M., and Sugden, D.E., 1988. Holocene glacier fluctuations in South America and Antartica. Quaternary Science Reviews 7, 185–190.

Costa, C.H., Smalley, R., Schwartz, D.P., Stenner, H.D., Ellis, M., and Ahumada, E.A., 2006. Paleoseismic observations of an onshore transform boundary: The Mafallanes-Fagnano Fault, Tierra del Fuego, Argentina. Revista de la Asociacion Geologica Argentina 61, 647–657.

Davis, P.T., Menounos, B., and Osborn, G., 2009. Holocene and latest Pleistocene alpine glacier fluctuations: A global perspective. Quaternary Science Reviews 28, 2021–2033, doi: 10.1016/j.quascirev.2009.05.020.

Denton, G.H., and Karlén, W., 1973. Holocene climatic variations – Their pattern and possible cause. Quaternary Research 3, 155–174.

Desloges, J.R., and Ryder, J.M., 1990. Neoglacial history of the Coast Mountains near Bella Coola, British Columbia. Canadian Journal of Earth Sciences 27, 281–290.

Desloges, J.R., and Gilbert, R., 1994. The record of extreme hydrological and geomorphological events inferred from glaciolacustrine sediments. *In* Variability in stream erosion and sediment transport. Proceedings of the Canberra Symposium. International Association of Hydrological Sciences (IAHS) Publication 224, 133–142.

Dominik, J., and Stanley, D.J., 1993. Boron, beryllium and sulfur in Holocene sediments and peats of the Nile delta, Egypt: Their use as indicators of salinity and climate. Chemical Geology 104, 203-216.

Easterbrook, D.J., and Donnell, C.B., 2007. Glacial and volcanic history of the Nooksack Middle Fork, Washington. Geological Society of America Abstracts with Programs 39 (4), 12.

Eyles, N., Eyles, C.H., and Miall, A.D., 1983. Lithofacies types and vertical profile models; An alternative approach to the description and environmental interpretation of glacial diamict and diamictite sequences. Sedimentology 30, 393–410.

Frederickson, A.F., and Reynolds, R.C., 1960. A geochemical method for determining paleosalinity. Clays and Clay Minerals 8, 203–213.

Gardner, J.S., and Jones, N.K., 1985. Evidence for a Neoglacial advance of the Boundary Glacier, Banff National Park, Alberta. Canadian Journal of Earth Sciences 22, 1753–1755.

Gibson, J.A.E., Vincent, W.F., Van Hove, P., and Belzile, C., 2002. Geochemistry of ice-covered, meromictic Lake A in the Canadian High Arctic. Aquatic Geochemistry 8, 97–119, doi: 10.1016/j.chemer.2003.11.004.

Gilbert, R., 1975. Sedimentation in Lillooet Lake, British Columbia. Canadian Journal of Earth Sciences 12, 1697–1711.

Glasser, N.F, Harrison, S., Winchester, V., and Aniya, M., 2004. Late Pleistocene and Holocene palaeoclimate and glacier fluctuations in Patagonia. Global and Planetary Change 43, 79–101.

Gordillo, S., Bujalesky, G., Pirazzoli, P., Rabassa, J, and Saliège, J., 1992. Holocene raised beaches along the northern coast of the Beagle Channel, Tierra del Fuego, Argentina. Palaeogeography, Palaeoclimatology, Palaeoecology 99, 41–45.

Gordillo, S., Coronato, A.M.J., and Rabassa, J.O., 1993. Late Quaternary evolution of subantarctic paleofjord, Tierra del Fuego. Quaternary Science Reviews 12, 889–897.

Hallet, B., Hunter, L., and Bogen, J., 1996. Rates of erosion and sediment evacuation by glaciers: A review of field data and their implications. Global and Planetary Change 12, 213–235.

Harvey, J.E., Smith, D.J., Laxton, S., Desloges, J., and Allen, S., 2012. Mid-Holocene glacier expansion between 7500 and 4000 cal. yr BP in the British Columbia Coast Mountains, Canada. The Holocene 22, 1–11, doi: 10.1177/0959683612437868.

Heiri, O., Lotter, A.F., and Lemcke, G., 2001. Loss on ignition as a method for estimating organic and carbonate content in sediments: Reproducibility and comparability of results. Journal of Paleolimnology 25, 101–110, doi: 10.1023/B:JOPL.0000042999.30131.5b.

Hodder, K.R., Gilbert, R., and Desloges, J.R., 2007. Glaciolacustrine varved sediment as an alpine hydroclimatic proxy. Journal of Paleolimnology 38, 365–394, doi: 10.1007/s10933-006-9083-9.

Holmlund, P., and Fuenzalida, H., 1995. Anomalous glacier responses to 20th century climactic changes in Darwin Cordillera, southern Chile. Journal of Glaciology 41, 465–473.

Ingall, E., Kolowith, L., Lyons, T., and Hurtgen, M., 2005. Sediment carbon, nitrogen and phosphorus cycling in an anoxic fjord, Effingham Inlet, British Columbia. American Journal of Science 305, 240–258.

Iturrizaga, L., 2008. Post-sedimentary transformation of lateral moraines. Journal of Mountain Science 5, 1–16, doi: 10.1007/s11629-008-0001-7.

Jackson, S.I., Laxton, S.C., and Smith, D.J., 2008. Dendroglaciological evidence for Holocene glacial advances in the Todd Icefield area, northern British Columbia Coast Mountains. Canadian Journal of Earth Sciences 45, 83–98, doi: 10.1139/E07-071.

Jibson, R.W., 1996. Use of landslides for paleoseismic analysis. Engineering Geology 43, 291–323.

Kaplan, M.R., Sterlin, J.A., Schaefer, J.M., Denton, G.H., Finkel, R.C., Schwartz, R., Putnam, A.E., Vandergoes, M.J., Goehring, B.M., and Travis, S.G., 2011. In situ cosmogenic ^{10}Be production rate at Lago Argentino, Patagonia: Implications for late-glacial climate chronology. Earth and Planetary Science Letters 309, 21–32.

Karlén, W., 1981. Lacustrine sediments studies: A technique to obtain a continous record of Holocene glacier variations. Geografiska Annaler 63, 273–281.

Karlstrom, T.N.V., 1964. Quaternary geology of the Kenai Lowland and glacial history of the Cook Inlet region, Alaska. U.S. Geological Survey Professional Paper 443, 69 pp.

Kemp, A.E.S. Dean, J., Pearcem R. B., and Pike, J., 2001. Recognition and analysis of bedding and sediment fabric features. *In* Tracking environmental changes using lake sediments: Physical and geochemical methods. Eds. Last, W.M. and Smol, J.P. Kluwer Academic, Dordrecht, Netherlands. pp. 7–22.

Koch, J., and Kilian, R., 2005. "Little Ice Age" glacier fluctuations, Gran Campo Nevado, southernmost Chile. The Holocene 15, 20–28, doi: 10.1191/0959683605hl780rp.

Koch, J., Clague, J.J., and Osborn, G.D., 2007a. Glacier fluctuations during the past millennium in Garibaldi Provincial Park, southern Coast Mountains, British Columbia. Canadian Journal of Earth Sciences 44, 1215–1233, doi: 10.1139/E07-019.

Koch, J., Osborn, G.D., and Clague, J.J., 2007b. Pre- " Little Ice Age " glacier fluctuations in Garibaldi Provincial Park, Coast Mountains, British Columbia, Canada. The Holocene 17, 1069–1078.

Koehler, L., and Smith, D.J., 2011. Late Holocene glacial activity in Manatee Valley, southern Coast Mountains, British Columbia, Canada. Canadian Journal of Earth Sciences 48, 603–618, doi: 10.1139/E10-087.

Kuylenstierna, J., Rosqvist, G., and Holmlund, P., 1996. Late-Holocene glacier variations in the Cordillera Darwin, Tierra del Fuego, Chile. The Holocene 6, 353–358.

Lamoureux, S.F., 1994. Embedding unfrozen lake sediments for thin section preparation. Journal of Paleolimnology 10, 141–146.

Land, L.S., and Hoops, G., 1973. Sodium in carbonate sediments and rocks: A possible index to the salinity of diagenetic solutions. Journal of Sedimentary Petrology 43, 614–617.

Larsen, D.J., Miller, G.H., Geirsdóttir, Á., and Thordarson, T., 2011. A 3000-year varved record of glacier activity and climate change from the proglacial lake Hvítárvatn, Iceland. Quaternary Science Reviews 30, 2715–2731, doi: 10.1016/j.quascirev.2011.05.026.

Leemann, A., and Niessen, F., 1994. Holocene glacial activity and climatic variations in the Swiss Alps: Reconstructing a continuous record from proglacial lake sediments. The Holocene 4, 259–268, doi: 10.1177/095968369400400305.

Leonard E.M., 1997. The relationship between glacial activity and sediment production: Evidence from a 4450-year varve record of neoglacial sedimentation in Hector Lake, Alberta, Canada. Jounal of Paleolimnology 17, 319–330.

Leonard, E.M., and Reasoner, M.A., 1999. A continuous holocene glacial record inferred from proglacial lake sediments in Banff National Park, Alberta, Canada. Quaternary Research 51, 1–13.

Leroy, S., Kazanci, N., Ileri, O., Kibar, M., Emre, M., Emre, O., McGee, E., and Griffiths, H.I., 2002. Abrupt environmental changes within a late Holocene lacustrine sequence south of the Marmara Sea (Lake Manyas , N-W Turkey): Possible links with seismic events. Marine Geology 190, 531–552.

Licciardi, J.M., Schaefer, J.M., Taggart, J.R., and Lund, D.C., 2009. Holocene glacier fluctuations in the Peruvian Andes indicate northern climate linkages. Science 325, 1677–1679, doi: 10.1126/science.1175010.

Loso, M.G., Anderson, R.S., Anderson, S.P., and Reimer, P.J., 2006. A 1500-year record of temperature and glacial response inferred from varved Iceberg Lake, southcentral Alaska. Quaternary Research 66, 12–24, doi: 10.1016/j.yqres.2005.11.007.

Luckman, B.H., 1986. Reconstruction of Little Ice Age events in the Canadian Rocky Mountains. Géographie physique et Quaternaire 40, 17–28.

Luckman, B.H., 1993. Glacier gluctuations and tree-ring records for the last millennium in the Canadian Rockies. Quaternary Science Reviews 16, 44 –450.

Luckman, B.H., 1995. Calendar-dated, early "Little Ice Age" glacier advance at Robson Glacier, British Columbia, Canada. The Holocene 5, 149–159, doi: 10.1177/095968369500500203.

Luckman, B.H., 2000. The Little Ice Age in the Canadian Rockies. Geomorphology 32, 357–384.

Luckman, B.H., Harding, K.A., and Hamilton, J.P., 1987. Recent glacier advances in the Premier Range, British Columbia. Canadian Journal of Earth Sciences 24, 1149–1161.

Lunde, G., 1977. Occurrence and transformation of arsenic in the marine environment. Environmental Health Perspectives 19, 47–52.

Matthews, J.A., Dahl, S.O., Nesje, A., Berrisford, M.S., and Andersson, C., 2000. Holocene glacier variations in central Jotunheimen, southern Norway based on distal glaciolacustrine sediment cores. Quaternary Science Reviews 19, 1625–1647.

Maurer, M.K., Menounos, B., Luckman, B.H., Osborn, G., Clague, J.J., Beedle, M.J., Smith, R., and Atkinson, N., 2012. Late Holocene glacier expansion in the Cariboo and northern Rocky Mountains, British Columbia, Canada. Quaternary Science Reviews 51, 71–80, doi: 10.1016/j.quascirev.2012.07.023.

Mayewski, P.A., Rohling, E.E., Stager, J.C., Karle, W., Maasch, K.A., Meeker, L.D., Meyerson, E.A., Gasse, F., Van Kreveld, S., Holmgren, K., Lee-thorp, J., Rosqvist, G., Rack, F., Staubwasser, M., Schneider, R.R., and Steig, E.J., 2004. Holocene climate variability. Quaternary Research 62, 243–255.

McCulloch, R.D., Bentley, M.J., Purves, R.S., Hulton, N.R.J., Sugden, D.E., and Clapperton, C.M., 2000. Climatic inferences from glacial and palaeoecological evidence at the last glacial termination, southern South America. Journal of Quaternary Science 15, 409–417.

Mendoza, L., Perdomo, R., Hormaechea, J.L., Cogliano, D. Del, Fritsche, M., Richter, A., and Dietrich, R., 2011. Present-day crustal deformation along the Magallanes-Fagnano fault system in Tierra del Fuego from repeated GPS observations. Geophysical Journal International 184, 1009–1022, doi: 10.1111/j.1365-246X.2010.04912.x.

Menounos, B., 2006. Anomalous early 20th century sedimentation in proglacial Green Lake, British Columbia, Canada. Canadian Journal of Earth Sciences 43, 671–678, doi: 10.1139/E06-016.

Menounos, B., Clague, J.J., Osborn, G., Luckman, B.H., Lakeman, T.R., and Minkus, R., 2008. Western Canadian glaciers advance in concert with climate change circa 4.2 ka. Geophysical Research Letters 35, 1–6, doi: 10.1029/2008GL033172.

Menounos, B., Koch, J., Osborn, G., Clague, J.J., and Mazzucchi, D., 2004. Early Holocene glacier advance, southern Coast Mountains, British Columbia, Canada. Quaternary Science Reviews 23, 1543–1550, doi: 10.1016/j.quascirev.2003.12.023.

Menounos, B., and Clague, J.J., 2008. Reconstructing hydro-climatic events and glacier fluctuations over the past millennium from annually laminated sediments of Cheakamus

Lake, southern Coast Mountains, British Columbia, Canada. Quaternary Science Reviews 27, 701–713, doi: 10.1016/j.quascirev.2008.01.007.

Menounos, B., Osborn, G., Clague, J.J., and Luckman, B.H., 2009. Latest Pleistocene and Holocene glacier fluctuations in western Canada. Quaternary Science Reviews 28, 2049–2074, doi: 10.1016/j.quascirev.2008.10.018.

Menounos, B., Clague, J.J., Clarke, G.K.C., Marcott, S.A., Osborn, G., Clark, P.U., Tennant, C., Novak, A.M., 2013a. Did rock avalanche deposits modulate the Late Holocene advance of Tiedemann Glacier, southern Coast Mountains, British Columbia, Canada?. Earth and Planetary Science Letters 384, 154–164.

Menounos, B., Clague, J.J., Osborn, G., Davis, P.T., Ponce, F., Goehring, B., Maurer, M., Rabassa, J., Coronato, A., and Maar, R., 2013b. Latest Pleistocene and Holocene glacier fluctuations in southernmost Tierra del Fuego, Argentina. Quaternary Science Reviews 77, 70–79, doi: org/10.1016/j.quasciriv.2013.07.008.

Mercer, J.H., 1965. Glacier variations in Southern Patagonia. Geography Reviews 55, 390–413.

Mercer, J.H., 1968. Variations of some Patagonian glaciers since the Late-Glacial. American Journal of Science 266, 91–109.

Mercer, J.H., 1970. Variations of some Patagonian glaciers since the Late-Glacial: II. American Journal of Science 269, 91–109.

Mercer, J.H., 1976. Glacial history of southernmost South America. Quaternary Research 6, 125–166.

Miller, G.H., Wolfe, A.P., Briner, J.P., Sauer, P.E., and Nesje, A., 2005. Holocene glaciation and climate evolution of Baffin Island, Arctic Canada. Quaternary Science Reviews 24, 1703–1721, doi: 10.1016/j.quascirev.2004.06.021.

Mitchell, J.M., 1976. An overview of climate variability and its causal mechanisms. Quaternary Research 6, 481–493.

Moernaut, J., De Batist, M., Charlet, F., Heirman, K., Chapron, E., Pino, M., Brümmer, R., and Urrutia, R., 2007. Giant earthquakes in south-central Chile revealed by Holocene mass-wasting events in Lake Puyehue. Sedimentary Geology 195, 239–256, doi: 10.1016/j.sedgeo.2006.08.005.

Moore, J.J., Hughen, K.A., Miller, G.H., and Overpeck, J.T., 2001. Little Ice Age recored in summer temperature reconstruction from varved sediments of Donard Lake, Baffin Island, Canada. Journal of Paleolimnology 25, 503–517, doi: 10.2307/1550544.

Motyka, R.J., and Begét, J.E., 1996. Taku Glacier, Alaska, U.S.A.: Late Holocene history of a tidewater glacier. Arctic and Alpine Research 28, 42–51.

Mulvaney, R., Abram, N.J., Hindmarsh, R.C.A., Arrowsmith, C., Fleet, L., Triest, J., Sime, L.C., Alemany, O., and Foord, S., 2012. Recent Antarctic Peninsula warming relative to Holocene climate and ice-shelf history. Nature 489, 141–144, doi: 10.1038/nature11391.

Neff, J.M., 1997. Ecotoxicology of arsenic in the marine environment. Environmental Toxicology and Chemistry 16, 917–927.

Nelson, E.P., Dalziel, I.W.D., and Ridley, W.I., 1978, Geological studies in Cordillera Darwin, Tierra del Fuego, southern Chile: R/VHero cruises 77-4 and 78-2, 14–15.

Neukom, R., Luterbacher, J., Villalba, R., Küttel, M., Frank, D., Jones, P.D., Grosjean, M., Wanner, H., Aravena, J.C., Black, D.E., Christie, D.A., D'Arrigo, R., Lara, A., and Morales, M., 2011. Multiproxy summer and winter surface air temperature field reconstructions for southern South America covering the past centuries. Climate Dynamics 37, 35–51, doi: 10.1007/s00382-010-0793-3.

Osborn, G., 1986. Lateral-moraine stratigraphy and Neoglacial history of Bugaboo Glacier, British Columbia. Quaternary Science Reviews 7, 115–128.

Osborn, G., and Karlstrom, E.T., 1988. Holocene history of the Bugaboo Glacier, British Columbia. Geology 16, 1015–1017, doi: 10.1130/0091-7613(1988)016<1015.

Osborn, G., and Karlstrom, E.T., 1989. Holocene moraine and paleosol stratigraphy, Bugaboo Glacier, British Columbia. Boreas 18, 311–322, doi: 10.1111/j.1502-3885.1989.tb00406.x.

Osborn, G.D., Robinson, B.J., and Luckman, B.H., 2001. Holocene and latest Pleistocene fluctuations of Stutfield Glacier, Canadian Rockies. Canadian Journal of Earth Sciences 38, 1141–1155, doi: 10.1139/cjes-38-8-1141.

Osborn, G., Menounos, B., Koch, J., Clague, J.J., and Vallis, V., 2007. Multi-proxy record of Holocene glacial history of the Spearhead and Fitzsimmons ranges, southern Coast Mountains, British Columbia. Quaternary Science Reviews 26, 479–493, doi: 10.1016/j.quascirev.2006.09.003.

Osborn, G., Menounos, B., Ryane, C., Riedel, J., Clague, J.J., Koch, J., Clark, D., Scott, K., and Davis, P.T., 2012. Latest Pleistocene and Holocene glacier fluctuations on Mount Baker, Washington. Quaternary Science Reviews 49, 33–51, doi: 10.1016/j.quascirev.2012.06.004.

Plouffe, A., and Levson, V.M., 2001. Late Quaternary glacial and interglacial environments of the Nechako River - Cheslatta Lake area, central British Columbia. Canadian Journal of Earth Sciences 38, 719–731, doi: 10.1139/cjes-38-4-719.

Porter, S.C., 2000. Onset of Neoglaciation in the Southern Hemisphere. Journal of Quaternary Science 15, 395–408.

Preston, R.S., Person, E., and Deevey, E.S., 1955. Yale natural radiocarbon measurments II. Science 122, 954–960.

Rabassa, J., Coronato, A., Bujalesky, G., Salemme, M., Roig, C., Meglioti, A., Heusser, C., Gordillo, S., Roig, F., Borromei, A., and Quattrocchio, M., 2000. Quaternary of Tierra del Fuego, southernmost South America: An updated review. Quaternary International 68-71, 217–240.

Reasoner, M.A., 1993. Equipment and procedure improvements for a lightweight, inexpensive, percussion core sampling system. Journal of Paleolimnology 8, 273–281, doi: 10.1007/BF00177859.

Reyes, A.V., and Clague, J.J., 2004. Stratigraphic evidence for multiple Holocene advances of Lillooet Glacier, southern Coast Mountains, British Columbia. Canadian Journal of Earth Sciences 41, 903–918, doi: 10.1139/E04-039.

Reyes, A.V, Wiles, G.C., Smith, D.J., Barclay, D.J., Allen, S., Jackson, S., Larocque, S., Laxton, S., Lewis, D., Calkin, P.E., and Clague, J.J., 2006. Expansion of alpine glaciers in Pacific North America in the first millennium A.D.. Geology 34, 57–60.

Rodbell, D.T., Smith, J.A., and Mark, B.G., 2009. Glaciation in the Andes during the Lateglacial and Holocene. Quaternary Science Reviews 28, 2165–2212, doi: 10.1016/j.quascirev.2009.03.012.

Rose, J., 1974. Small-scale spatial variability of some sedimentary properties of lodgement till and slumped till. Proceedings of the Geologists' Association 85, 239–258.

Röethlisberger, F., 1987. 10000 Jahre Gletschergeschichte der Ede. Sauerlander, Aarau, Switzerland.

Rubio, B., Nombela, M., and Vilas, F., 2000. Geochemistry of major and trace elements in sediments of the Ria de Vigo (NW Spain): An assessment of metal pollution. Marine Pollution Bulletin 40, 968–980, doi: 10.1016/S0025-326X(00)00039-4.

Ryder, J.M., 1987. Neoglacial history of the Stikine-Iskut area, northern Coast Mountains, British Columbia. Canadian Jounal of Earth Sciences 24, 1294–1301.

Ryder, J.M., and Thomson, B., 1986. Neoglaciation in the southern Coast Mountains of British Columbia: Chronology prior to the late Neoglacial maximum. Canadian Journal of Earth Sciences 23, 273–287.

Samolczyk, M., 2011. Latest Pleistocene and Holocene glacier fluctuations in Mount Rainier National Park, Washington, USA. M.Sc. thesis, University of Calgary, Calgary, AB.

Santisteban, J.I., Mediavilla, R., López-Pamo, E., Dabrio, C.J., Blanca Ruiz Zapata, M., José Gil García, M., Castaño, S., and Martínez-Alfaro, P.E., 2004. Loss on ignition: A qualitative or quantitative method for organic matter and carbonate mineral content in sediments?. Journal of Paleolimnology 32, 287–299, doi: 10.1023/B:JOPL.0000042999.30131.5b.

Schaefer, J.M., Denton, G.H., Kaplan, M., Putnam, A., Finkel, R.C., Barrell, D.J.A., Andersen, B.G., Schwartz, R., Mackintosh, A., Chinn, T., and Schlüchter, C., 2009. High-frequency Holocene glacier fluctuations in New Zealand differ from the northern signature. Science 324, 622–625, doi: 10.1126/science.1169312.

Schiefer, E., Hassan, M.A., Menounos, B., Pelpola, C.P., and Slaymaker, O., 2010. Interdecadal patterns of total sediment yield from a montane catchment, southern Coast Mountains, British Columbia, Canada. Geomorphology 118, 207–212, doi: 10.1016/j.geomorph.2010.01.001.

Schnellmann, M., Anselmetti, F.S., Giardini, D., Mckenzie, J.A., and Ward, S.N., 2002. Prehistoric earthquake history revealed by lacustrine slump deposits. Geology 30, 1131–1134, doi: 10.1130/0091-7613(2002)030<1131.

Shilts, W.W. and Clague, J.J. 1992. Documentation of earthquake-induced disturbance of lake sediments using subbottom acoustic profiling. Canadian Journal of Earth Sciences 29, 1018-1042.

Smith, S.V., 1984. Phosphorus versus nitrogen limitation in the marine environment. Limnology and Oceanography 29, 1149–1160.

Snowball, I., Sandgren, P., and Petterson, G., 1999. The mineral magnetic properties of an annually laminated Holocene lake-sediment sequence in northern Sweden. The Holocene 9, 353–362, doi: 10.1191/095968399670520633.

Souch, C., 1994. A methodology to interpret downvalley lake sediments as records of Neoglacial activity: Coast Mountains, British Columbia, Canada. Geografiska Annaler, Series A, Physical Geography 76, 169–185, doi: 10.2307/521036.

Sperazza, M., Moore, J.N., and Hendrix, M.S., 2004. High-resolution particle size analysis of naturally occurring very fine-grained sediment through laser diffractometry. Journal of Sedimentary Research 74, 736–743, doi: 10.1306/031104740736.

Strelin, J.A., and Malagnino, E.C., 2000. Late-glacial history of Lago Argentino, Argentina, and age of the Puerto Bandera moraines. Quaternary Research 54, 339–347.

, J., and Iturraspe, R., 2007. Recent evolution and mass balance of Cordón Martial glaciers, Cordillera Fueguina Oriental. Global Planetary Change 59, 17–26.

Strelin, J., Casassa, G., Rosqvist, G., and Holmlund, P., 2008. Holocene glaciations in the Ema Glacier valley, Monte Sarmiento Massif, Tierra del Fuego. Palaeogeography, Palaeoclimatology, Palaeoecology 260, 299–314, doi: 10.1016/j.palaeo.2007.12.002.

Stuiver, M., Reimer, P.J., and Reimer, R.W., 2010. CALIB 6.0. [http://calib.qub.ac.uk/calib/].

Sugden, D.E., Bentley, M.J., Fogwill, C.J., Hulton, N.R.J., McCulloch, R.D., and Purves, R.S., 2005. Late-Glacial glacier events in southernmost South America: A Blend of "Northern" and "Southern" Hemispheric climatic signals?. Geografiska Annaler 87, 273–288, doi: 10.1111/j.0435-3676.2005.00259.x.

Villalba, R., 1994. Tree-ring and glacial evidence for the Medieval Warm Epoch and the Little Ice Age in southern South America. Climatic Change 26, 183–197.

Weber, G., 2006. Dendrochronologische untersuchungen moderner und historischer glestscherstände in den vorfeldern von Eagle, Herbert und Mendenhall gletscher (Juneay Icefield, Südost Alaska). Diplomarbeit, Geografisches Institut der Universität Zürich, Birmensdorf, Switzerland.

Wenzens, G., 1999. Fluctuations of outlet and valley glaciers in the southern Andes (Argentina) during the past 13,000 years. Quaternary Research 51, 238–247, doi: 10.1006/qres.1999.2043.

Westman, P., and Hedenström, A., 2002. Environmental changes during isolation processes from the Litorina Sea as reflected by diatoms and geochemical parameters – A case study. The Holocene 12, 531–540, doi: 10.1191/0959683602hl560rp.

Wiles, G.C., Calkin, P.E., 1994. Late Holocene, high-resolution glacial chronologies and climate, Kenai Mountains, Alaska. Geological Society of America Bulletin 106, 281–303.

Wiles, G.C., Jacoby, G.C., Davi, N.K., McAllister, R.P., 2002. Late Holocene glacier fluctuations in the Wrangell Mountains, Alaska. Geological Society of America Bulletin 114, 896–908.

Wiles, G.C., D'Arrigo, R.D., Villalba, R., Calkin, P.E., and Barclay, D.J., 2004. Century-scale solar variability and Alaskan temperature change over the past millennium. Geophysical Research Letters 31, 2–5, doi: 10.1029/2004GL020050.

Winkler, S., and Matthews, J.A., 2010. Holocene glacier chronologies: Are "high-resolution" global and inter-hemispheric comparisons possible?. The Holocene 20, 1137–1147, doi: 10.1177/0959683610369511.

Wood, C., and Smith, D., 2004. Dendroglaciological evidence for a Neoglacial advance of the Saskatchewan Glacier, Banff National Park, Canadian Rocky Mountains. Tree-Ring Research 60, 59–65.

Appendices

Appendix A: Stratigraphy of the northeast lateral moraine of Stoppani Glacier.

Table A.1: Stratigraphy section at the Main Gully site, northeast lateral moraine of Stoppani Glacier.

Unit	Height above base of section (m) (approximate)	Description
1	0 – 13	Massive sandy gravel diamicton with angular to subangular clasts up to two meters across. Unit dips towards glacier with sharp upper contact.
2	13 – 15	Horizontally stratified, sand and sandy gravel with scattered cobbles and boulders up to one meter across. Gradational upper contact. The unit is discontinuous along the length of the exposure.
3	15 – 25	Weakly stratified, matrix-supported sandy gravel diamicton with angular to subrounded clasts up to two meters across. Sharp upper contact.
4	25 – 26	Weakly stratified, matrix-supported sandy gravel diamicton with scattered boulders. Sharp upper contact.
5	26 – 38	Matrix-supported sandy diamicton with angular to subrounded clasts up to three meters across. Lower half of unit is massive and upper half is weakly stratified. Sharp upper contact.
6	38 – 39	Silty to sandy gravel with peat lenses. Sharp upper contact. The unit is discontinuous along the length of the exposure.
7	39 – 57	Weakly stratified sandy gravel diamicton with angular to subrounded clasts up to three meters across. Gradational upper contact.
8	57 – 74	Horizontally stratified, matrix-supported sandy gravel diamicton with boulders up to three meters across. Gradational upper contact.
9	74 – 84	Weakly stratified to massive sandy gravel diamicton with scattered boulders up to three meters across.

Appendix B: Sediment analysis procedures.

Procedure for LOI analysis modified from Heiri et al. (2001):

I collected about 1 cm^3 samples of sediment at 1 cm intervals along the length of the cores. I transferred the wet samples into pre-weighed crucibles and placed them in an oven at 105°C for 24 hours. After drying, I re-weighed the crucibles to determine the dry weight of the samples. The difference between the wet and dry sample weights represents the percent water content of the sediment.

$$W = \frac{[(Ww - Wc) - (Wd - Wc)]}{(Ww - Wc)} * 100$$

where W = percent water content, Ww = total wet weight (g), Wd = total dry weight of solids (g), and Wc = total weight of crucible (g).

I then placed the samples in the muffle furnace at 550°C for 6 hours. After burning off the organic material, I re-weighed the samples. The difference in weight between the dry sample and the combusted sample represents the percent organic matter (LOI).

$$LOI = \frac{[(Wd - Wc) - (Wi - Wc)]}{(Wd - Wc)} * 100$$

where LOI = percent loss-on-ignition, Wi = weight of inorganic residue (g), Wd = total dry weight of solids (g), and Wc = total weight of crucible (g).

Procedure for particle-size analysis modified from (Sperazza et al., 2004):

I treated the residues from 20 samples for the total elemental composition with 35% hydrogen peroxide (H_2O_2) to remove any remaining organic matter. I placed each of the 20 samples in a clean beaker with 20 mL of distilled water (dH_2O) and then added 20 mL of H_2O_2. I placed each beaker on a hot plate set to 70°C and continuously stirred the mixture until no more bubbles were produced. Once the reaction between the organic matter and the H_2O_2 was complete, I allowed most of the remaining water to evaporate off and transferred the samples into vials.

I treated each sample at Simon Fraser University with sodium metaphosphate ($(NaPO_3)_6$ or Calgon) to prevent flocculation of the fine particles during analysis. Before introducing a small amount of each sample into the Mastersizer, I stirred the sample to ensure no settling was taking place and that I would get a representative analysis. I measured each sample three times.

The Mastersizer software separates the measured particles into different size fractions and also calculates the mean particle size (d50) for each sample. I took the average d50 of the three measurements as the average particle size for each of the 20 samples.

Appendix C: Elemental concentrations determined by Inductively Coupled Plasma Mass Spectrometry (ICP-MS).

Figure C.1: Elemental concentrations in core 09-LRoca(02).

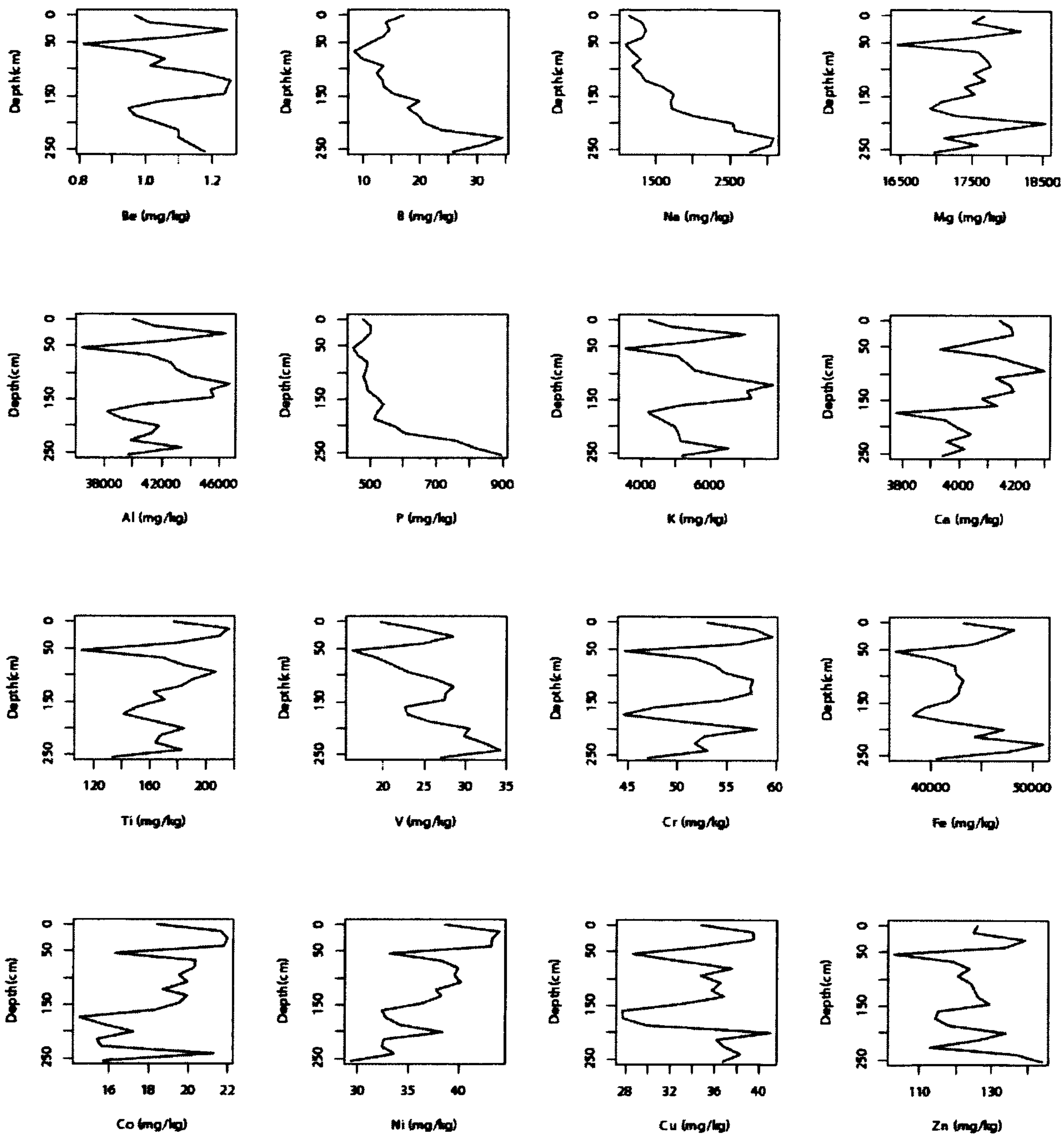

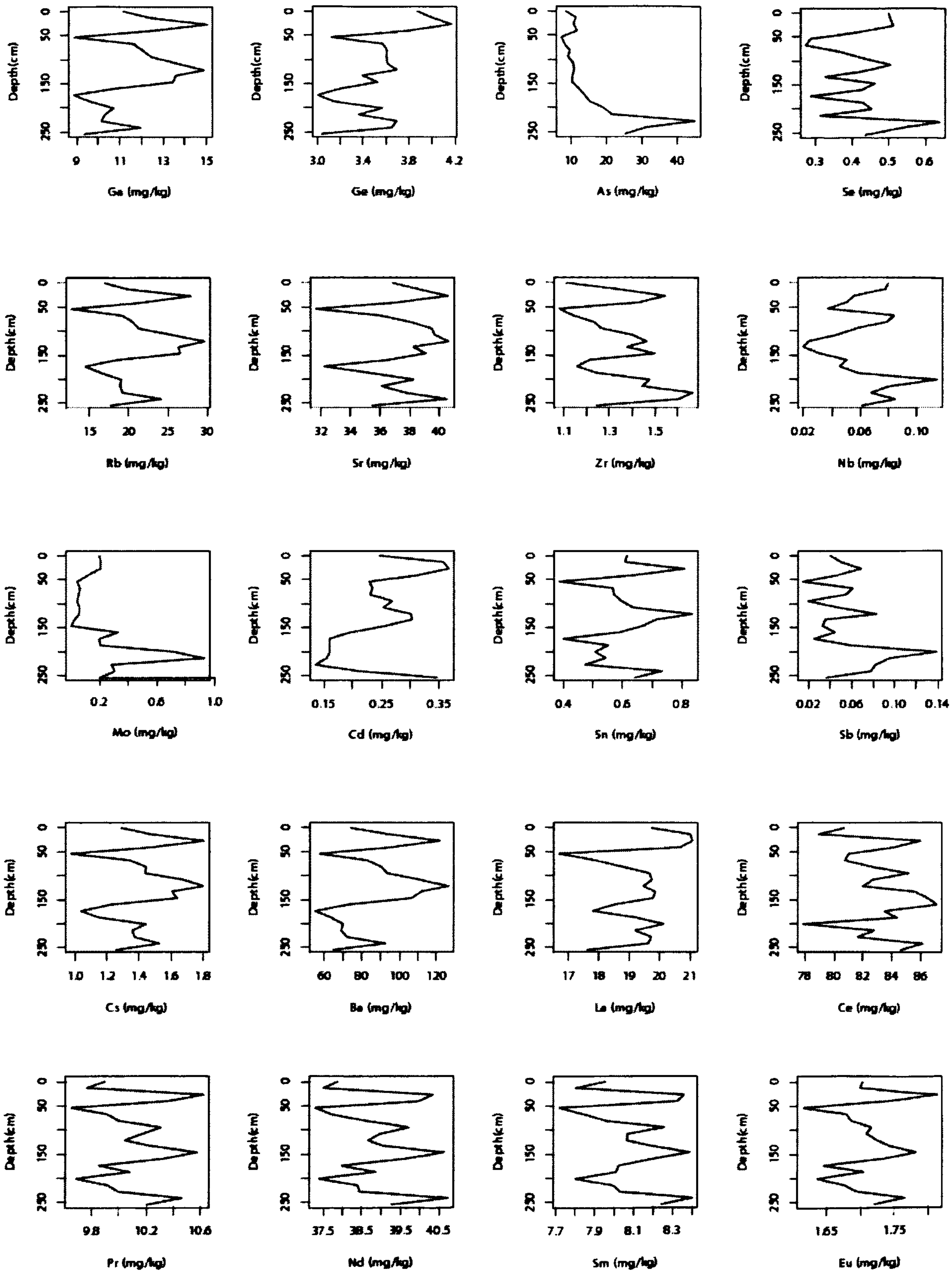

Depth(cm)
0
50
150
250
Ga (mg/kg)
9 11 13 15
Ge (mg/kg)
3.0 3.4 3.8 4.2
As (mg/kg)
10 20 30 40
Se (mg/kg)
0.3 0.4 0.5 0.6
Rb (mg/kg)
15 20 25 30
Sr (mg/kg)
32 34 36 38 40
Zr (mg/kg)
1.1 1.3 1.5
Nb (mg/kg)
0.02 0.06 0.10
Mo (mg/kg)
0.2 0.6 1.0
Cd (mg/kg)
0.15 0.25 0.35
Sn (mg/kg)
0.4 0.6 0.8
Sb (mg/kg)
0.02 0.06 0.10 0.14
Cs (mg/kg)
1.0 1.2 1.4 1.6 1.8
Ba (mg/kg)
60 80 100 120
La (mg/kg)
17 18 19 20 21
Ce (mg/kg)
78 80 82 84 86
Pr (mg/kg)
9.8 10.2 10.6
Nd (mg/kg)
37.5 38.5 39.5 40.5
Sm (mg/kg)
7.7 7.9 8.1 8.3
Eu (mg/kg)
1.65 1.75

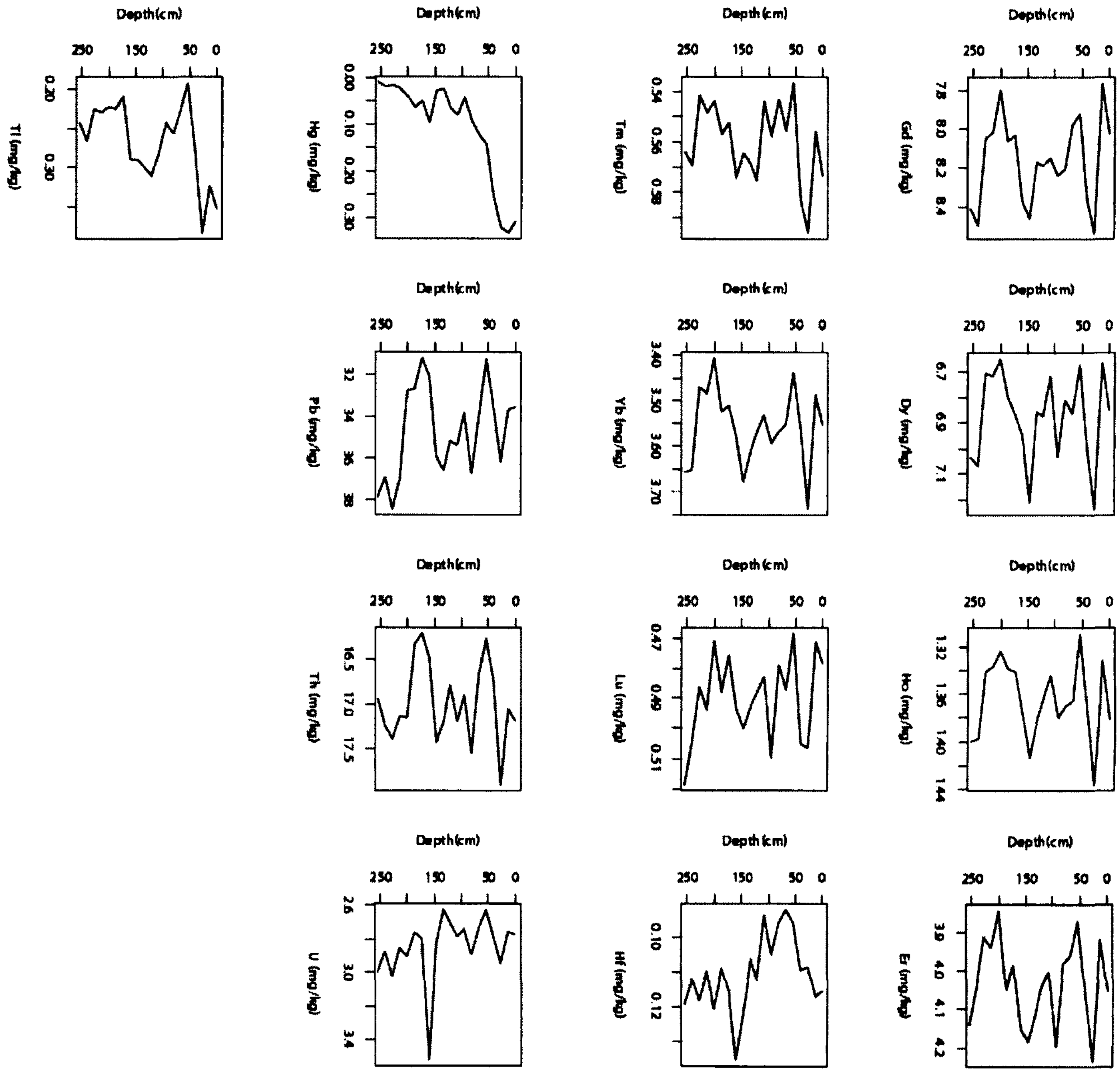
Depth(cm)
Tl (mg/kg)
Hg (mg/kg)
Tm (mg/kg)
Gd (mg/kg)
Pb (mg/kg)
Yb (mg/kg)
Dy (mg/kg)
Th (mg/kg)
Lu (mg/kg)
Ho (mg/kg)
U (mg/kg)
Hf (mg/kg)
Er (mg/kg)

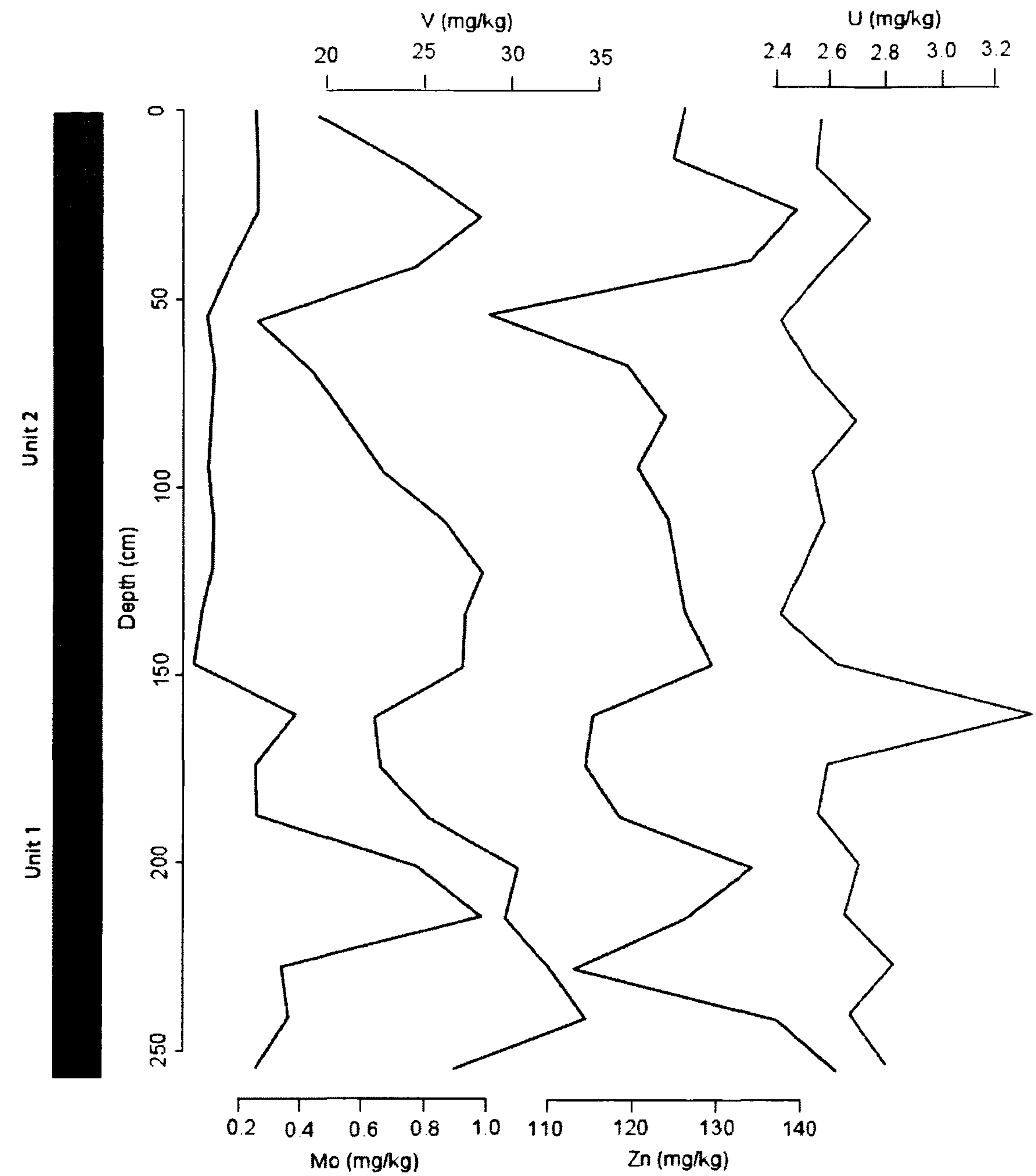

Figure C.2: Total concentration of redox-indicator elements molybdenum, vanadium, zinc and uranium in core 09-LRoca(02).

Appendix D: Principal component analysis of total elemental concentrations after standardization for differences in clay content.

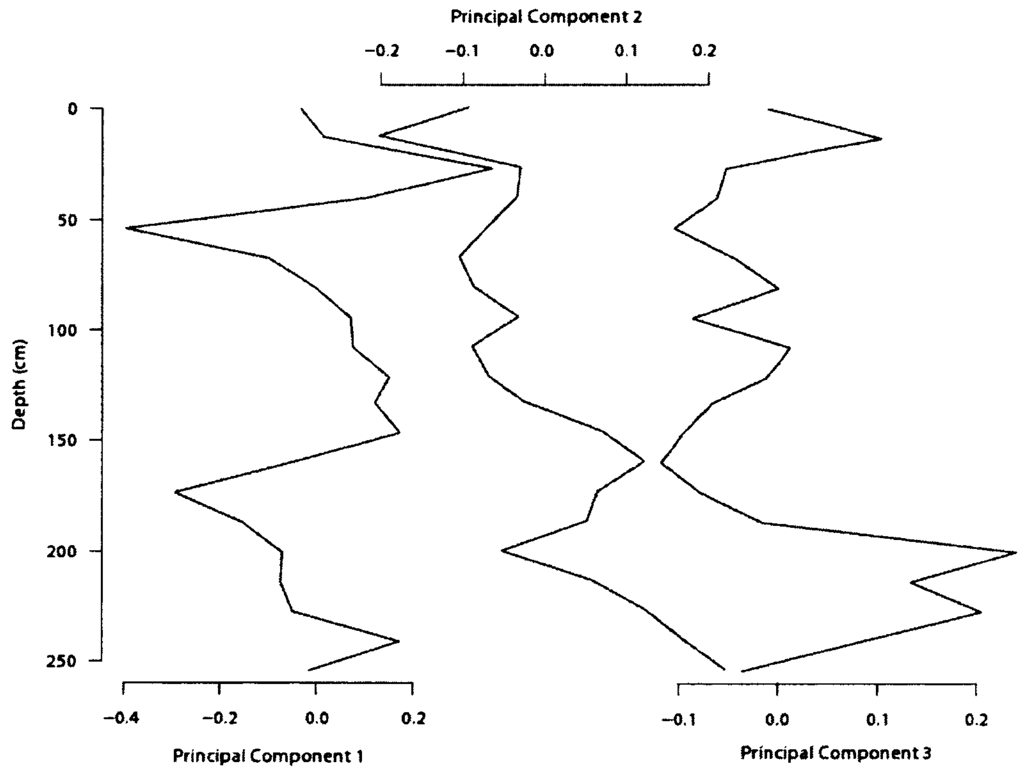

Figure D.1: Principal component 1, 2 and 3 of 20 geochemistry samples from 09-LRoca(02).

Table D.1: Correlation between principal component 1, 2 and 3, percent clay, water density, water content, organic matter and magnetic susceptibility.

	PC1	PC2	PC3	% Clay	Wet density	Dry density	Water content	Organic matter	Magnetic susceptibility
PC1	1	-4.0E-16	-4.3E-17	0.37	0.053	0.011	0.091	-0.027	-0.19
PC2	-4.0E-16	1	-1.3E-16	0.057	-0.42	-0.53	0.61	0.44	0.048
PC3	-4.3E-17	-1.3E-16	1	0.51	-0.39	-0.49	0.52	0.43	-0.58
% Clay	0.37	0.057	0.51	1	-0.06	-0.11	0.20	0.18	-0.61
Wet density	0.053	-0.42	-0.39	-0.06	1	0.96	-0.51	-0.25	0.26
Dry density	0.011	-0.53	-0.49	-0.11	0.96	1	-0.72	-0.43	0.35
Water content	0.091	0.61	0.52	0.20	-0.51	-0.72	1	0.73	-0.43
Organic matter	-0.027	0.44	0.43	0.18	-0.25	-0.43	0.73	1	-0.37
Magnetic susceptibility	-1.9E-01	4.8E-02	-0.58	-0.61	0.26	0.35	-0.43	-0.37	1

Appendix E: Calibrated radiocarbon ages for northwestern North America Neoglacial sites.

Table E.1: Calibrated age ranges of in situ fossil plants that span the Neoglacial period in northwestern North America.

Region	Glacier name	Calibrated age (cal yr BP) Maximum	Minimum	Reference
Canadian Coast Mountains	Tiedemann	4410	4180	Menounos et al., 2009
	Tiedemann	4380	3930	Menounos et al., 2009
	Tiedemann	4290	4100	Menounos et al., 2009
	Tiedemann	4220	3890	Menounos et al., 2009
	Decker	3580	3260	Osborn et al., 2007
	Lillooet	3360	3080	Reyes and Clague, 2004
	Bridge	3340	2980	Allen and Smith, 2007
	Decker	3320	2990	Osborn et al., 2007
	Decker	3240	2900	Osborn et al., 2007
	Tiedemann	3210	3000	Menounos et al., 2009
	Tiedemann	2970	2860	Menounos et al., 2009
	Tiedemann	2920	2750	Menounos et al., 2009
	Tiedemann	2870	2730	Menounos et al., 2009
	Tiedemann	2750	2370	Menounos et al., 2009
	Jacobsen	2710	2360	Desloges and Ryder, 1990
	Manatee	2700	2170	Koehler and Smith, 2011
	Lillooet	2300	1930	Reyes and Clague, 2004
	Bridge	1520	1300	Allen and Smith, 2007
	Lillooet	1340	1280	Reyes and Clague, 2004
	Beare	1180	920	Barclay et al., 2009
	Beare	1050	790	Barclay et al., 2009
	Llewellyn	960	780	Clague et al., 2010
	Warren	950	780	Koch et al., 2007a
	Llewellyn	910	800	Clague et al., 2010
	Scud	900	320	Ryder, 1987
	Llewellyn	900	560	Clague et al., 2010
	Franklin	900	680	Ryder and Thomson, 1986
	Kilinaklin	740	920	Ryder and Thomson, 1986
	Helm	730	550	Koch et al., 2007a
	Bridge	690	550	Ryder and Thomson, 1986
	Purgatory	680	530	Ryder and Thomson, 1986
	Herbert	670	560	Weber, 2006

Region	Glacier name	Calibrated age (cal yr BP) Maximum	Minimum	Reference
Canadian Rocky Mountains	Boundary	4820	4410	Gardner and Jones, 1985
	Boundary	4510	4100	Gardner and Jones, 1985

	Boundary	4420	4160	Wood and Smith, 2004
	Robson	4280	3850	Luckman, 1995
	Robson	4150	3830	Luckman, 1995
	Robson	3690	3380	Luckman, 1993
	Robson	3640	3280	Luckman, 1993
	Peyto	3250	2930	Luckman, 1993
	Saskatchewan	3210	2800	Wood and Smith, 2004
	Saskatchewan	3140	2780	Wood and Smith, 2004
	Bugaboo	2930	2720	Osborn and Karlsrom, 1989
	Peyto	1550	1320	Luckman, 2006
	Stulfield	960	730	Osborn et al., 2001
	Peyto	940	710	Luckman, 1993
	Robson	920	740	Luckman, 1993
	Peyto	900	670	Luckman, 1994
Interior mountain ranges	Castle	4960	4450	Maurer et al., 2012
	Castle	4850	4620	Menounos et al., 2008
	Harworth	4410	4160	Menounos et al., 2008
	Castle	4150	3980	Menounos et al., 2008
	Castle	4150	3990	Maurer et al., 2012
	Castle	2730	2490	Maurer et al., 2012
	Castle	1870	1720	Maurer et al., 2012
	Castle	1540	1420	Maurer et al., 2012
	Castle	910	800	Maurer et al., 2012
Washington Cascade Mountains	Deming	2150	2010	Osborn et al., 2012
	Deming	1810	1710	Osborn et al., 2012
	Deming	1810	1550	Osborn et al., 2012
	Deming	1540	1410	Osborn et al., 2012
	Deming	930	800	Osborn et al., 2012
	Deming	930	800	Osborn et al., 2012
	Deming	500	330	Osborn et al., 2012

		Calibrated age (cal yr BP)		
Region	**Glacier name**	**Maximum**	**Minimum**	**Reference**
Alaska	Herbert	3200	2790	Barclay et al., 2009
	Gilkey	2340	2010	Röethlisberger, 1986

Mendenhall	2320	1990	Röethlisberger, 1986
Mendenhall	2300	1900	Röethlisberger, 1986
Nabesna	2150	1870	Wiles et al., 2002
Mendenhall	2100	1720	Röethlisberger, 1986
Mendenhall	1970	1620	Röethlisberger, 1986
Kuskulana	1820	1540	Wiles et al., 2002
Kuskulana	1820	1450	Wiles et al., 2002
Bartlett	1730	830	Karlstrom, 1964
Mendenhall	1700	1570	Weber, 2006
Beare	1520	1290	Reyes et al., 2006
Dinglestadt	1520	1190	Wiles and Calkin, 1994
Gilkey	1300	1010	Röethlisberger, 1986
Mendenhall	1170	920	Preston, 1955
Kennicott	1050	750	Wiles et al., 2002
Gilkey	1040	680	Röethlisberger, 1986
Kennicott	950	730	Wiles et al., 2002
Kennicott	910	690	Wiles et al., 2002
Herbert	670	560	Weber, 2006
Herbert	660	540	Motyka and Beget, 1996